Volume 13 | Number 4 | 17 February 2026

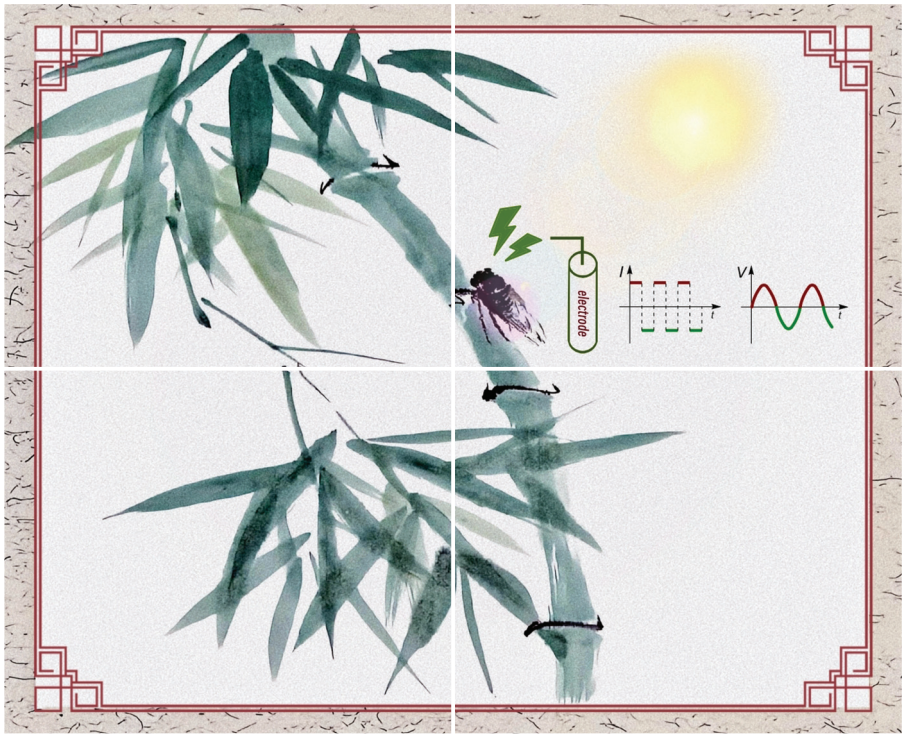

ORGANIC CHEMISTRY

FRONTIERS

CCS 中国化学会 CHINESE CHEMICAL SOCIETY
SIOC 1950
ROYAL SOCIETY OF CHEMISTRY
rsc.li/frontiers-organic

ORGANIC CHEMISTRY FRONTIERS

REVIEW

View Article Online
View Journal | View Issue

Cite this: *Org. Chem. Front.*, 2026, **13**, 1337

Metallic electrocatalyzed C–N bond formation: new catalytic modes and technologies

Zhao-Zhao Zhou [a,b]

Received 22nd October 2025,
Accepted 5th December 2025

DOI: 10.1039/d5qo01467k

rsc.li/frontiers-organic

The current state-of-the-art hot research topic of C–N bond formation is focused on versatile and mild transformations. Conventional transition metal-catalyzed methods are typically conducted using specific ligands, high temperatures and stoichiometric alkoxide bases or oxidants. In this regard, metallic electrocatalyzed protocols have emerged as elegant strategies with electronic oxidative or reductive agents. This synergistic catalytic system exhibits many potential advantages compared to direct electrolysis by overcoming the energy barrier and facilitating the rate-limiting steps in oxidative addition, transmetalation or reductive elimination. This review comprehensively highlights the recent developments in metallic electrocatalyzed C–N bond formation with new methodologies and technologies. Major emphasis is placed on key factors during methodology development as well as detailed mechanism verification and description. The synthetic applications and prospects are also provided in the field of metallic electrosynthesis.

1. Introduction

Nitrogen-containing molecules, including amines, anilines, amides, sulfonamides, sulfoximines, carbamates, benzylamines and imines, are one of the most important classes of organic compounds and these ubiquitous skeletons play crucial roles in a wide range of biological processes, pharmaceuticals and synthetic organic chemistry.[1] To date, more than 75% of the top 200 selling drugs and most pesticide molecules contain amine moieties, making C–N bond formation one of the most valuable and widespread transformations in organic synthesis.[2] Considering the significance of the carbon–nitrogen bond, tremendous progress had been made in this area, including C–N bond coupling reaction,[3] C–H amination,[4] alkene hydroamination[5] and N-centered radical-based transformations.[6] The extensive development of these methods has greatly expanded the applications of nitrogen-containing compounds.

1.1 Classical transition metal-catalyzed C–N cross-coupling and key factors

The past decades have witnessed a flourishing resurgence of C–N cross-coupling in both academia and industry and enduring efforts have been devoted to developing transition metal-catalyzed strategies (Scheme 1).[3] Copper-catalyzed Ullmann–Ma-type amination was originally proven to be a powerful strategy due to its extremely facile reductive elimination step from high-valent Cu(III) species.[7] However, relatively low rate and high energy barriers of Cu-haloarene oxidative addition often lead to the requirement for specialized ligands, high temperatures and weak C–X bonds such as aryl iodides and activated aryl bromides. Thus, Cu-catalyzed Chan–Lam amination coupling has been developed as an alternative pathway to bypass these typical challenges, despite the slow transmetalation with organoboronic acids.[8] It is worth noting that the disproportionation of Cu(II) species would generate Cu(I) and high-valent Cu(III) species to accelerate oxidative addition and reductive elimination, respectively, without an exogenous stoichiometric oxidant.[9]

Meanwhile, the reactivity of palladium catalysis is relatively moderate in the elementary steps of cross-coupling reactions, and constantly the evolving Pd-catalyzed Buchwald–Hartwig

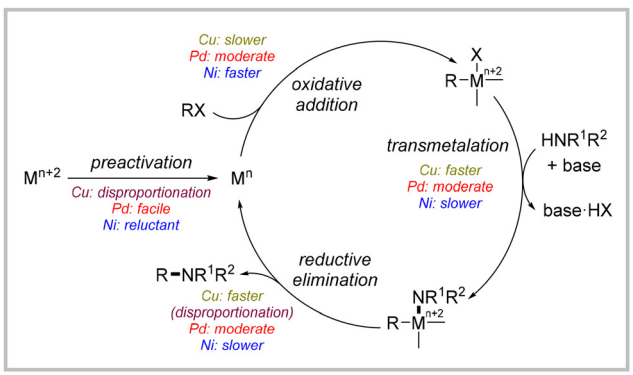

Scheme 1 Conventional transition metal-catalyzed C–N cross-coupling.

[a]*College of Chemistry and Food Science, Nanchang Normal University, Nanchang, 330000, P.R. China*
[b]*State Key Laboratory of Food Science and Technology, Nanchang University, Nanchang 330000, P.R. China. E-mail: zhouzz@lzu.edu.cn*

amination has demonstrated good efficiency.[10] The relatively high stability of the easily accessible low-valent active Pd(0) species often provides predictable and controllable catalytic properties through the typical Pd(0)/Pd(II) catalytic cycle. More importantly, the continuous development of the ligand library has made this reaction highly applicable.[11]

Furthermore, since Buchwald's pioneering work on Ni(0)-catalyzed amination in 1997,[12] earth-abundant nickel catalysts have been widely employed as low-cost alternatives to palladium catalysts among the group 10 metals and exhibited significant advantages in C–N cross-coupling reactions,[13] as follows: (1) more negative redox potential of low-valent Ni species results in higher reactivity in oxidative addition with less reactive electrophiles such as aryl chlorides and fluorides.[14] (2) Alkyl electrophiles could be well compatible due to inhibited β-hydrogen elimination with higher persistence of alkyl–Ni intermediates.[15] (3) Diverse and interconvertible oxidation states of nickel species provide tremendous potential in catalytic modes. (4) A radical pathway could be involved in catalytic system.[16] However, despite the aforementioned advancements, the developed thermodynamic nickel catalytic systems for C–N bond formation still suffer from the following limitations: (1) special strong reductants such as alkoxide bases or NHC (N-heterocyclic carbenes) ligands are essential to give low-valent Ni species.[17] (2) High catalyst loadings are often needed due to air-sensitive Ni(0) catalysts or instability of the Ni(I) species. (3) Inevitable high-temperature conditions should be used to bypass high energy barriers of unfavorable reductive elimination with Ni(II) species.

1.2 Early-stage modification of thermodynamic catalytic system

Generally, thermodynamic transition metal-catalyzed C–N cross-couplings require the adjustment of multiple parameters to overcome the drawbacks in different catalytic stages. Under harsh conditions, the effective conversion of some specific substrates still has not been well addressed, including aryl fluorides, alkyl halides and ammonia. This limited application scope should be attributed to the lack of understanding of the catalytic system, such as its rate-determining step (RDS), valence state/redox potential of transition metal species/intermediates, and even dynamic equilibrium process.[10d,18]

Current cutting-edge and hot research topics focused on elegant conversions under mild catalytic conditions and more advanced reaction strategies have gradually been developed to make this field greener. Representative examples have been presented from the perspective of elementary reactions in catalytic cycles, as follows: (1) preactivation of low-valent transition metal: air-insensitive Ni(0) catalysts were successfully developed by several groups[19] and the [(NHC)Ni(allyl)Cl] precatalyst led to the first amination reaction at room temperature by the Nicasio group in 2010.[20] (2) Oxidative addition: oxalic diamides[7a,21] and anionic N^1,N^2-diarylbenzene-1,2-diamine ligands[22] both promoted copper-catalyzed Ullmann–Ma-type C–N coupling at room temperature. (3) Transmetalation or ligand exchange: the enhanced Lewis acidity of palladium species by JackiePhos facilitated the ligand exchange of weak nucleophilic amides.[23] (4) Reductive elimination: oxidation-induced reductive elimination with 1,2-dichloroisobutane (DCIB) smoothly achieved accelerated nickel-catalyzed Kumada coupling.[24]

1.3 Advantages and advances of metallic electrocatalyzed C–N bonds formation

These advanced reaction strategies have expanded the reactivity to a certain extent; however, the limited parameter control has failed to trigger revolutionary innovations in terms of reaction conditions of C–N bond formation, such as redox neutral atmosphere, ligand free, no base and ambient reaction temperature. The emergence of photocatalysis has brought about several new opportunities and the capacity of photocatalysts as both strong single-electron oxidants and reductants has enabled the simultaneous adjustment of multiple parameters in one catalytic cycle.[25] For example, in the pioneering photo-induced C–N cross-coupling reaction with nickel catalysis, Buchwald, MacMillan and co-workers employed an iridium photocatalyst to achieve the preactivation of Ni(0) species and the thermodynamically favored reductive elimination of Ni(III) intermediates in the same catalytic cycle under extremely mild conditions.[26] Subsequently, bulky σ-donating ligands, direct photoexcited Ni(II) intermediates and EnT (energy transfer) process to Ni(II) were also innovatively developed to facilitate the reductive elimination stage.[27] Importantly, the superiority of mild conditions not only enhanced the reaction efficiency and substrate compatibility, but also provided the potential possibility for asymmetric coupling.[28]

As an alternative to electron transfer, organic electrochemistry represents the most direct means for mild transformation and its adjustable current or voltage could avoid the screening of photosensitizers with specific redox potential.[29] Direct metal-free electrochemical aminations were typically developed,[30] and further remarkable advances in the field of metallic electrocatalyzed C–N bond formation have been made since 2017.[31] Compared to photocatalysis, electrochemical transition metal-catalyzed C–N cross-coupling exhibits more advantages in terms of flexible reaction control, including: (1) paired electrolysis simultaneously promoted reduction elimination and oxidation addition with the combination of anodic oxidation and cathodic reduction and this redox-neutral reaction unleashed the catalytic potential with maximized atom and energy efficiencies. (2) Individual oxidation or reduction in half-reactions at anode or cathode could selectively facilitate the RDS in elementary reactions, in which electrons transferred to the electrodes could be interpreted as oxidizing or reducing agents. (3) Mediator-enabled electrocatalysis employing an organo-mediator facilitates electrochemical reactions *via* outer-sphere electron transfer between active mediators and substrates. The selection of the mediator could adjust the redox potential to lower the reaction energy barrier and avoid side reactions (Scheme 2A).[32] (4) An alternating current (AC) enables a pair of redox processes to occur on the same electrode, avoiding the transfer of high-active reaction intermedi-

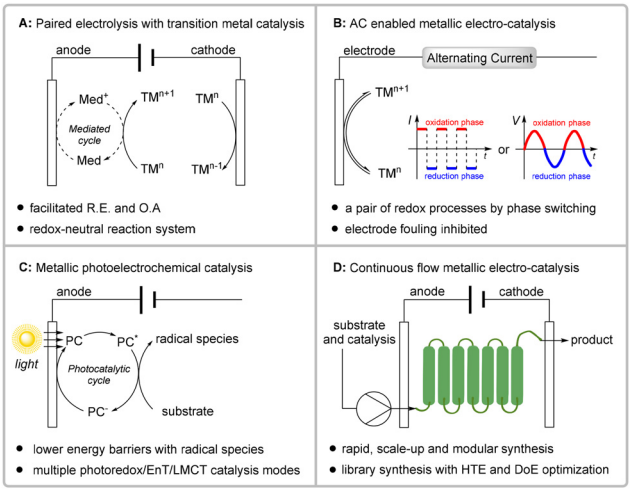

Scheme 2 New metallic electrocatalytic technologies for the C–N bond formation.

ates between electrodes and facilitating the conversion of short-lived species. Electrode fouling caused by a plated zero-valent metal catalyst could also be inhibited (Scheme 2B).[33] (5) The introduction of photochemistry in the metallic electrocatalytic process further lowers the energy barriers of ligand exchange through radical species, and multiple photoredox, EnT and LMCT (ligand-to-metal charge transfer) catalysis modes could be integrated (Scheme 2C). (6) Continuous flow chemistry with metallic electrocatalysis reveals more advantages than conventional batch reactions owing to its higher reproducibility as well as rapid, scale-up, modular and customizable synthesis. Meanwhile, library synthesis with HTE (high throughput experiment) and DoE (Design of Experiments) could simultaneously screen multiple parameters to accelerate reaction optimization (Scheme 2D).

Besides these new technologies adopted in a novel manner, a variety of new electrocatalytic methodologies have emerged to establish reliable C–N bond formation, including metallic electroreductive hydrogenative and cross-electrophile couplings, electrooxidative cross-dehydrogenative, Chan–Lam and carbonylative couplings, C–H amination and C–H/N–H annulation, and photoelectrooxidative decarboxylative couplings. Furthermore, significant breakthroughs in enantioselective metallic electrocatalyzed C–N couplings have also been efficiently achieved.

1.4 Scope of this review

Over the past two decades, a variety of review articles summarizing the impressive advances made in the field of electrochemical C–N bond formation have been published. The pioneering reviews include those by Yoshida, Baran, Waldvogel, Moeller, Little and Lin.[34] Subsequently, reviews detailing either electrochemical C–H amination or transition metal-free oxidative cross-coupling processes were summarized by Kärkäs, Lei, Roy, Qiu and Zhang.[35] From the perspective of reaction mechanism, the progress on electrochemically generated nitrogen-centered radicals was further summarized by Xia and Xu.[36] In terms of synthesis, the electrochemical construction of nitrogen-based heterocycles was reviewed by Xu, Zhang, Voskressensky and Huang.[37] Meanwhile, advanced urea electrosynthesis in the cutting-edge field of CO_2 conversion was gradually reviewed by Hou, Zhu and Wang.[38] Photoelectrochemical strategies, as milder and greener pathways, were also contemporaneously summarized by Lambert and Shi.[39]

Despite the aforementioned results, reviews on metallic electrocatalyzed C–N bond formation are rather scattered and mainly limited to C–H functionalization summarized by Ackermann, Minteer, Roy and Xu.[40] Considering the advantages brought by unique synergistic catalysis, such as milder reaction conditions and remarkable extension of the substrate scope, metallic electrocatalyzed strategies had witnessed explosive growth in the past five years, simultaneously accompanied by a wide variety of reaction types and techniques. Therefore, it is extremely essential to summarize the cutting-edge reactions and clarify the overall framework in this field.

In this review, an overview of new metallic electrocatalyzed reaction systems and technologies for carrying out C–N bond formation is macroscopically presented. The specific content of this article includes key factors during condition optimization and detailed mechanism verification and description. Taking into account the complexity of the different reaction types, the reaction classification in this review is organized based on the substrate and reaction types and the logical development sequence of the same reaction types is integrated beginning from early pioneering works, but not strictly in chronological order. The aim of this review is to encourage researchers to accurately grasp the characteristics of metallic electrocatalytic synthesis to develop more efficient, milder and greener reaction conditions over conventional C–N coupling reactions. A general synthetic toolbox is expected to be established and applied modularly to other coupling reactions.

2. Metallic electrocatalyzed cross-coupling for C–N bond formation

Direct C–N cross-couplings represent one of the most attractive and challenging topics in synthetic chemistry owing to their widespread application in natural and synthetic organic molecules. Thus, this section mainly summarizes the recent advances in metallic electrocatalyzed C–N bond formation between *C*-electrophilic and *N*-nucleophilic substrates for primary/secondary amination as well as sulfoximination.

2.1 Metallic electrocatalyzed cross-coupling for secondary amination

In 2017, Baran and co-workers reported a pioneering electrochemical Ni-catalyzed amination (e-amination) between (hetero)aryl halides/triflates and aliphatic amines (Scheme 3).[31] During the optimization of the conditions, a commercial RVC (reticulated vitreous carbon) anode and Ni-

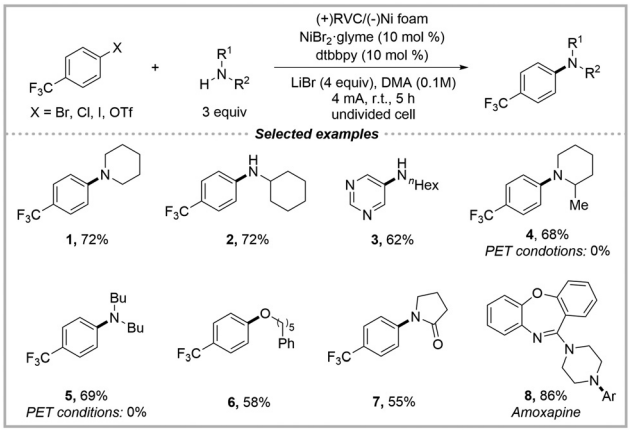

Scheme 3 Pioneering nickel-catalyzed electrochemical amination with aryl bromides.

foam cathode in concert with Ni catalysis provided the highest isolated yield of 72% of product **1**. Importantly, the inhibited anodic oxidation with sacrificial zinc rather than RVC (reticulated vitreous carbon) anode resulted in almost reductive homocoupling biaryl byproducts with only 7% e-amination products, which explained the necessity of high-valent nickel species favored in reductive elimination. Furthermore, the addition of an external base was unnecessary and the employment of oxygen showed no significant impact on this electrochemical transformation, with 42% yield under air. The final optimized conditions were confirmed to be LiBr electrolyte (4 equiv.) and a constant current of 4.0 mA in an undivided cell with DMA solvent (dimethylacetamide) at room temperature for five hours.

Compared to thermodynamically palladium-, copper-, nickel-catalyzed or photochemical conditions, this groundbreaking electrocatalysis could afford comparable yields at lower temperature without external base. (Hetero)aryl bromides/chlorides/iodides/triflates, especially for electron-withdrawing aryl substrates, as well as primary and secondary cyclic amines were satisfactorily compatible (**1**–**3**), though electron-donating aryl halide coupling partners were largely limited. Specific substrates, such as 2-methyl-piperidine **4** and dibutylamine **5** partners, further revealed the advantages of electrocatalysis in the PET (photoinduced electron transfer) process with higher yields, as reported by Buchwald, MacMillan and co-workers.[26] Meanwhile, other nucleophilic primary alcohol **6**, amide **7** and drug **8** substrates were also suitable for this versatile system. This electrochemical Ni-catalyzed reaction represented a rare and novel amination example through paired electrolysis, where both the anode and cathode contributed to the formation of Ni species with different oxidation states. More importantly, the drawbacks of Ni-catalyzed amination including use of air-sensitive Ni(0) catalysts, high temperatures and strong alkoxide bases were significantly resolved.

Later, in 2019, Neurock, Minteer, Baran and co-workers completely uncovered the key mechanistic characteristics of Ni-catalyzed e-aminations through a series of spectroscopy, electrochemical, computational, kinetic and empirical experiments (Scheme 4).[41] In their mechanistic studies, UV-Vis (ultraviolet-visible) spectroscopy firstly indicated that the ligand/Ni(II) ratio determined the predominant species of the mixed dynamic Ni(II) ligation states and a substantial portion of Ni(II) remained unligated with only 1.0 equivalent ligand. Cathodic overreduction of the unligated Ni(II) species would result in black excessive plated Ni(0), indicating that a higher ligand loading was essential for a high reaction efficiency. Next, DFT (density functional theory) calculations revealed competitive binding within ligand/DMF/amine nucleophiles to form dynamic Ni(II) complexes and the observed redox potentials in subsequent SWV (square wave voltammetry) experiments showed that the predominantly formed Ni(I) species by cathodic reduction were most likely to initiate oxidative addition. CV (cyclic voltammogram) experiments further revealed the rapid oxidative addition of LNi(I)Br and an exothermic process.

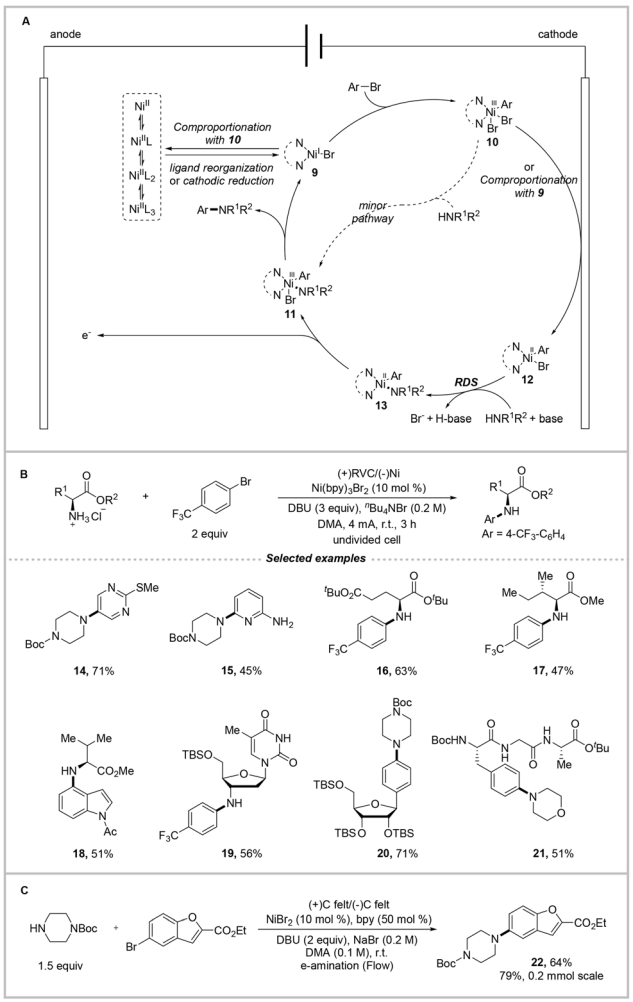

Scheme 4 Mechanism studies and enlarged applications of the electrochemical amination.

Next, DFT calculations indicated that the generated Ar–Ni(III)L–Br_2 could be readily reduced to Ar–Ni(II)L–Br species and the subsequent amine coordination of Ar–Ni(II)L–Br was exothermic. A high energy barrier should be required for the rate-determining deprotonation of the Ar–Ni(II)L–amino species and the addition of an exogenous base would be energetically favorable. Meanwhile, the anodic oxidized Ar–Ni(III) Br–amino species would drastically decrease the energy barrier compared to the direct reductive elimination of Ar–Ni(II)L–amino. Finally, continuous electrolysis was necessary to achieve appreciable yields as only 5% product yield was achieved after 15 min electrolysis during 3 h stirring.

A persuasive electrocatalytic mechanism was proposed (Scheme 4A). This catalytic cycle began with the reduction of the dynamic ligation-state Ni^{II} precatalyst at the cathode, and then generated Ni^{I} species **9** underwent rapid oxidative addition with aryl halide to give Ni^{III} species **10**. Next, further reduction of **10** at the cathode and subsequent amine coordination/deprotonation resulted in intermediate **13**, followed by the formation of high-valent Ni^{III} complex **11** with electrooxidation at the anode. Finally, a complete catalytic system was achieved with the regeneration of Ni^{I} species **9** and arylamine product after reductive elimination. It is worth noting that minor pathway with a self-sustaining Ni(I)/Ni(III) cycle exhibited apparent inefficiency, which is probably due to the generated Ni(II) intermediate from the comproportionation of **9** and **10** failing to promote reductive elimination under the base-free and room temperature conditions. From this perspective, the developed nickel-catalyzed electrochemical system with continuous electrolysis could constantly promote the generation of Ni(III) and Ni(I) species, which further simultaneously accelerated reduction elimination and oxidation addition, respectively.

Based on the above-mentioned mechanistic discussion, the revised electrochemical C–N bond formation conditions had been optimized with a higher ligand/Ni(II) ratio and external base (Scheme 4B). The e-amination 2.0 conditions successfully expanded the substrate scope to heteroaryl **14–15**, amino acid ester **16–18**, nucleoside **19–20**, and oligopeptide **21** coupling partners. The increased reaction efficiency was attributed to the following two key factors: (1) a higher ligand loading (ligand/Ni^{II} ratio from 2 : 1 to 3 : 1) resulted in a significantly increased yield with the restrained deposition of nickel black on the cathode, which was also conducive to the favorable process of cathodic reduction of Ni^{II} to Ni^{I} species, which had been preliminarily verified by the mechanism research. (2) The addition of an exogenous base such as DBU (1,8-diazabicyclo [5.4.0]undec-7-ene) would facilitate displacement of the bromide on intermediate **12** during amine nucleophilic attack to Ni^{II} species in the rate-determining deprotonation step. Furthermore, an encouraging 100 g scaled-up reaction was also successfully carried out by employing a flow system with only a slight decrease in the yield of **22** to 64% (Scheme 4C).

The aforementioned results represent the well-established conventional strategies for metallic electro-catalyzed C–N bond formation. Although the mechanistic studies and description are relatively complete, specific unclear fields still exist. In 2023, Ess, Liu and co-workers conducted comprehensive research on the interaction of Ni-amino intermediates in the e-amination 2.0 reaction (Scheme 5).[42] Detailed and in-depth experimental research had made sufficient supplements and further improvements to the mechanism proposed by Baran.

Based on UV-Vis spectroscopy, CV experiments and DFT calculations, the crucial transformation details were further confirmed, as follows: (1) coordination of the amine to the Ni(II) catalyst occurred before the cathodic reduction and oxidative addition steps. (2) A stable Ar–Ni(II)–amino intermediate was produced from the cathodic half reaction, which was a critical step in controlling the selectivity between cross-coupling and undesired homo-coupling reaction pathways. (3) DBU additive shifted the aryl bromide oxidative addition mechanism from an Ni(I)-based pathway to an Ni(0)-based pathway, as DBU could displace Br^- to coordinate to the Ni(II) center. (4) The redox-active bromide in the supporting electrolyte acted as a redox mediator to promote the oxidation of the stable Ar–Ni(II)–amino intermediate to an Ar–Ni(III)–amino intermediate.

Two electrocatalytic cycles were, proposed as follows: **Path A** (without DBU): Coordination of Ni(II) species **23** with amine formed Ni(II)–amine **24**, which was then reduced to Ni(I)–amine species **25** through cathodic single-electron reduction. Then, **25** underwent oxidative addition with aryl halide to produce high-valent Ni(III) species **26**, accompanied by subsequent comproportionation with Ni(I) species to aryl–Ni(II)–amine **27**. **Path B** (with DBU): Coordination of Ni(II) species **23** with amine and DBU formed DBU–Ni(II)–amine **31**, allowing further cathodic two-electron reduction to Ni(0) species **32**. Low-valent **32** underwent oxidative addition to produce Ni(II) species **33**, followed by amine coordination to give aryl–Ni(II)–amine **27**. Furthermore, subsequent deprotonation with amine or base yielded the stable Ar–Ni(II)–amino intermediate **28**, which transformed into high-valent aryl–Ni(III)–amine inter-

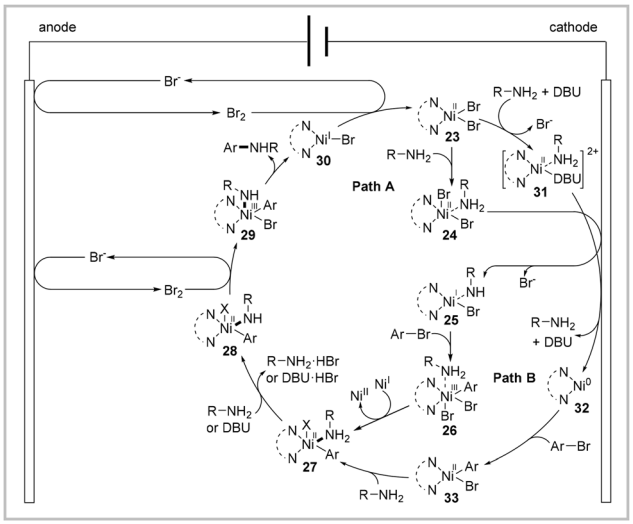

Scheme 5 Mechanism studies of the nickel species in the electrochemical amination.

mediate **29** through Br-mediated anodic oxidation.[32] Finally, reductive elimination of **29** produced the final amination product and Ni(I) species **30** was released, followed by the regeneration of **23** after Br-mediated anodic oxidation to finish the catalytic cycle.

Based on the above-mentioned achievements, electrochemically driven, transition metal-catalyzed C–N bond formation reactions have achieved rapid development. To expand the substrate scope of the coupling reactions, in 2021, Yue, Rueping and co-workers developed a more general e-amination protocol with a series of weak *N*-nucleophiles (Scheme 6).[43] During the optimization of the conditions, the anode was re-optimized to graphite, with the nickel foam cathode remaining unchanged compared to Baran's conditions[41] and 72% yield of the desired product **34** was smoothly obtained. Differently, DBU resulted in no reaction owing to the increased overall activation energy due to its coordination to the Ni intermediate, while Et_3N (triethylamine) promoted the transformation well.

Pharmaceutical-related compounds **38–40** and electron-rich aryl halides **35–37** as well as electron-deficient anilines **35–36**, sulfonamides **38–40**, sulfoximines **41**, carbamates **42**, benzylamines **43** and imines **45–46** were all successfully compatible, demonstrating the effectiveness. For a specific *N*-nucleophile, fine-tuning the electrodes and base was necessary to accommodate the electrocatalytic system (**41–46**). Uniquely, the sulfonamidation reaction proceeded smoothly using an alternating current (AC) and paired electrolysis of the e-amination process was proven by no observed product **44** with sulfonamide in a divided cell (Scheme 6C). Furthermore, either imine product **45** or amine product **46** was selectively obtained by simply adjusting the type of base (Scheme 6D). Mechanism studies with DFT and current efficiency calculations revealed that the generation of Ni(II) species from the comproportionation of unstable Ni(I) and Ni(III) species without electricity caused the reaction to proceed with low efficiency, while the role of electricity was to suppress the comproportionation process and facilitate reductive elimination from the Ni(III) intermediate.

Considering that continuous electrolysis was necessary for the redox-neutral electrochemical C–N formation, namely rate-limiting electroreduction to Ni(I) in oxidative addition and electrooxidation to Ni(III) species in reductive elimination, the alternating current (AC) mode also authentically fitted the idea of a catalytic cycle assisted by a pair of redox processes. In 2021, Semenov and co-workers developed an AC-assisted Ni-catalyzed amination of aryl bromides in a divided cell, in which electrode fouling caused by plated Ni(0) could be prevented (Scheme 7).[44] An appropriate voltage should be applied to simultaneously perform the desired oxidation and reduction of nickel species on the two electrodes. The frequency of the applied voltage was another key parameter, with the highest yield of 87% achieved around 2.0 Hz, while higher frequencies destroyed the reversible Ni(II)/Ni(I) and Ni(II)/Ni(0) oxidation/

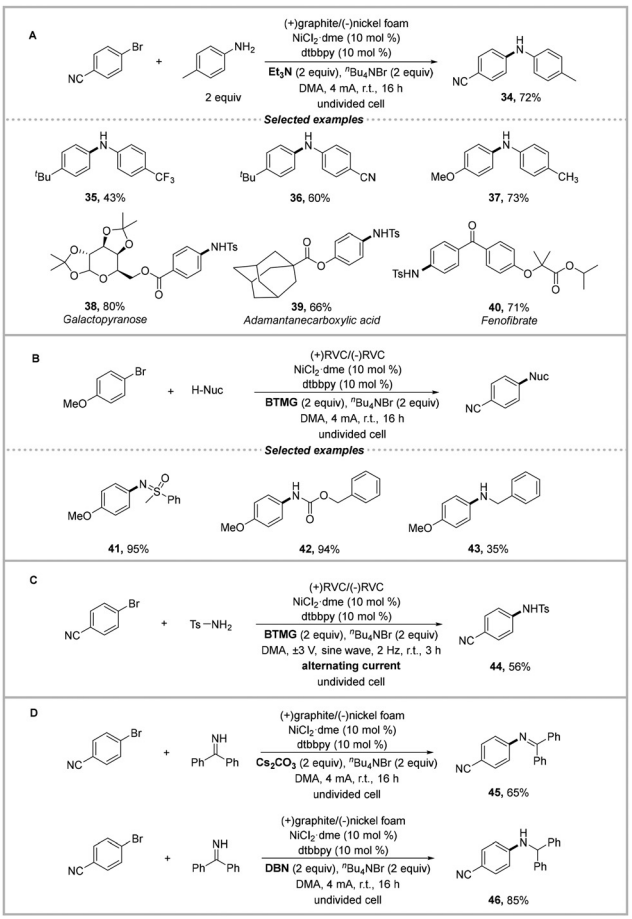

Scheme 6 Nickel-catalyzed electrochemical amination with weak *N*-nucleophiles.

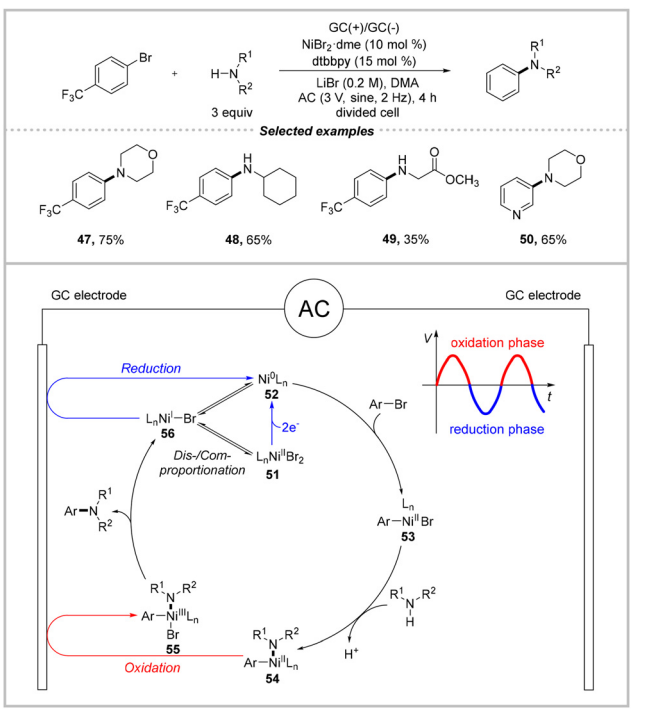

Scheme 7 AC-assisted nickel-catalyzed electrochemical amination.

reduction cycles and decreased frequency as well as the use of DC led to diminished yields and more byproducts.

After careful studies, a persuasive AC-assisted mechanism was presented.[33] This catalytic cycle began with the reduction of Ni(II) precatalyst **51** to Ni(0) species **52** at the electrode, which then underwent oxidative addition to Ni(II) species **53**. Next, ligand exchange to **54** occurred during the low-voltage phase with no valence state change. Finally, the oxidation phase of the AC cycle led to high-valent Ni(III) species **55**, which furnished the desired coupling after reductive elimination. The released Ni(I) **56** would be reduced to Ni(0) **52** either through direct electrode reduction or disproportionation, along with subsequent reduction of Ni(II) to Ni(0). Meanwhile, current-assisted catalytic cycles involving oxidative addition to Ni(I) species **56** proposed by Phil. S. Baran may coexist.[31,41] Uniquely, the AC-assisted cycle, especially in a divided cell with single electrode, could facilitate the conversion of short-living intermediates and avoid the transfer of reactive intermediates between electrodes. The adjustable frequency and wave form of AC also represented easily tunable parameters to control the selectivity of the reactions.

Although the developed electrochemical system employing a direct or alternating current exhibited excellent reaction efficiency and adaptability, the addition of transition metal catalysts, ligands and bases made the reaction system more complex. Therefore, developing a reaction system where transition metal catalysts are directly released from the electrodes is of high novelty. In 2021, Sengmany, Léonel and co-workers adopted a convenient sacrificial anode process for the amination of (hetero)aryl halides (Scheme 8).[45] The nickel species generated from the sacrificial anode could catalyze the electrochemical C–N cross-coupling reaction under constant current electrolysis (CCE) in an undivided cell at room temperature without additional base or ligand.

During the optimization of the conditions, in the presence of 5 mol% of Ni(bpy)Br_2 precatalyst, replacing the Fe/Ni alloy anode with an Ni sacrificial anode observably increased the yield of product **56** from <10% to 60% in DMF (*N*,*N*-dimethylformamide) with inhibited hydrodebromination byproducts. Surprisingly, without the nickel precatalyst, a sufficient efficiency could also be maintained, even with a higher yield of 74%. No reaction occurred without electricity and the current intensity was the key factor in the reaction, as a higher current intensity would produce more aryl dimer byproducts. Finally, the mixed solvent MeCN : DMF (8 : 2) provided the highest yield of 79% for **56** with freshly *in situ* generated nickel species. Electron-withdrawing aryl bromides and secondary cyclic amines **57–59** were well tolerated, and modified conditions with higher amine loading (10 equiv.) and lower current intensity (50 mA) also gave moderate yields of heteroaryl bromide **60**.

In mechanistic studies, the reaction in a divided cell with 10 mol% $NiCl_2$ did not generate the product, which reflected the necessity of anodic oxidation for high-valent nickel species before reductive elimination. A preliminary sacrificial anode process electrochemical mechanism was proposed. Initially, Ni

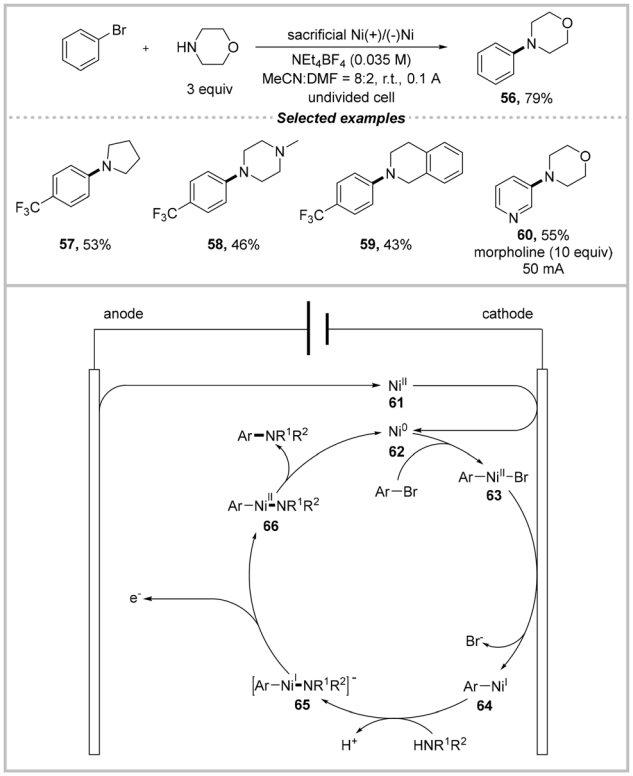

Scheme 8 Electrogenerated nickel-catalyzed amination with a sacrificial anode process.

(II) species **61** generated from the sacrificial nickel anode was reduced at the cathode to Ni(0) **62**, which then underwent oxidative addition to Ni(II) species **63**. Next, single-electron cathodic reduction and subsequent ligand exchange of **63** with amine led to Ar–Ni(I)–NRR′ intermediate **65**. Finally, anodic oxidized Ni(II) species **66** gave rise to the amination product and the release of Ni(0) after reductive elimination. Nevertheless, the alternative catalytic cycle through the Ni(I)/Ni(III) system could not be completely ruled out.[29]

In the above-mentioned early-stage sacrificial anode process for C–N coupling, a stoichiometric amount of freshly electrogenerated nickel species could not be avoided under a constant current, which resulted in electrode over-consumption and restricted the substrate scope. To address this problem, later in 2023, Sengmany and co-workers further reported a stepwise sacrificial anode e-amination process with an *in situ*-generated catalytic amount of nickel salts, which was achieved by replacing the sacrificial nickel anode with a platinum grid anode after 16 min preliminary reaction, which generated 10 mol% Ni(II) species (Scheme 9).[46]

During the conditional optimization, extra 10% ligand 2,2-bipyridine (bpy) accompanied with a catalytic amount of Ni(II) species smoothly gave a higher isolated yield of 91% of product **67** in DMF. The control experiment indicated that a constant current, sacrificial nickel anode and ligand were crucial to the for the transformation. Importantly, to reduce the amine amount (1.5 equiv.), the addition of Et_3N was sig-

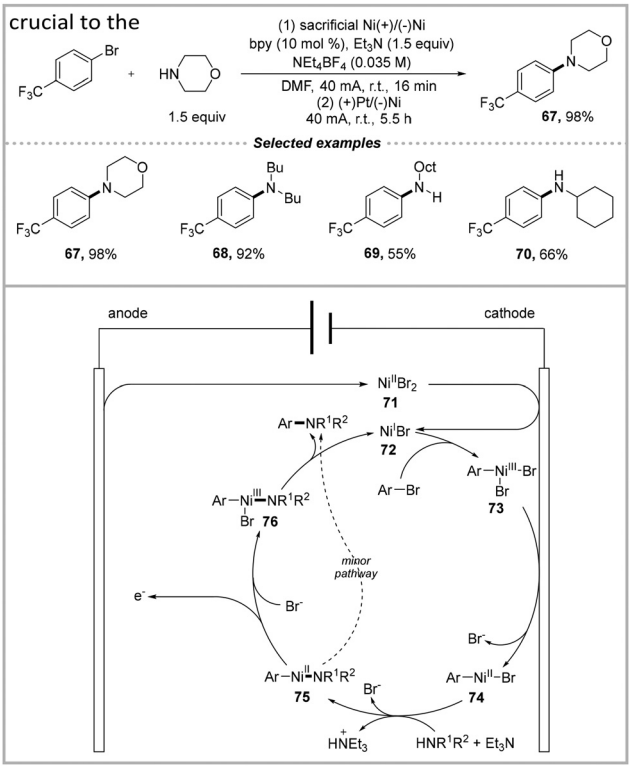

Scheme 9 Stepwise sacrificial anode electrochemical amination process.

nificantly effective, with 98% optimized yield of product **67**. Compared with the sacrificial anode process developed before, the compatible range of substrates had been expanded to secondary acyclic amines **68** and primary amines **69–70**.

In mechanistic studies, CV experiments confirmed the oxidative addition of Ni(bpy)Br_2 species to aryl bromide around a potential of −1.2 V (*vs.* Ag/AgCl). Subsequent control experiments further indicated the essential role of current in maintaining the process for the electrogeneration of nickel. Meanwhile, the results with trace products and more aryl dimer byproducts observed in the divided cell also revealed the homocoupling of aryl bromides through the cathodic reduction of Ar–Ni(II)L–Br and oxidation addition of generated Ar–Ni(I)L to ArBr. A feasible mechanism distinguished from the stoichiometric sacrificial anode process was proposed. Initially, electrogenerated Ni(II)Br_2 **71** was released from the sacrificial anode, which then gave Ni(I)–Br species **72** through cathodic reduction or comproportionation with Ni(0). Next, Ar–Ni(III)L–Br_2 species **73**, produced from the oxidative addition of **72** with aryl bromide, was reduced at the cathode to the more stable Ar–Ni(II)–Br species **74**. Subsequent ligand exchange with amine and anodic oxidation gave high-valent Ar–Ni(III)Br–amino species **76**. Finally, the amination product and regenerated Ni(I) species **72** was obtained after reductive elimination to finish the catalytic cycle.

Although the sacrificial anode process avoided the direct employment of transition metal catalysts, the inherent electrode consumption made it difficult to precisely control the reaction, which also exhibited certain limitations from the perspective of sustainable reactions. Meanwhile, N-centered radicals (NCRs) have been extensively employed to construct C–N bonds because high reactivity and mild conditions are often associated with a radical-mediated catalytic cycle.[47] In the initial stage, transition metal-catalyzed C–N coupling reactions with NCRs mainly relied on stoichiometric chemical oxidants, while new reaction technologies with photoredox and electrochemical catalysis made this process greener and more efficient.[48] Although electrocatalytic C–H amination with NCR species was developed,[49] the direct anodic oxidation of amines remained challenging,[50] especially with metallic electrocatalysis.

To overcome the high energy barrier and bypass the sluggish rate-determining step of *N*-attack and deprotonation in conventional metallic electrochemical amination methods, a new and elegant strategy employing amine radicals was presented. In 2024, Jiang, Li, Wu, Tang and co-workers reported the first metallic photoelectrochemical (PEC) aryl amination with a three-electrode configuration (Scheme 10).[51] Photoanodic oxidation together with a HAT (hydrogen atom transfer) process generated an amine radical, which facilitated subsequent ligand exchange and reduction elimination under an ultra-low potential of −0.4 V (*vs.* Ag/$AgNO_3$).

During the optimization of the conditions, a $BiVO_4$ photoanode, Ni foam cathode and Ag/$AgNO_3$ reference electrode were employed. Meanwhile, the HAT reagent DABCO (1,4-diaza [2.2.2]bicyclooctane) promoted charge transfer between the photoanode and amines in the photo-induced process, resulting in 82% yield and 89% selectivity for product **77**. The trace

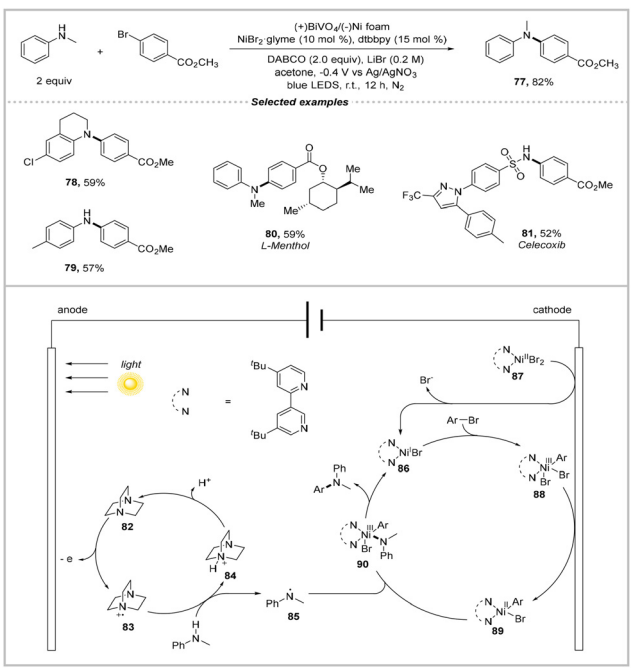

Scheme 10 Nickel-catalyzed photoelectrochemical amination.

product with no nickel precatalyst, ligand, DABCO or electricity (one parameter at a time) revealed their crucial roles in this reaction. Importantly, no product was detected in the dark until the oxidation potential was increased to +1.5 V (*vs.* Ag/$AgNO_3$), and the decrease in the yield to 16% and product selectivity to 62% demonstrated the superiority of the PEC system over conventional electrocatalysis. Primary/secondary amines **78–80**, sulfonamide **81** as well as drug frameworks **80–81** were widely tolerated.

In mechanistic studies, CV experiments indicated that preferential anodic oxidation occurred with DABCO (with lower oxidation potential of +0.41 V *vs.* Ag/$AgNO_3$) before *N*-methyl aniline (+0.53 V *vs.* Ag/$AgNO_3$). Moreover, interactions between oxidized DABCO and amines, as well as Ni(I)-participated oxidation addition had also been verified. In the control experiment, the trace product yield in the divided cell and amine dimers in the absence of nickel catalyst further demonstrated the essential roles of anodic oxidation and nickel catalysis in this PEC C–N cross-coupling, respectively. Finally, the much lower energy barrier of radical attack to Ni(II) species in the DFT calculations provided a more thermodynamically favourable pathway for high-valent Ni(III) species from a theoretical perspective.

A plausible reaction mechanism of photoelectrochemical C–N coupling was proposed. Under irradiation, excited $BiVO_4$ photoanodic single-electron oxidation of DABCO **82** produced DABCO cation radical **83**, which next induced a HAT process with aniline to protonated DABCO **84** and aniline radical **85**. Simultaneously, Ni(I) intermediate **86**, generated from the cathodic reduction of Ni(II) precatalyst **87**, underwent oxidative addition of aryl bromide to form Ni(III) species **88**. After cathodic reduction again, Ni(II) intermediate **89** was produced and captured the photoanode-generated amine radical to form Ni(III) intermediate **90**. Finally, a reductive elimination process occurred by releasing the amination product and Ni(I) species **86** to complete the catalytic cycle. It is worth mentioning that the ultra-low potential could prevent the overoxidation of the amine products in conventional electrochemical process, which further provided synthetic potential for asymmetric catalysis.

Considering the problems associated with conventional batch devices, such as miniaturization issues, limited number of vials per plate and glovebox required for inert atmosphere, continuous-flow reactors have been proven to be an excellent alternative, though suffering from high material consumption, potential long-run issues and additional optimization parameters. Therefore, the development and optimization of continuous flow reactions would facilitate the industrial application of C–N coupling. In 2024, Eggenweiler, Kappe, Laudadio and co-workers reported an automated electrochemical flow platform for C–N cross-coupling and drug molecular libraries (Table 1).[52] This developed automated electrochemical flow platform had been efficiently built with the

Table 1 Nickel-catalyzed electrochemical amination with flow platform and library synthesis

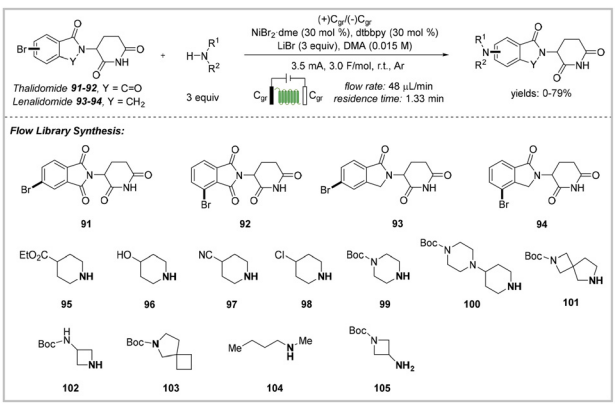

Partners and yields (%)	**91**	**92**	**93**	**94**
95	72	62	27	73
96	73	51	0	25
97	77	68	43	82
98	75	54	40	73
99	79	65	47	74
100	56	34	26	42
101	32	11	8	**6**
102	37	31	18	16
103	3	4	0	7
104	44	12	33	44
105	19	16	18	12

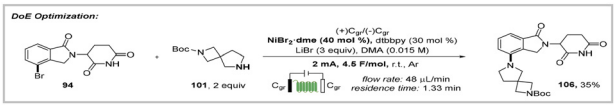

advantages of low material consumption, reduced reaction time, closed inert system, improved reaction control with script, equipment modularity and flexibility amenability to HTE (high throughput experiment).

At the initial stage of reaction condition optimization, drug molecule precursors thalidomide **91–92** and lenalidomide **93–94** bromides as well as eleven amines **95–105** were employed under Baran's electrochemical Ni-catalyzed amination conditions[29] by transferring the reaction protocol to single-pass flow operation. Inspiringly, a better performance was observed in flow library synthesis compared to the batch system within 8 h of continuous operation under inert conditions without a glovebox.

Meanwhile, the difficult-to-introduce spirocyclic amines **101** in medicinal chemistry with poor yield of 6% were further optimized in the automated platform by screening multiple parameters simultaneously through a DoE experiment (Design of Experiments). The results revealed that the catalyst loading and current were the crucial factors and an ideal 35% yield of product **106** was finally obtained with a high nickel catalyst loading (40 mol%) and low current (2.0 mA), which was 6-times higher than the result of the initial library protocol. The efficient and modular nature of the automated electrochemical flow platform would accelerate drug R&D and push organic electrochemistry HTE to the forefront.

In 2025, Carvalho, Jones and co-workers described a continuous flow platform for the metallic electrocatalytic library synthesis of C–N and C–O coupling (Scheme 11).[53] The flow cell significantly increased the product yield and selectivity compared to the batch reactor. During the optimization of the conditions, the conditions reported by Semenov (conditions **A**)[44] and Baran (conditions **B**)[31,41] under a direct current (DC) with an Analytical Sales 24-well HTE-chem device resulted in poor yields of **107**, which was attributed to the dibrominated, aryl dimeric byproducts and inconsistent results with multiple reaction parameters. Switching to a Vapourtec Ion electrochemical flow reactor with conditions **C**, and thus minimizing the electrode spacing, which was favorable for the required rate-limiting catalyst diffusion for turnover between the electrodes in the paired-electrolysis, accelerated the mass transfer with 38% yield after interelectrode gap screening (membrane thickness). However, these DC-assisted conditions involving passivation of the GC (glassy carbon) anode prevented a further yield improvement, while the potentiostatic alternating polarity from the alternating current (AC) with 3.0 V and 1.0 Hz SqW (square waveform) provided good reproducibly over 24 reactions and improved the product selectivity, though in 32% LC (liquid chromatography) yield (conditions **D**). This represented the first application of AC-assisted flow electrolysis in C–N and C–O coupling.

Subsequent HTE screening one parameter at a time gave an increased yield of 40% with the optimized Ni source ($NiCl_2$·glyme), ligand (di-OMebpy, 4,4′-dimethoxy-2,2′-bipyridine), base (quinuclidine), electrodes (GC/GC), additive (LiBr) and waveform (SqW) in air. Furthermore, DoE optimization with seven continuous factors indicated a major non-linear

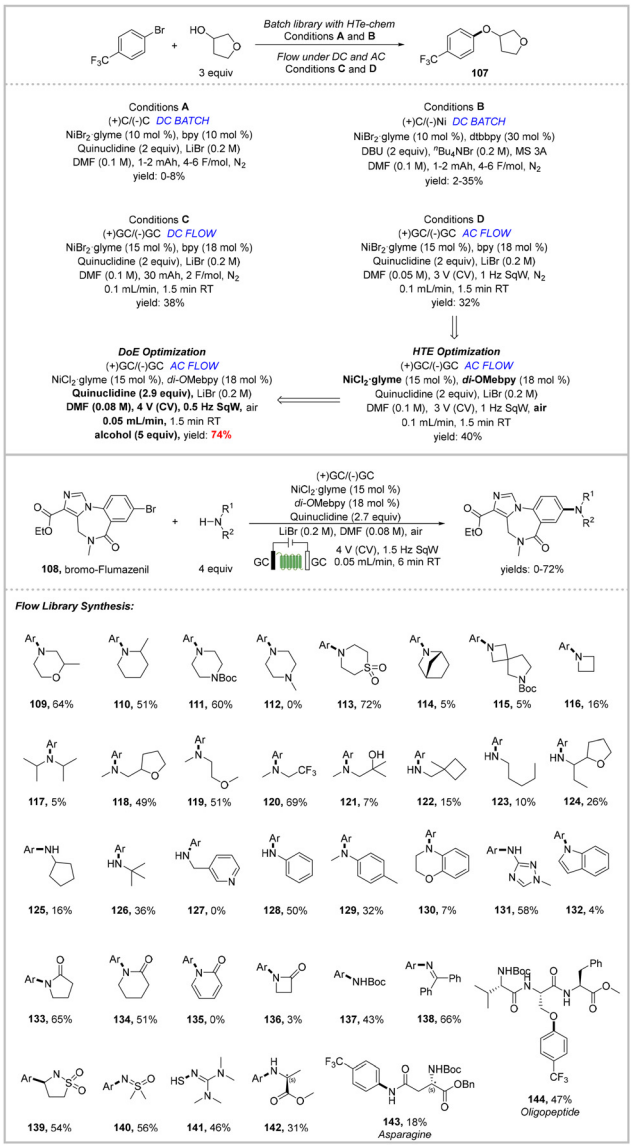

Scheme 11 Nickel-catalyzed electrochemical amination with the AC-flow platform and library synthesis.

influence from the substrate concentration, alcohol and voltage, namely attainment of the highest yield should depend on the simultaneous optimization of these three factors. Finally, a 74% LC yield of product **107** was obtained with alcohol (5 equiv.), substrate concentration (0.08 M), voltage (4 V), flow rate (0.05 mL min^{-1}), AC frequency (0.5 Hz), and base (2.9 equiv.) at 20 °C.

The uniform set of conditions without modification of the base, nucleophile equivalents or AC frequency in this flow electrolysis demonstrated superiority compared to previously reported reactions in the batch system. It is worth noting that the first example of electrochemical serine arylation of an oligopeptide **144** was achieved in 47% isolated yield. Moreover, the automated flow library synthesis was efficiently extended to secondary alkyl amine, branched primary amine and elec-

tron-deficient amine substrates. For example, electron-deficient amines such as sulfonamide **139**, dimethylsulfoximine **140**, tetramethylguanidine **141**, alanine **142** as well as asparagine **143** were well tolerated. The success rate of the library synthesis of **109–138** was 20/30, and benzyl amine **127**, indole **132** or hindered diisopropylamine **117** showed low reaction efficiency. Meanwhile, primary amines gave lower yields due to product dimerization. In conclusion, the successfully developed continuous flow system would dramatically facilitate the adoption of metallic electrocatalytic C–N coupling in industry.

2.2 Metallic electrocatalyzed cross-coupling for sulfoximination

Transition metal-catalyzed sulfoximination has received significant attention owing to the key role of sulfoximines in drug discovery and ligand design. In the early stage, copper and palladium catalysis were widely employed with aryl coupling partners,[54] but the transformation of aryl chlorides and fluorides had not been well resolved though the rapid development of nickel catalysis or photoredox/nickel co-catalysis.[55] Meanwhile, its high temperatures, restricted substrate scope, use of expensive iridium catalysts and the reliance on alkoxide bases also suppressed its application. Delightedly, metallic electro-catalyzed sulfoximination would be a cutting-edge approach, which was not only reflected in its mild reaction conditions, but also in the accelerated elementary reaction process. In this section, the key challenges in conventional sulfoximination have been resolved through electrochemical processes.

In 2021, Mei and co-workers also reported nickel-catalyzed electrochemical sulfoximination involving weakly nucleophilic sulfoximines (Scheme 12).[56] This protocol provided an efficient and convenient approach to diverse sulfoximidoyl derivatives and overcame the drawbacks of high temperatures, restricted substrate scope and strong bases. During the optimization of the conditions, base had the most significant impact on the results and DBN (1,5-diazabicyclo[4.3.0]non-5-ene), DABCO, and Et_3N were proven to be ineffective besides DBU. Meanwhile, the electron-rich bipyridine ligand di-OMebpy (4,4′-dimethoxy-2,2′-bipyridine) achieved full substrate conversion and 90% yield of product **145**. Delightfully, gram-scale synthesis with 85% isolated yield could be obtained on a 5 mmol scale. The catalytic system exhibited excellent functional group tolerance to both (hetero)aryl bromides **146** and sulfoximines **147** with different electron-properties. It is worth noting that chiral-substituted sulfoximines **148** proceeded smoothly with no racemization phenomenon, and aryl chlorides on drug frameworks also gave sulfoximine product **149** in moderate yields.

In mechanistic studies, the control experiment with Ar–Ni(II)L–Br complex **150** indicated that anodic oxidation of Ar–Ni(II)L–Br species to Ar–Ni(III)L–sulfoximine was crucial for the product formation. A conventional Ni(I)/Ni(III)/Ni(II)/Ni(I) catalysis sequence was analogously proposed. Initially, the Ni-foam cathode reduced the $LNi(II)X_2$ precatalyst to LNi(I)X species **152**, followed by oxidative addition with aryl halides to give Ar–Ni(III)L–X_2 **153**. After cathodic reduction, the generated Ar–Ni(II)L–X **154** further underwent ligand exchange (*N*-attack and deprotonation facilitated by DBU) to afford the corresponding Ar–Ni(II)L–sulfoximine intermediate **155**. High-valent Ar–LNi(III)X–sulfoximine species **156** formed by anodic oxidation induced the final reductive elimination to give the desired product and regenerate LNi(I)X species **152**.

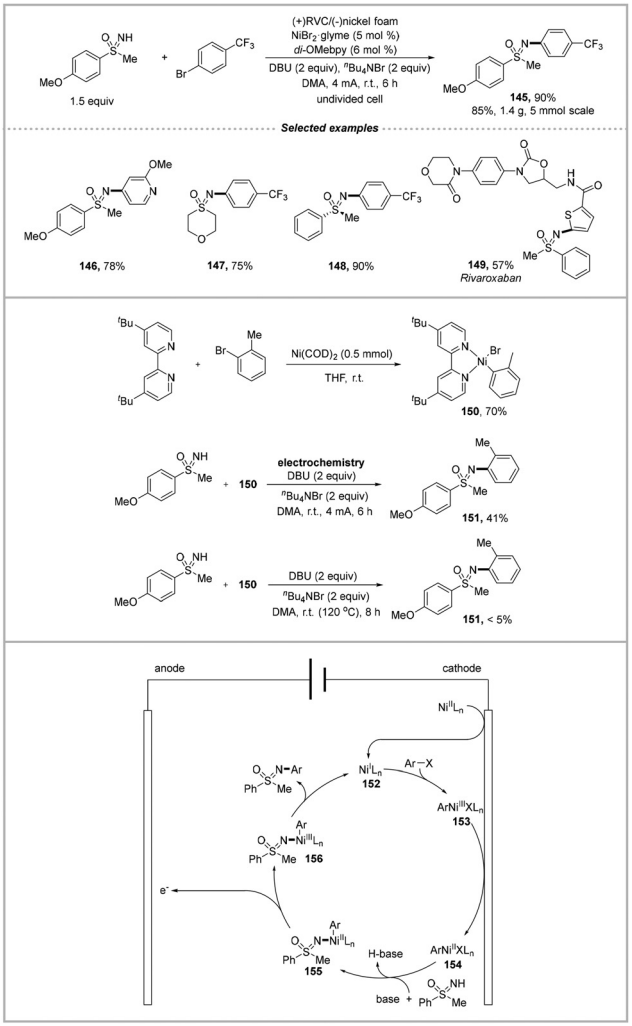

Scheme 12 Nickel-catalyzed electrochemical amination with *NH*-sulfoximines.

In 2024, Ma, Mei and co-workers further merged a highly efficient paired electrochemical nickel-catalyzed intramolecular C–N coupling with sulfoximines (Scheme 13).[57] Optimization of the reaction conditions revealed that both ligand and base significantly influenced the transformation and di-OMebpy (4,4′-dimethoxy-2,2′-bipyridine) ligand (15 mol%) as well as DBU (2 equiv.) afforded the highest isolated yield of 88% of **157**. A series of 1,2-benzothiazines **158–160** was synthesized, featuring mild reaction conditions and good functional group tolerance.

In mechanistic studies, CV and square wave voltammetry (SWV) experiments revealed the multiple conversional signal

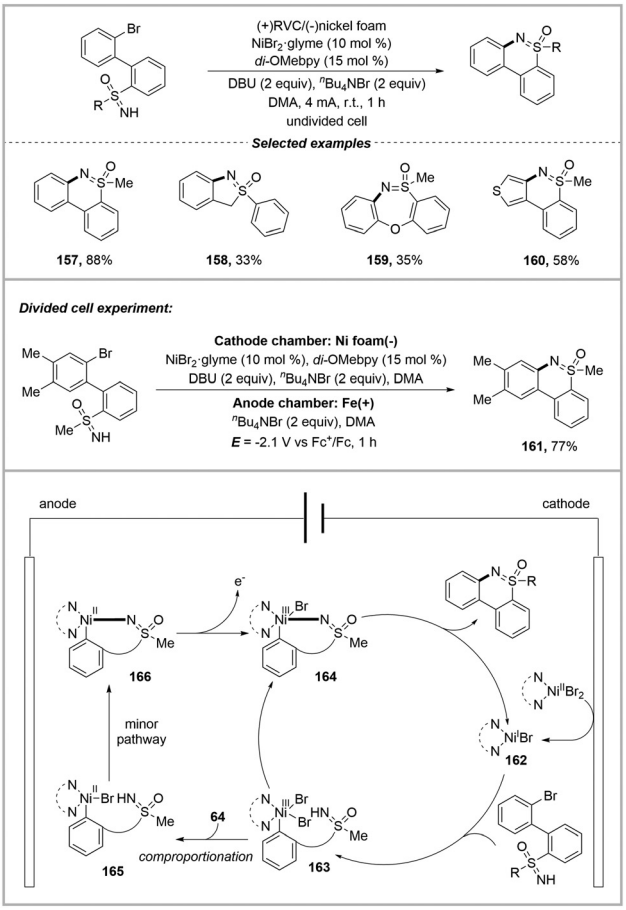

Scheme 13 Nickel-catalyzed electrochemical intramolecular amination.

of active species Ni(I)/Ni(0) or Ni(II)/Ni(I) as complicated coordination situations from excessive ligands (1.5 equiv.). Considering the measured stable cathodic potential of −2.28 V (*vs.* Fc/Fc^+), the reduction of Ni(II)/Ni(I) species (−1.6 to −1.9 V *vs.* Fc/Fc^+) should be favorable for the reduction of the Ni(I)/Ni(0) species (−2.5 V *vs.* Fc/Fc^+), which clearly explained the initial role of Ni(I) species in the electrocatalytic cycle. Meanwhile, the on/off experiment also ensured the essential role of electricity and the high 118% current efficiency indicated that a sustained flow of electrons was not required to obtain the final product. This result was consistent with the subsequent 77% yield of product **161** in divided cells, which explained the formation of Ni(III) species before reductive elimination without the role of anodic oxidation.

A probable mechanism was then proposed. Cathodic reduction of the Ni(II) precatalyst produced Ni(I) species **162**, which then underwent oxidative addition with aryl bromide to Ni(III) species **163**. Rapid base-assisted sulfoximine ligand exchange, followed by reductive elimination of **164**, resulted in the formation of the product. However, the conventional Ni(I)/Ni(III)/Ni(II)/Ni(I) catalysis sequence mechanism including chemical reduction to Ni(II) **165** *via* comproportionation between Ni(III) and Ni(I) could be considered as a minor pathway.

In 2025, Kong, Cao and co-workers developed a challenging electrochemical Ni-catalyzed defluorinative sulfoximination of non-activated aryl fluorides (Scheme 14).[58] Compared with the developed defluorinative strategies such as C–F oxidative addition, nucleophilic substitution with Ru/Rh η^6-coordinated complexes or aryl radical cations, this cathodic single-electron reduction model seemed difficult and rare as very negative reduction conditions were needed to effectively reduce PhF (E_{red} = −3.0 V *vs.* SCE).

Optimization of the reaction conditions revealed that no extra ligands were needed as DMA could be a good ligand for the $NiCl_2{\cdot}H_2O$ catalyst. Importantly, electrosynthesis was essential as totally inhibited reactivity was observed when replacing electrocatalysis with Mn or Zn reductant. This defluorinative sulfoximination protocol demonstrated good substrate compatibility, including multifold aryl electrophiles and exhibiting excellent reactivity for some challenging substrates. Gram-scale reactions of **167** and late-stage modifications of bioactive molecules **168–171** also confirmed this superiority.

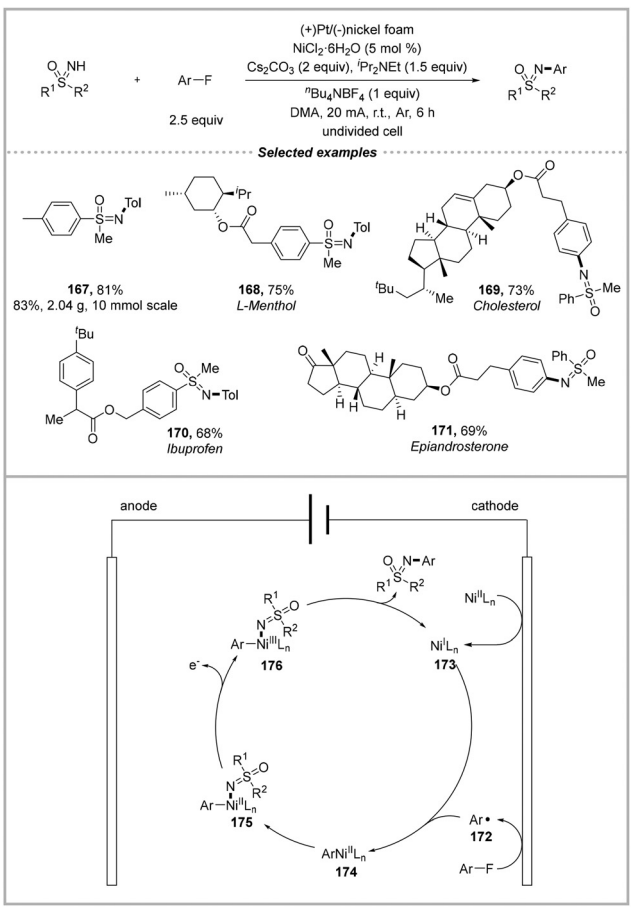

Scheme 14 Nickel-catalyzed electrochemical amination with nonactivated aryl fluorides.

In mechanistic studies, the dramatic decrease in yield in a divided cell revealed the essential roles of both the anodic and cathodic processes in paired electrolysis. Radical scavenger experiments with TEMPO (2,2,6,6-tetramethylpiperidin-1-oxyl) and EPR (electron paramagnetic resonance) spectroscopy also confirmed the aryl radical intermediate. Subsequent CV experiments demonstrated that Ni(I) species served as the active catalytic intermediate. A probable mechanism was then proposed. Single-electron cathodic reduction occurred with both a fluorinated substrate and Ni(II) precatalyst, which produced key aryl radical intermediate **172** (by releasing fluoride ions from the aryl radical anion) and Ni(I) species **173**, respectively. Next, the generated Ar–Ni(II)–X complex **174** with aryl radical was coordinated with sulfoximine, facilitated by Cs_2CO_3, yielding intermediate **175**. Subsequent anodic oxidation of **175** produced Ar–Ni(III)–sulfoximino intermediate **176**, which underwent final reductive elimination to afford the desired product with the regeneration of the active Ni(I) species **173**.

2.3 Metallic electrocatalyzed cross-coupling for primary amination

Primary aryl amines represent fundamental building blocks of various biological scaffolds. However, the direct synthesis of primary aryl amines is challenging in conventional transition-metal-catalyzed amination, which is mainly due to the requirement of a highly reductive ligand to overcome the slow reductive elimination and further oxidation of the product with a low oxidation potential.[59] Metallic photocatalyzed strategies with azides as the nitrogen source also demonstrated the positive impact of light on elementary reactions from various perspectives.[60] In this section, metallic electrocatalyzed primary amination is described as the cutting-edge research and development of a greener and direct method to synthesize primary arylamines.

Despite the achievements in secondary amination, the direct synthesis of monoaryl amines with an $-NH_2$ moiety had not yet been achieved through the electrochemical nickel-catalyzed approach.[61] Encouragingly, a pioneering advancement was realized by Wei, Xu and co-workers in 2025 and the first direct metallic electrocatalyzed amination to obtain monoaryl amines was selectively developed by employing $TMSN_3$ (trimethylsilyl azides) as the nitrogen source (Scheme 15).[62]

During the optimization of the conditions, the selection of electrodes, ligands and bases enabled the chemoselective synthesis of both monoaryl amines and diaryl amines. Employing a nickel anode, bpy (2,2′-bipyridine) and DBU was conducive to obtain monoaryl amine **177** and additional H_2O and TEMPO promoted this transformation with 70% isolated yield at 60 °C. Notably, the reaction could still proceed in the absence of nickel catalyst with 45% yield of monoaryl amines, which could be due to the Ni(II) species generated through a sacrificial anode process. Furthermore, other appropriate conditions with aluminum anode, dtbbpy (4,4-di-*tert*-butyl bipyridine) and Et_3N gave diaryl amine product **182** in moderate yield with high chemoselectivity. This protocol demonstrated excellent compatibility with the electronic property and steric

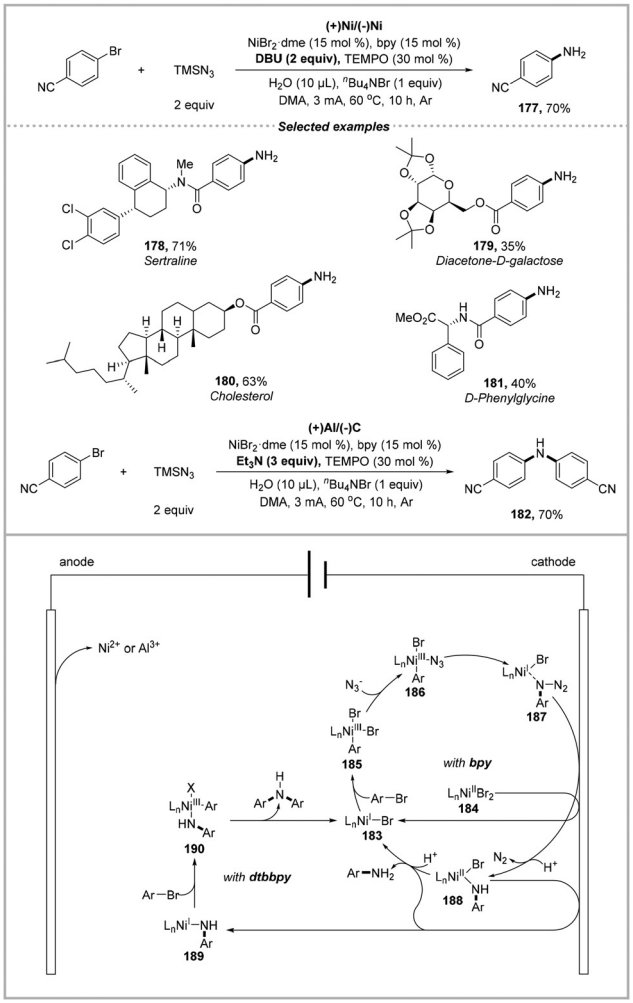

Scheme 15 Nickel-catalyzed electrochemical amination with $TMSN_3$.

hindrance of (hetero)aryl halides, and amination/diarylamination of various bromo-drug molecules **178–181** also proceeded smoothly.

In mechanistic studies, controlled experiments primarily highlighted the important intermediate role of aryl azide rather than aniline. Subsequent DFT calculations indicated that the Ni(III) complex was more prone to undergo reduction elimination owing to its lower energy barrier of 12.7 kcal mol^{-1} compared to 39.8 kcal mol^{-1} with the Ni(II) complex. A probable mechanism was then proposed. Initially, Ni(I) species **183** was reduced from Ni(II) precatalyst **184** at the cathode, which then underwent oxidative addition with aryl bromide to Ni(III) species **185**. Transmetalation between $TMSN_3$ and **185** resulted in ligand exchanged Ar–Ni(III)X–N_3 intermediate **186**, followed by reductive elimination to produce Ni(I) intermediate **187**. Sequential cathodic reduction gave ArNH–Ni(II)–X intermediate **188** (with the liberation of N_2 and hydrogenation) and the final reductive elimination product monoaryl aniline by regenerating Ni(I) species **183**. Encouragingly, when changing the ligand from bpy to dtbbpy, the difference was mani-

fested in the conversion of intermediate **188**. Further cathodic reduction of **188** and secondary oxidative addition of **189** generated Ar–Ni(III)X–Ar intermediate **190**. The reductive elimination of **190** provided the diarylamine product and regenerated **183**, initiating another catalytic cycle.

Meanwhile, in 2025, Qiu and co-workers reported a rare and rapid access to electrochemical Ni-catalyzed amination for primary arylamines (Scheme 16).[63] The weak nucleophilic reagent NH_3 was directly employed as an ammonia surrogate and aryl chlorides, bromides, and iodides were proven to be quite compatible with high efficiency. During the optimization of the conditions, the sacrificial Zn anode material had a significant effect on the reaction by releasing the Lewis acid to activate C–X bonds and avoiding over-oxidation reactions.

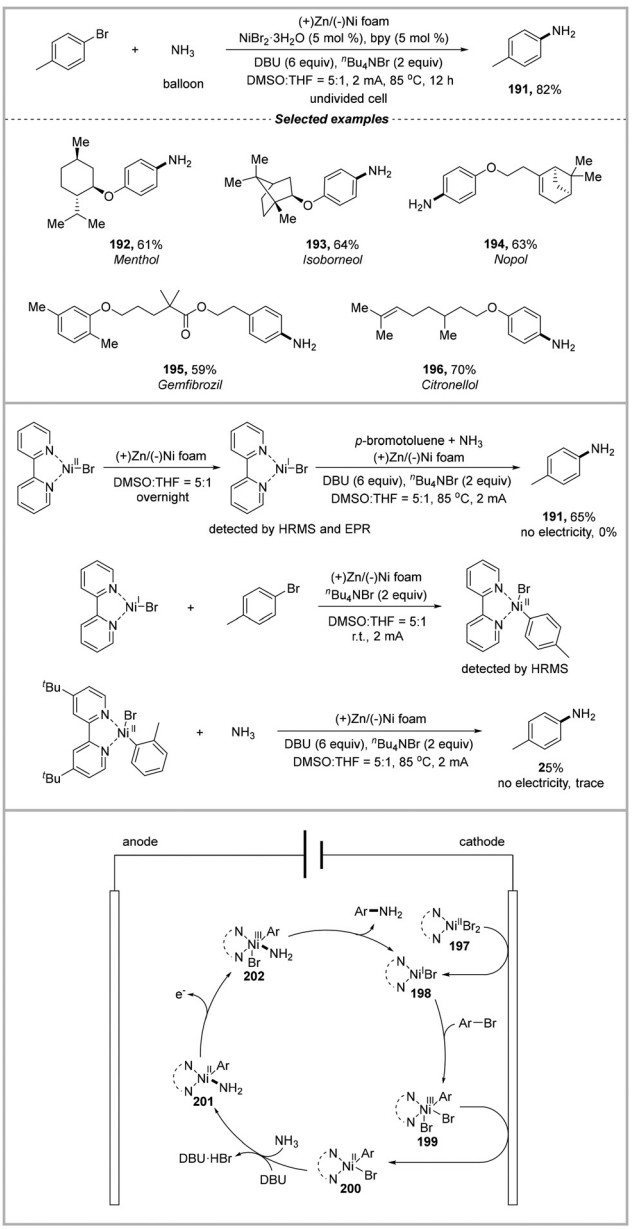

Scheme 16 Nickel-catalyzed electrochemical amination with NH_3.

Meanwhile, a high temperature of 60 °C and thermodynamically favored NH_3 liberation were essential, as they facilitated activation of the N–H bond and inhibited deactivation of the nickel species coordinated by NH_3, respectively. Furthermore, a mixed solvent of DMSO : THF = 5 : 1 was crucial to obtain a high yield probably due to the good solubility of nickel complexes and NH_3 in DMSO (dimethyl sulfoxide) and high alkalinity of DBU in THF (tetrahydrofuran). Notably, in the case of primary amine product **191** with a lower oxidation potential, this catalytic system could prevent further oxidation by employing a reductive microenvironment with a sacrificial Zn anode and NH_3 gas. Meanwhile, drug-containing molecules **192–196** were well tolerated in moderate yields, showing the excellent substrate compatibility.

In mechanistic studies, cathodic reduction of LNi(II)Br_2 to LNi(I)Br was first detected by HRMS (high-resolution mass spectrometry) and EPR experiments and subsequent electrochemical reaction with aryl bromides and NH_3 indicated the initiated role of LNi(I)Br species. Then, the Ar–Ni(II)bpy–Br intermediate generated from LNi(I)Br and ArBr revealed the cathodic reduction of Ar–Ni(III)L–Br_2 and subsequent electrochemical reaction with NH_3 demonstrated its existence throughout the catalytic cycle. Furthermore, divided cell experiments with the desired product in the anodic cell revealed the possible anodic oxidation of Ar–Ni(II)L–NH_2 to Ar–Ni(III)Br–NH_2 before reductive elimination, and CV experiments also confirmed this process.

A plausible mechanism was proposed. Firstly, the Ni-foam cathode reduced Ni(II) precatalyst **197** to Ni(I) species **198**. Ni(III) intermediate **199** was formed through oxidative addition of **198** with aryl halide, which led to key Ni(II) intermediate **200** by cathodic reduction. After that, under an reductive atmosphere of DBU and NH_3 gas, ammonia attack to **200** and deprotonation produced Ni–amino intermediate **201**, followed by the formation of high-valent Ni(III) intermediate **202** with anodic oxidation. Finally, the reductive elimination of **202** to primary arylamines and regeneration of Ni(I) intermediate **198** completed the entire cycle.

2.4 Metallic electroreductive hydrogenative couplings for C–N bond

Transition metal-catalyzed hydrogenative coupling represents a higher-order variant of the classical reductive aminations. Conventional research focused on the conversion of aldehydes and ketones with amines to *N*-alkyl amines.[64] However, the harsh reaction conditions with precious metal catalysts, excessive metal hydrides and poor selectivity limited its application. Compared to the classical thermal hydrogenation, the development trend of cross-hydrogenative C–N couplings was employing protons and electrons as the hydrogen source and redox equivalent, respectively. In this section, metallic electroreductive hydrogenative C–N couplings are superiorly described with relatively inert coupling partners as well as green and sustainable synthesis.

In 2024, Liu and co-workers described the electroreductive cobalt-catalyzed hydrogenative cross-coupling of less electro-

philic nitriles with amines (Scheme 17).[65] Co(II)–H species, generated from cathodic reduction and protonation with electrons and protons as the redox equivalent and hydrogen source, induced the selectivity control of nitrile reduction and C–N coupling, respectively. Diverse secondary and tertiary amines were efficiently synthesized, which was quite challenging in early-stage developed methods for primary amine substrates.

During the optimization of the conditions, the bidentate bipyridine ligand di-Mebpy (5,5′-dimethy-2,2′-bipyridine) obviously increased the yield of product **203** to 85%, while conventional hydrogenation with H_2 rather than electrohydrogenation could not directly generate the product. The acid additive HFIP (10 equiv., hexafluoroisopropanol) played a crucial role in this transformation (condition A) and a comparable yield of 82% could also be obtained with a lower loading of HFIP (3 equiv.) and higher temperature 70 °C (condition B). Functionalized aromatic, aliphatic nitriles **204–206**, acetonitrile **207** as well as anilines **203**, heterocyclic **208**, aliphatic primary/secondary amines **209–210**, and nitrogen-containing drug frameworks **210–212** were widely tolerated (except bromo- and iodo-benzene substrates) and intramolecular electroreductive amination of **213** or homocoupling **214** was also feasible. It is gratifying that reductive deuteration of *N*-α-CD_2 labelled amines **215** with methanol-D_4 could smoothly afford the corresponding amines in moderate yield with high deuterium incorporation.

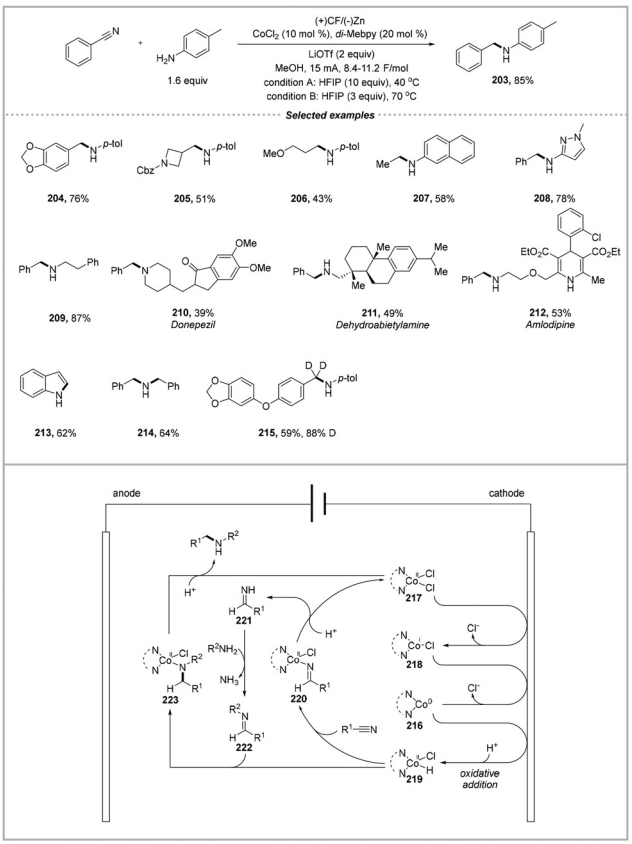

Scheme 17 Cobalt-catalyzed electrochemical hydrogenative cross-coupling with nitriles.

In mechanistic studies, the kinetic experiment clearly indicated that hydrogenation of condensed intermediate **222** was fast and the preceding cobalt-hydrogenation of cyano was the rate-determining step (also proven by kinetic isotope effect experiment). Further kinetic studies on RDS indicate the roles played by the cobalt catalyst, benzonitrile and HFIP, accompanied by a competitive thermodynamically preferred hydrogen evolution reaction (HER) with higher HFIP concentration. Moreover, increased cyano electrophilic reactivity with HFIP was detected through NMR experiments, which facilitated the cobalt-hydride reduction. Subsequent CV experiments indicated that Co(0) species was generated *via* cathodic reduction, followed by *in situ* protonation of the Co(II)–H species and a more efficient hydride transfer to nitrile in the presence of HFIP.

A probable mechanism was then proposed. Initially, Co(0)L species **216**, generated from the stepwise cathodic reduction of $LCo(II)X_2$ **217**, resulted in LCo(II)X–H complex **219** in the presence of an acid. Cobalt-hydrogenation of nitrile gave Co(II)–imine complex **220**, and its subsequent protonation with acid reproduced **217** and semi-hydrogenation product **221**. Next, imine **222**, generated from the fast condensation of amine substrate and **221**, underwent secondary cobalt-hydrogenation to afford Co(II)–amino complex **223**. Finally, protonation of **223** produced the desired amine product, and regenerated **217** ensured the continuity of the catalytic cycle.

In 2025, Qu, Liu and co-workers sequentially reported an electroreductive cobalt-catalyzed hydrogenative cross-coupling of low electrophilic and thermodynamically stable carboxylic acids with amines, which overcame the conventional obstacles of high negative carboxylic reductive potential, Kolbe decarboxylation byproducts and catalyst deactivation by carboxylate over-coordination (Scheme 18).[66] The developed electrocatalytic system effectively generated the cobalt hydride species and enable *N*-alkylation products without superstoichiometric metal hydrides in classical thermal hydrogenations.

During the optimization of the conditions, the bidentate phosphine ligand dppf (1,1′-bis(diphenylphosphino)ferrocene) promoted the efficient conversion of TFA (trifluoroacetic acid) with good chemoselectivity and the more electrophilic carbonyl group activated by the Lewis acid additive $Ti(O^nBu)_4$ was prone to undergo protonation reactions to generate β-fluoroalkylamine products. Meanwhile, electrocatalysis exhibited superiority in this coupling owing to the rapidly diminishing reaction activity with stoichiometric reductants such as Zn, Mn, $PhSiH_3$ and H_2. This reductive *N*-trifluoroethylation exhibited excellent compatibility with anilines **224–225**, though alkylamines such as benzylamine and morpholine were unfavorable. Inspiringly, by replacing the Lewis acids with $BF_3{\cdot}OEt_2$, formic acid, HCOOH, could also enable efficient *N*-methylation with anilines **226**, secondary amine **227** as well as drug molecules **231**, and less electrophilic aliphatic or polyfluorocarboxylic acids **228–230** were also com-

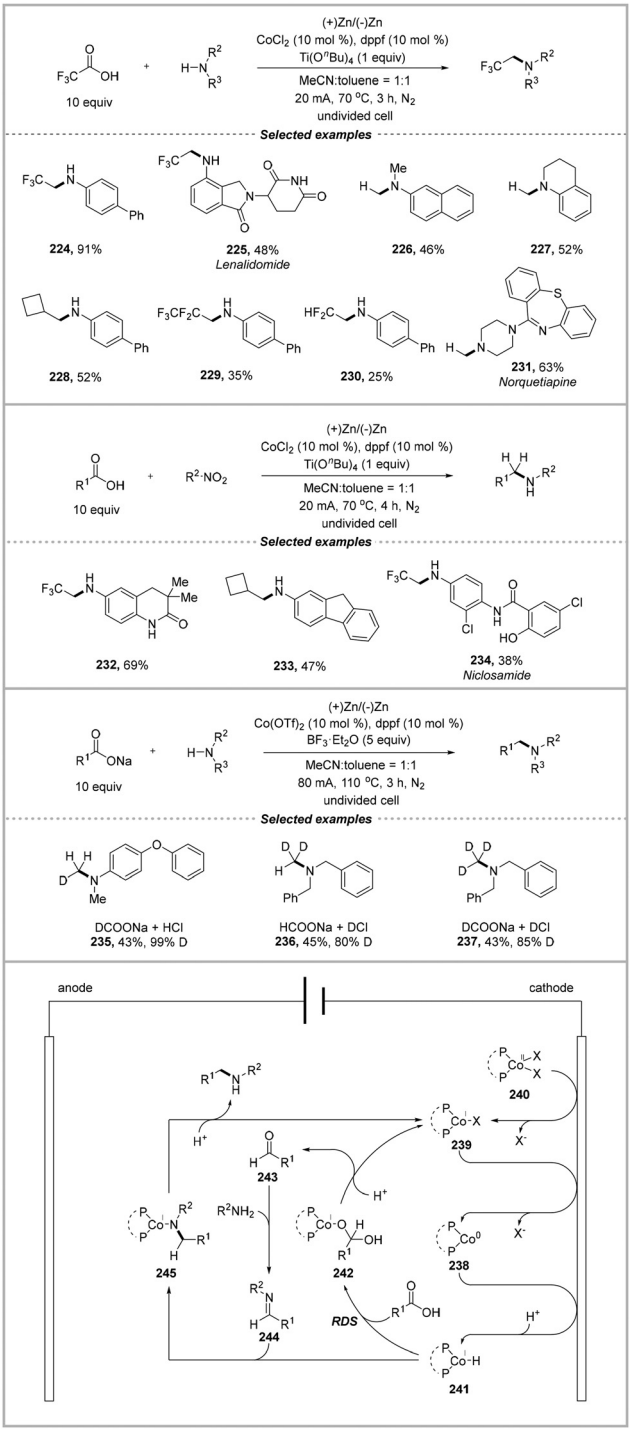

Scheme 18 Cobalt-catalyzed electrochemical hydrogenative cross-coupling with carboxylic acids.

patible, albeit in lower yields. Its synthetic applications were further extended to electroreductive *N*-alkylation with nitroarenes[67] **232–234** and chemodivergent deuteration (namely $-CH_2D$, $-CHD_2$ or $-CD_3$) at the α-positions of *N*-methyl amines **235–237**.

In mechanistic studies, the possibility of amide formation, followed by deoxygenative reduction was initially excluded with no coupling product, and trifluoroacetaldehyde was confirmed as an effective intermediate. Meanwhile, KIE (kinetic isotope effect) experiments revealed hydrogen transfer was the turnover-limiting step with the cobalt catalyst and TFA. CV experiments indicated the interaction between the cobalt complex and TFA with a lower potential of −1.5 V (*vs.* Ag/AgCl) for the cobalt–TFA complex and negative potential of −2.1 V (*vs.* Ag/AgCl) for Co(0)–H species, respectively. ^{1}H NMR spectra further provided evidence for the Co(I)–H intermediate and acid reduction product aldehyde and alcohol. Density functional theory (DFT) calculations also provided theoretical evidence for the hydride transfer step as the rate-determining step with the overall activation barrier of 18.9 kcal mol^{-1}.

A probable mechanism was proposed. Firstly, Co(0)L species **238** was obtained through stepwise cathodic reduction of LCo(II)X_2 **240**, which next interacted with acid to give corresponding LCo(I)–H complex **241**. The rate-determining carboxylic reduction by **241** resulted in hemiacetal intermediate **242**, followed by rapid protonation to aldehyde **243** by releasing LCo(I)–X species **239**. Subsequently, imine intermediate **244**, condensed from **243** and amine substrates, underwent cobalt-hydrogenation to give Co(I)–amino intermediate **245**. Final hydrogenative cross-coupling products were obtained, with acid and regenerated LCo(I)–X species **239** completing the electrocatalytic cycle.

2.5 Metallic electroreductive cross-electrophile coupling for C–N bond

Transition metal-catalyzed oxidative decarboxylation coupling represents the classical transformation of bench-stable alkyl carboxylic acids to obtain alkyl amines, while excess oxidant decreases the reaction compatibility.[68] Meanwhile, electrochemically promoted anodic oxidation is an alternative method, but the reaction is highly dependent on the substrate structure, which is mainly due to the required stable carbocations.[69] Considering these limitations, reductive cross-electrophile coupling with electrophilic carboxylic acid derivatives would be a flexible pathway.[70] In this section, metallic electroreductive cross-electrophile coupling is described in a highly controlled metal catalytic process with multiple active species.

In 2024, Shang and co-workers reported the first example of an Ni-catalyzed electroreductive decarboxylative C(sp^3)–N cross-electrophile coupling reaction (Scheme 19).[71] This strategy avoided the strict structural requirement of carboxylic acids to form stabilized carbon cations in the classical Ritter-type amination. During the optimization of the conditions, a zinc plate anode and nickel foam cathode were required, and control experiments indicated that nickel catalyst, ligand, and electricity were all crucial to promote this reaction. Importantly, no reaction occurred by replacing electricity with stoichiometric Mn or Zn reductant, indicating the indispensable role of electrocatalysis. Furthermore, electron-withdrawing benzophenone-derived oxime esters **247** and ligand Phen (1,10-phenanthroline) were favorable for the highest isolated

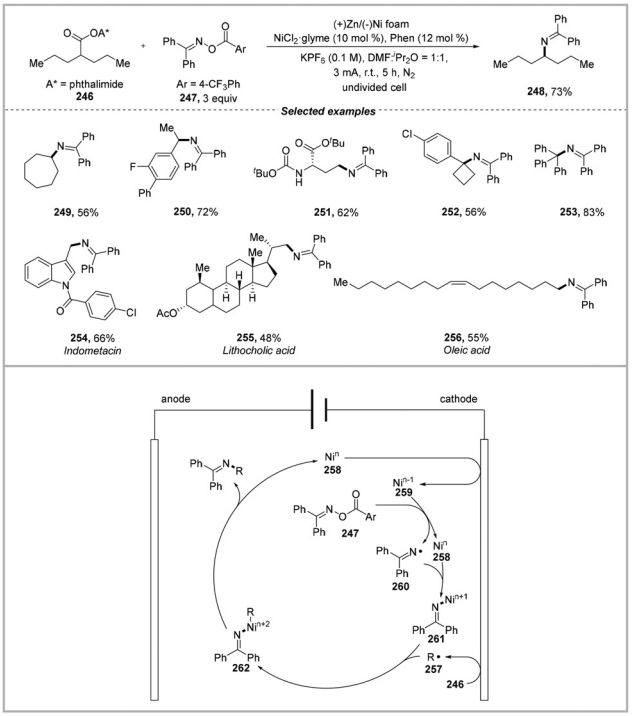

Scheme 19 Nickel-catalyzed electrochemical cross-electrophile coupling for C–N bonds.

yield of product **248** of 73%. Secondary **249–250**, primary **251** or even tertiary **252–253** carboxylic acid redox active esters (RAEs) as well as bioactive substrates **254–256** could successfully react with benzophenone derived oxime esters to obtain protected alkyl amines under the optimized mild conditions.

In mechanistic studies, radical trap and radical clock experiments both revealed the involvement of alkyl radicals. Control experiments and CV experiments demonstrated the engagement of iminyl radicals, direct cathodic reduction of RAEs as well as reduction of oxime ester with low-valent nickel species. It is worth noting that the co-solvent $^{i}Pr_2O$ (diisopropyl ether) could significantly increase the yield, as it inhibited N–N dimeric byproducts as well as synchronization between the alkyl radical formation rates and reduced iminyl radical generation rates. Meanwhile, a direct radical–radical coupling process rather than nickel-mediated pathway was strictly excluded.

A probable mechanism was proposed. Firstly, direct cathodic reduction of alkyl carboxylic acid RAEs **246** generated alkyl radical species **257**, in which nickel-mediated reduction could be a minor pathway. Meanwhile, Ni(n − 1) species **259** was also produced with cathodic reduction of Ni(n) species **258**, which further reduced oxime ester **247** to iminyl radical **260**, with the regeneration of Ni(n) **258**. Next, Ni(n + 1)-amino species **261** was obtained with radical recombination of **260** and Ni(n) species **258**, and subsequently captured alkyl radical **257** to high-valent R–Ni(n + 2)–amino species **262**. Finally, reductive elimination occurred to finish the catalytic cycle by delivering the amination product and Ni(n) species **258**.

3. Metallic electrooxidative C–H activation for C–N bond formation

C–H activation has emerged as a powerful tool for C–N bond formation. In the early stages, C–H activation was mainly focused on palladium-catalyzed systems, which are limited to strongly *N*-coordinating directing groups. The subsequent rhodium(III) and ruthenium(II) catalysis expanded the means to the use of weakly coordinating amides and acids. However, stoichiometric amounts of expensive and toxic metal oxidants were largely involved in conventional oxidative C–H activations, compromising their overall sustainable nature.[72] In sharp contrast, metallic electrooxidative C–H activation had been identified as a more efficient strategy.[73] However, given the scarcity and high cost of 4d transition metals (Pd, Rh, and Ru), recent breakthroughs have mainly focused on the transformation by earth-abundant and cheap 3d transition metals, such as cobalt, nickel, and copper catalysis.[74] Considering the sustainable nature of electrochemical C–H activation, significant development had been made in this rapidly evolving research area, especially for C–H amination and enantioselective synthesis.[75] In this section, the late-stage development on metallic electrocatalyzed C–N bond formation is summarized, mainly from the aspect of C–H amination and C–H/N–H annulations,[76] respectively.

3.1 Metallic electrooxidative C–H aminations

In 2018, Ackermann and co-workers reported the first cobalt-catalyzed electrooxidative C–H amination at 40 °C (Scheme 20).[77] A greener approach to aryl amines was achieved by employing sustainable electricity as the terminal oxidant instead of stoichiometric sacrificial and toxic metal oxidants. Optimization of the reaction conditions indicated that the *N*,*O*-bidentate coordinated substrate exhibited a distinctive reactivity compared with *N*,*N*-bidentate chelation and electron-deficient amides. Meanwhile, biomass-derived, renewable solvent γ-valerolactone (GVL) significantly increased the yield of product **264** to 77% under an ambient air atmosphere.

In mechanistic studies, kinetic experiments as well as isotopically labelled with cosolvent D_2O indicated a facile C–H cleavage process. Furthermore, the higher oxidation potential of **263** (+1.51 V *vs.* SCE) than the Co(II) precatalyst (+1.05 V *vs.* SCE with KOAc) in the cyclic voltammetry analysis suggested an SET (single-electron transfer) route from **263** to preferentially form Co(III). A probable mechanism was proposed. Initially, Co(III) species **267** was produced through anodic oxidation, which induced SET and C–H cleavage of **263** to achieve carboxylate-assisted C–H activation intermediate **268**. Then, subsequent amino ligand exchange after deprotonation gave Co(III) species **269**, followed by C–N bond formation with reductive elimination to Co(I) species **270**. Finally, the catalytic C–H amination cycle was achieved by demetallation of **270**, protonation of amino for **264** and further anodic oxidation of regenerated Co(I) for Co(III) species **257**.

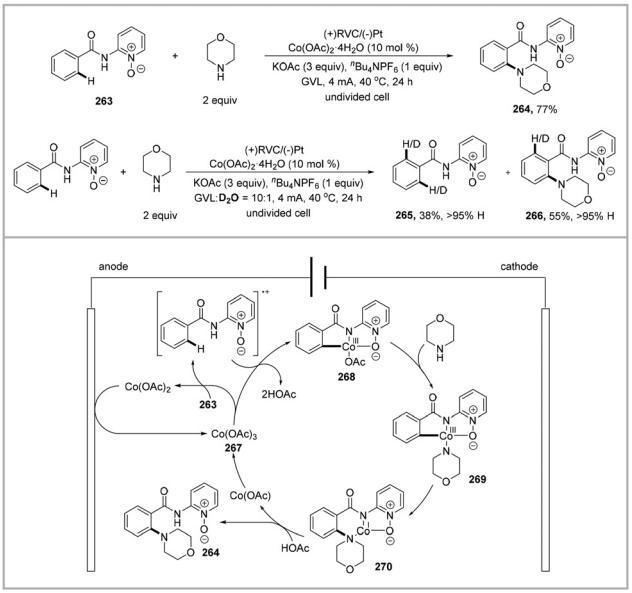

Scheme 20 Cobalt-catalyzed electrochemical C–H amination with the *N*,*O*-bidentate chelation.

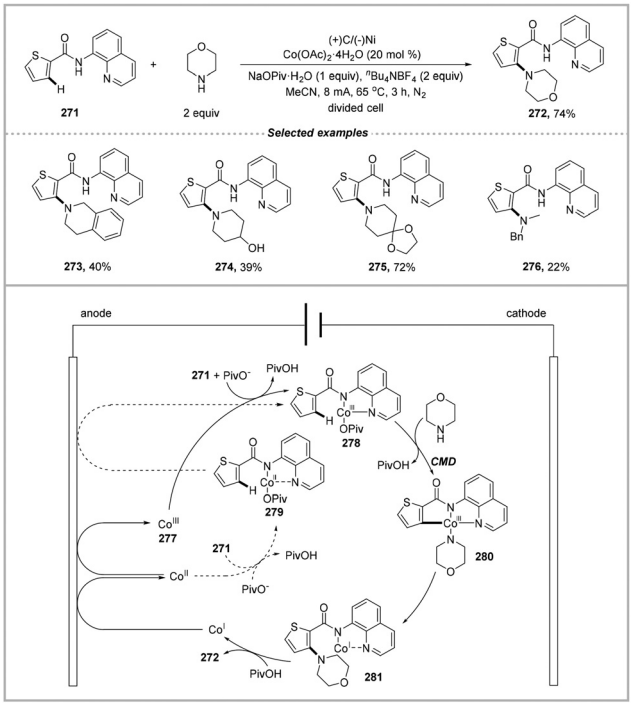

Scheme 21 Cobalt-catalyzed electrochemical C–H amination with the AQ-directed benzamide.

Simultaneously, Lei and co-workers reported an oxidant-free cobalt-catalyzed electrochemical C–H amination between AQ-directed benzamide and secondary amine at 65 °C (Scheme 21).[78] During the optimization of the conditions, no reaction occurred under an undivided cell, which is probably due to the loss of metal catalytic activity and formation of undesired byproducts with cathodic reduction. The reaction exhibited good compatibility with secondary cyclic amine substrates **273–275**. Primary alkylamines proved to be invalid for this electrocatalytic system and only *N*-methylbenzylamine **276** gave 22% isolated yield when using chain amines.

In mechanistic studies, the kinetic isotope effect (KIE) experiment indicated that C–H cleavage might not be involved in the rate-limiting step. Meanwhile, the CV experiment explained the effective coordination between the benzamide substrate and Co(II) precatalyst by monitoring the naught potential E° = 1.269 V for $Co(OAc)_2{\cdot}4H_2O$, which changed to E° = 1.460 V for the Co(II)-coordinated complex. A probable mechanism was proposed. Initially, Co(III) species **277** was obtained through anodic oxidation, which then coordinated to *N*-(quinolin-8-yl)benzamide to produce Co(III)-complex **278**. The reversed sequence of anodic oxidation and coordination through **279** could be a compatible pathway. Next, the pivalate-assisted concerted-metalation–deprotonation (CMD) process gave Co(III)–amino complex **280**, which further resulted in the desired product after the reductive elimination of **280** and demetallation of **281**. The Co(II) species was regenerated by anodic oxidation to finish the electrocatalytic cycle.

In 2018, Ackermann and co-workers reported the first nickel-catalyzed electrooxidative C–H amination at 120 °C (Scheme 22).[79] In contrast to the cobalt catalysis manifold, biomass-derived solvent GVL failed to provide the desired product and NaOPiv would be the optimal additive without an essential redox-mediator. Meanwhile, various *N*,*N*-coordinated and *N*,*O*-bidentate chelated benzamides exhibited limited activity, except bidentate aminoquinoline (AQ)-directed benzamide **282**. Heterocyclic benzamides **284–286** and challenging secondary acyclic amine **287** could be well tolerated.

In the detailed mechanistic studies with cyclic voltammetry, an Ni(II)/Ni(III) event was obviously observed with the oxidation potential (E_p = +0.26 V *vs* Fc/Fc^+) of benzamide, NaOPiv and nickel precatalyst mixture at 25 °C, while the elevated temperature of 120 °C promoted the formation of cyclometalated Ni(III) species with a lower oxidation potential (E_p = −0.18 V *vs.* Fc/Fc^+). Importantly, the additional reversible oxidation potential (E_p = +0.49 V *vs.* Fc/Fc^+) further indicated the subsequent oxidation of Ni(III) to Ni(IV) species during the electrocatalytic cycle. Meanwhile, isotopically labelled and kinetic experiments with cosolvent CD_3OD indicated fast C–H scission.

A probable mechanism was proposed. Initially, pivalate-assisted C–H nickelation with Ni(II) precatalyst **290** and *N*-(quinolin-8-yl)benzamide **282** gave Ni(II) intermediate **292** through C–H cleavage. Then, deprotonation of coordinated amine and anodic oxidation delivered Ni(III)–amino intermediate **293**. Subsequent oxidation-induced reductive elimination of high-valent Ni(IV)–amino species **294** give the desired product. The regeneration of catalytically competent Ni(II) species **290** ensured the integrity of the electrocatalytic cycle.

In 2018, Mei and co-workers reported the first copper-catalyzed electrooxidative C–H amination of *N*-phenylpicolinamides with cyclic secondary amines at room

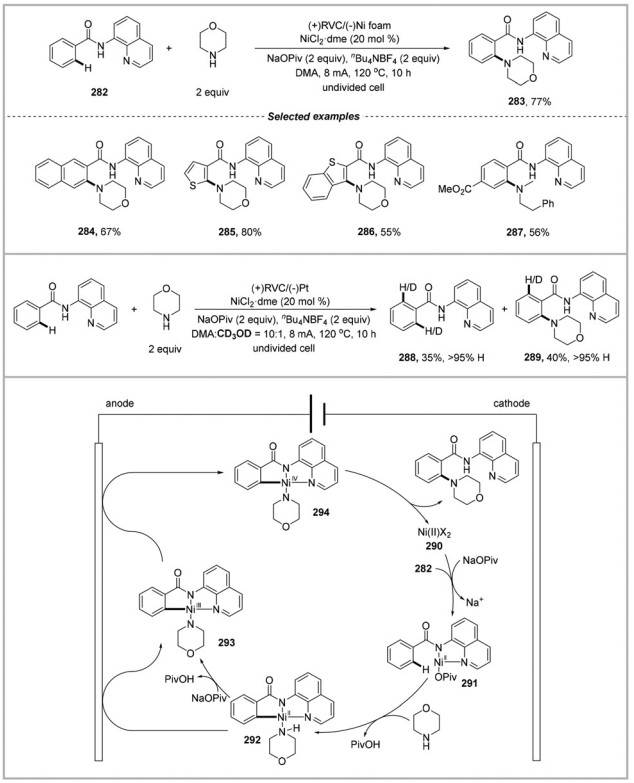

Scheme 22 Nickel-catalyzed electrochemical C–H amination with the AQ-directed benzamide.

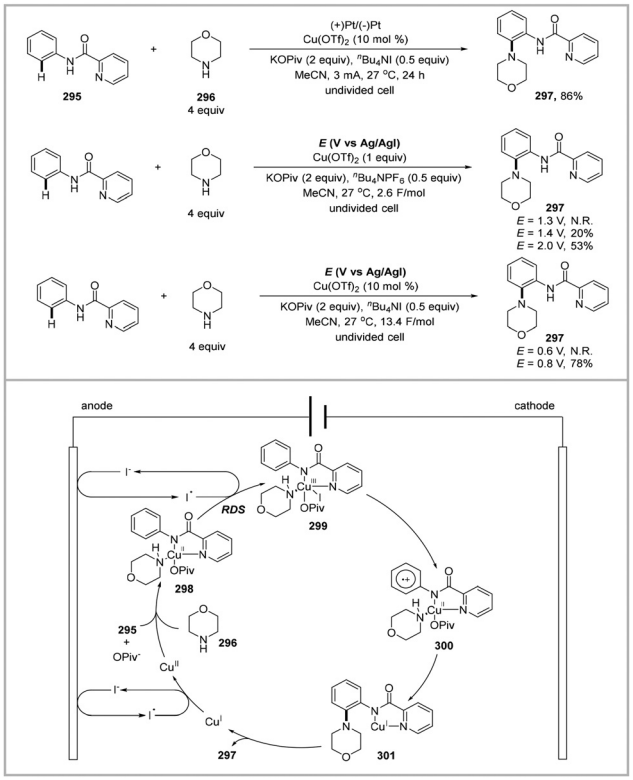

Scheme 23 Copper-catalyzed electrochemical C–H amination with picolinamide.

temperature (Scheme 23).[80] The redox mediator $^{n}Bu_4NI$ was employed to promote this electrocatalytic system by decreasing the required oxidation potential. During optimization of the reaction conditions, stoichiometric copper salts could not give any desired amination product in the absence of an electrical current, which was quite distinct from the thermodynamic copper-mediated C–H amination process. Meanwhile, the NHCO-2-Py group demonstrated superiority compared to other directing groups and the synthetically important 3-NHCO-2-Py pyridine substrate **295** was employed, with predominate *ortho*-position products.

In mechanistic studies, faster initial rates with electron-donating substrates and negative slope in the Hammett plot analysis revealed an SET mechanism for this copper-catalyzed C–H oxidation reaction. Meanwhile, the KIE experiment excluded the role of the rate-determining step of C–H cleavage. Importantly, according to the cyclic voltammetric analysis, the onset oxidation potential for various component combinations clearly revealed the lowest value of 1.51 V (*vs.* Ag/AgI) with a mixture of Cu(II), substrate **295** and morpholine **296**, indicating that the redox mediator preferentially oxidized the Cu(II)-complex prior to Cu(II) (2.42 V), **295** (2.06 V) or **296** (1.61 V). Furthermore, catalytic current test experiments provided favorable evidence that in the presence of morpholine **296**, iodine radical oxidized the Cu(II) complex to Cu(III) species, further promoting C–H amination in the absence of $^{n}Bu_4NI$. A subsequent controlled experiment under a high oxidation potential (E = 2.0 V *vs.* Ag/AgI) without $^{n}Bu_4NI$ verified this inference and that the accompanied lower yield may be due to the partial decomposition of the aminated product.

A probable mechanism was proposed. Firstly, Cu(II)-complex **298** with a low oxidation potential was obtained through iodine-mediated anodic oxidation of Cu(I)[32] and pivalate-assisted coordination with amine **296** and substrate **295**, which then underwent rate-determining iodine-mediated anodic oxidation to give Cu(III)-complex **299**. Next, intermediate **300**, generated from intramolecular SET of **299**, underwent amine transfer to a radical-cation and further SET to the Cu(II) core generated Cu(I) species **301**. The desired product was released and iodine-mediated anodic reoxidation of Cu(I) to Cu(II) guaranteed the catalytic cycle.

During the same period, Kathiravan, Nicholls and co-workers also described C–H amination with AQ-directed benzamide through a synergistic combination of copper catalysis and electrocatalysis under mild conditions (Scheme 24).[81] By employing excess additive NaOAc (4 equiv.), a series of benzamides and secondary cyclic amines successfully generated the corresponding products **283**. It is worth noting that coupling fragments of established significance in pharmaceutical chemistry (buspirone **302**, haloperidol **303**, and amoxapine **304**) as well as acyclic *N*-methylamine drug derivatives fluoxetine **305** were applied smoothly by using electricity as a green oxidant.

The preliminary mechanism was proposed. Firstly, anodic oxidation of Cu(II) precatalyst **306** resulted in Cu(III) species

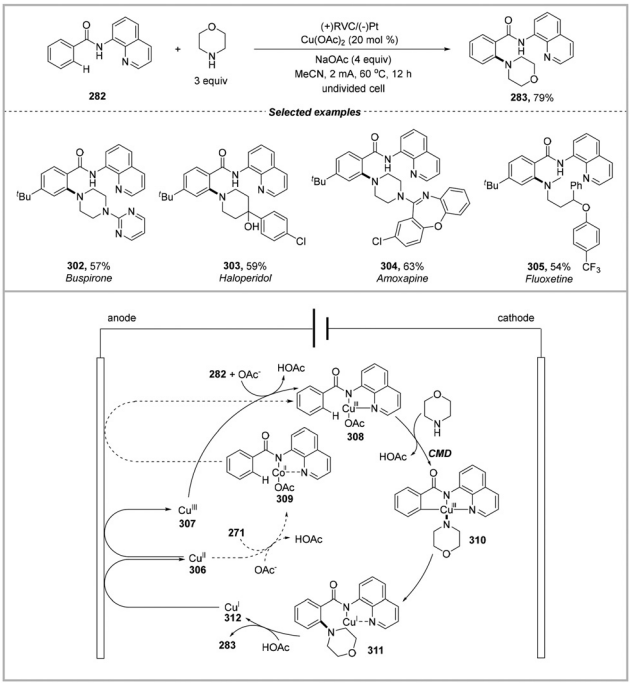

Scheme 24 Copper-catalyzed electrochemical C–H amination with the AQ-directed benzamide.

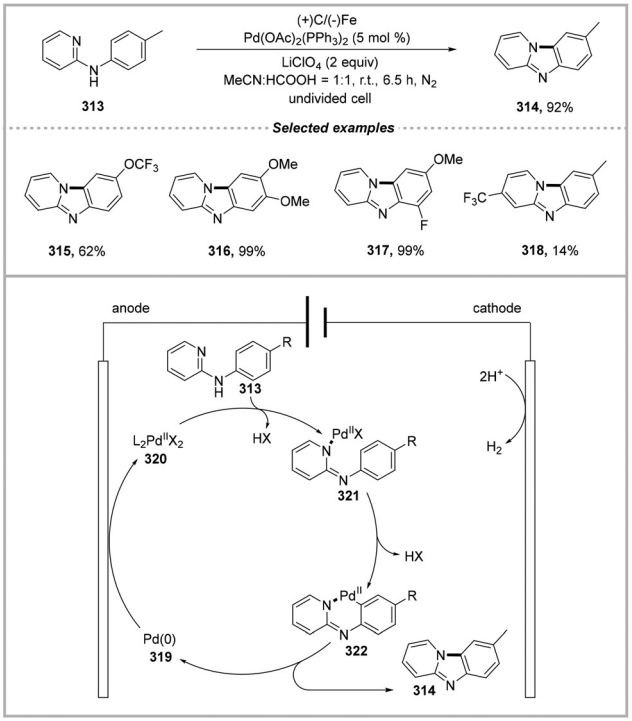

Scheme 25 Palladium-catalyzed electrooxidative C–H amination for pyrido[1,2-α]benzimidazoles.

307 and its further acetate-assisted coordination with AQ-directed benzamide **282** gave Cu(III) intermediate **308**. The reversed sequence of anodic oxidation and coordination through **309** could be a compatible pathway. Next, the CMD process, namely nucleophilic attack of amine and deprotonation, led to Cu(III)-complex **310**. Finally, Cu(I)-complex **311** was generated, along with a C–H amination process, and subsequent anodic oxidation of released Cu(I) **312** to Cu(II) species **306** indicated a sustainable catalytic cycle by achieving the desired product **283**.

3.2 Metallic electrooxidative C–H/N–H annulations

In 2020, Lei and co-workers reported a palladium-catalyzed electrooxidative intramolecular C–H amination annulation reaction without an external stoichiometric oxidant, which represented the first example of the synthesis of pyrido[1,2-α]benzimidazoles without copper among transition-metal catalysis (Scheme 25).[82] During the optimization of the conditions, the choice of electrode material played a vital role, namely an anodic carbon cloth plate and cathodic Fe plate gave the highest isolated yield of 92% product **314** with CH_3CN/HCOOH mixed solvent. Evaluation of the substrate scope showed that electron-rich substrates **315–317** reacted better than the electron-poor one **318**, indicating a palladium-catalyzed electrophilic metalation mechanism.

In mechanistic studies and CV experiments, the lower oxidation peak of $Pd(PPh_3)_4$ than *N*-(*p*-tolyl)pyridin-2-amine **313** revealed that Pd(0) **319** may be oxidized before **313**. A probable mechanism was proposed. Firstly, Pd(II) species **320** coordinated with substrate **312**, and then a two-step acetate-assisted electrophilic deprotonation process occurred to generate intermediate **321** and **322** in sequence. Next, reductive elimination of Pd(II) intermediate **322** gave the desired product **314** by releasing Pd(0) **319**. Anodic oxidation of Pd(0) to Pd(II) and cathodic reduction of proton to H_2 ensured the continuity of the electrocatalytic cycle.

In 2021, Zhang, Lei and co-workers reported a palladium-catalyzed electrooxidative intramolecular cross-dehydrogenative coupling (CDC) reaction for C–H amination with 2-amidobiaryls (Scheme 26).[83] Compared with the developed methods, the electrochemical strategy could facilitate the reduction elimination process smoothly by merging electrons as traceless reagents under mild conditions without a stoichiometric amount of oxidant or expensive photoredox catalyst. During the optimization of the conditions, the decreased yield of 9% and 29% product **323** in the absence of palladium catalyst and 4-methylbenzenesulfonic acid (*p*-TsOH), respectively, revealed the pivotal mediating role of the transition metal in the synergistic catalytic system, rather than the single electrode-mediated process. Evaluation of the substrate scope showed that electron-rich substrates **324** were more prone to react than those with electron-withdrawing groups **325**. Other arenes such as thienyl **326** and *N*-substituted substrate **327** also performed well in the reaction. The scaled-up reaction with a cheaper graphite rod cathode also gave 1.56 g target carbazole **323** in 56% yield. In mechanistic studies, KIE experiments indicated that cleavage of the C–H bond might not be involved in the rate-limiting step. Meanwhile, considering the ambient

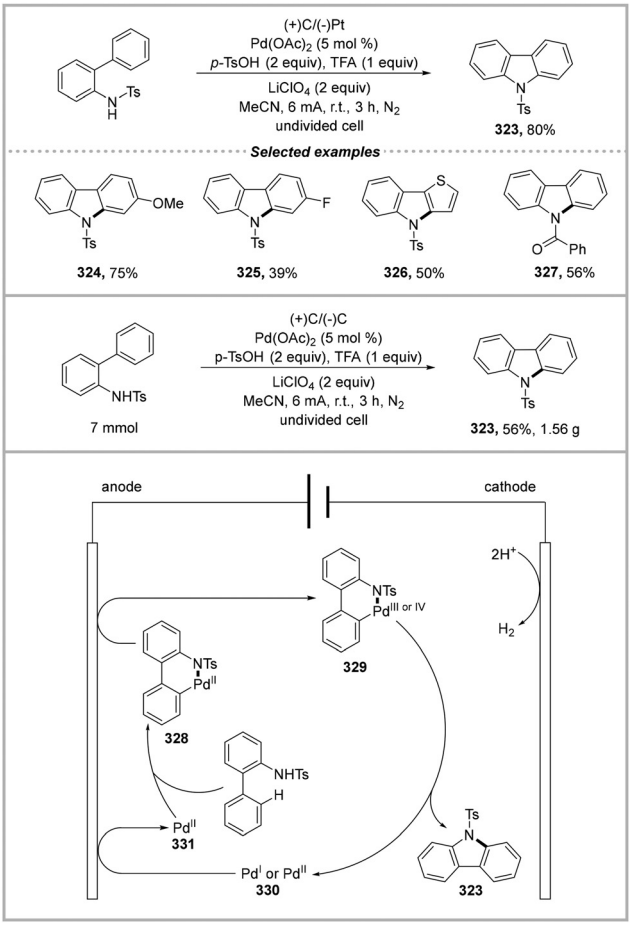

Scheme 26 Palladium-catalyzed electrochemical intramolecular C–H amination for carbazoles.

temperature employed in this electrochemical catalysis and the fact that high-valent Pd(III) or Pd(IV) facilitates reduction elimination with strong oxidants, a hypothetical mechanism was proposed. Initially, six-membered palladacycle **328** was obtained through amine coordination and *p*-TsOH-assisted C–H activation. Next, anodic oxidation of **328** generated oxidative Pd(III) or Pd(IV) palladacycle intermediate **329**. Pd(I) or Pd(II) species **330** was released after subsequent reductive elimination with the desired product, which further oxidized to Pd(II) **331** at the anode to initiate a new catalytic cycle. Concomitant cathodic reduction reaction with the detected proton reduction product H_2 guaranteed the continuity of the electrocatalytic cycle.

In 2022, Ni, Huang, Ackermann and co-workers reported a rhodium-catalyzed electrooxidative [5 + 2] C–H/N–H annulation for rarely reported seven-membered azepino[3,2,1-*hi*] indoles with alkynes **333** and 7-arylindoles **332** (Scheme 27).[84] The reaction system avoided stoichiometric chemical oxidants such as hypervalent iodine(III) reagents, as well as copper(II) and silver(I) salts for the regeneration of high-valent catalyst species in the conventional strategy. During the optimization of the conditions, the reaction was highly sensitive to the

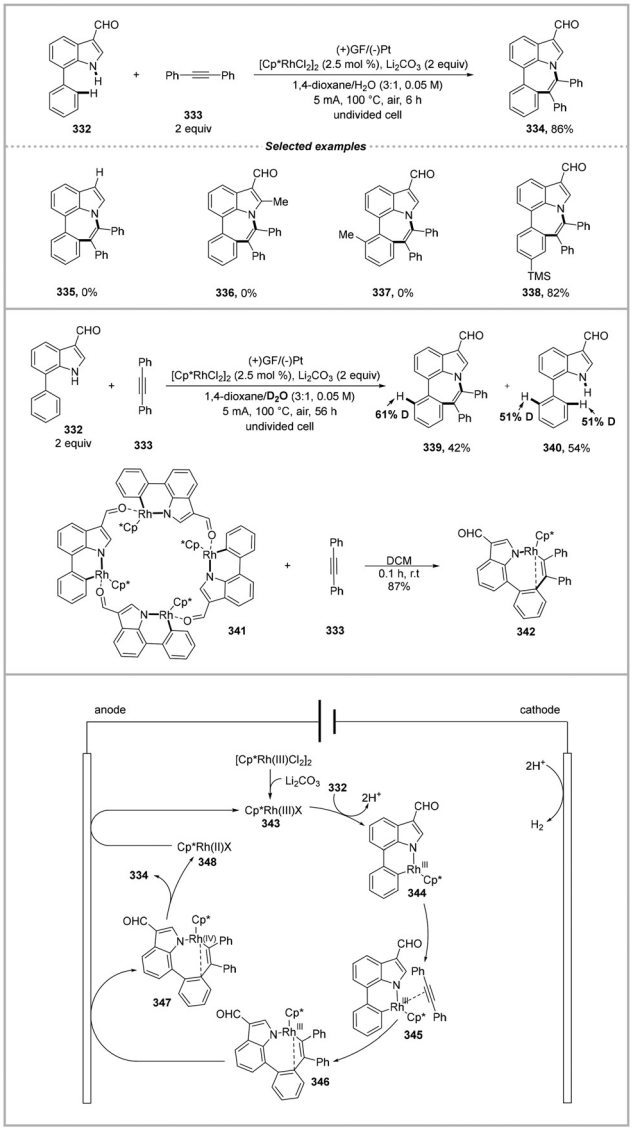

Scheme 27 Rhodium-catalyzed electrochemical [5 + 2] C–H/N–H annulation.

$[Cp^*RhCl_2]_2$ catalyst, Li_2CO_3 additive and 1,4-dioxane solvent. Meanwhile, the 3-formyl on the indole ring was essential to achieve the successful transformation. Evaluation of the substrate scope showed that substituents at the 2-position of the indole ring or the benzene ring disabled the reaction (**335–338**) and this electrolytic protocol generally provided a superior performance to the conventional reoxidation strategy ($[Cp^*RhCl_2]_2/Ag_2CO_3$) in terms of yield.

In mechanistic studies, the deuterium-labeling and competition experiments suggested reversible C–H cleavage and the obvious electronic effect from the 7-aryl group of substrate **332**, respectively. Meanwhile, X-ray crystallography of tetrameric six-membered cyclometalated rhodium(III) complex **341** from C–H activation of **332** indicated the coordination role of the carbonyl oxygen to rhodium and the eight-membered cyclometalated rhodium(III) crystal **342** further revealed the

kinetically and thermodynamically unfavorable two-electron reductive elimination process, as it maintained its stability even at 130 °C. Importantly, the X-ray photoelectron spectroscopy (XPS) results suggested both the reduction elimination process of the Rh(IV) intermediate to Rh(II) species and the reoxidation of low valent state rhodium(II) to Rh(III). Namely, it existed an oxidation-induced reductive elimination within the Rh(III/IV) regime, where the irreversible oxidation peak at E_p = +0.349 V (*vs.* Fc/Fc^+) in the CV experiments and lower energy barrier of 6.7 kcal mol^{-1} in the DFT calculations further confirmed the results.

A probable mechanism was proposed. Firstly, in the presence of the additive, six-membered cyclometalated Rh(III) species **344** was generated through subsequent N–H/C–H cleavage with active rhodium(III) species **343**, which then coordinated with alkyne to induce migratory insertion to generate eight-membered cyclic Rh(III) species **346**. Next, anodic oxidation-induced reductive elimination of **347** gave the product through an Rh(III)/Rh(IV)/Rh(II) catalysis sequence. Finally, the release of H_2 at the cathode and regeneration of **343** from the anodic oxidation of Rh(II) species **348** completed the catalytic cycle.

In 2025, Ackermann, Mo and co-workers reported an efficient rhodium-catalyzed electrooxidative C–H/N–H annulation with *N*-pyridinyl benzamide pharmacophores and alkynes (Scheme 28).[85] A range of medicinally relevant structures were synthesized with the convergence of metal catalysis and electrosynthesis, avoiding the use of toxic and waste-generating stoichiometric oxidants, such as copper(II) and silver(I) salts in the classical method. During the optimization of the conditions, the sodium pivalate (NaOPiv) additive and electricity input were essential to promote the reaction with the Rh(III) catalyst $[Cp^*RhCl_2]_2$. Meanwhile, the mixed solvent hexafluoroisopropanol (HFIP)/H_2O (3 : 1) gave the best catalytic performance. This strategy showed excellent tolerance toward *N*-pyridinyl-substituted benzamides and a variety of diaryl-, dialkyl-, and unsymmetric alkynes, such as high efficiency for *ortho*-substituted benzamide **350**, excellent regioselectivity with *meta*-substituted benzamide **351**, naphthamide **352** and unsymmetrically substituted alkynes **352–354**. Surprisingly, 1,4-butynediol also proceeded smoothly with tandem dehydroformylation/dihydroxylation product **355**. The late-stage functionalization of bioactive molecules **356–357** also revealed its superiority over conventional strategies owing to its selectivity and mild conditions.

In mechanistic studies, the deuterium-labeling, KIE and competition experiments indicated reversible C–H cleavage and the electron-deficient benzamide was conducive to the C–H metalation process. DFT calculations revealed the possible N–H/C–H activation processes as well as the rate-determining reductive elimination step. A probable mechanism was shown, as follows. Firstly, with the assistance of $OPiv^-$, active catalyst $Cp^*Rh(III)(OPiv)_2$ **359** coordinated with the pyridine ring of *N*-pyridinyl benzamide **348** to induce consecutive N–H/C–H activation. Generated rhodium(III) species **360** further coordinated with alkyne to give thermodynamically stable seven-membered cyclic Rh(III) species **362** through migratory insertion. Then, upon the coordination of the directing group, more exergonic Rh(III) species **363** underwent reductive elimination (energy barrier of 25.1 kcal mol^{-1}) to give final product **349**. However, anodic oxidation-induced reductive elimination through the Rh(III)/Rh(IV)/Rh(II) catalysis sequence was not explicitly stated.

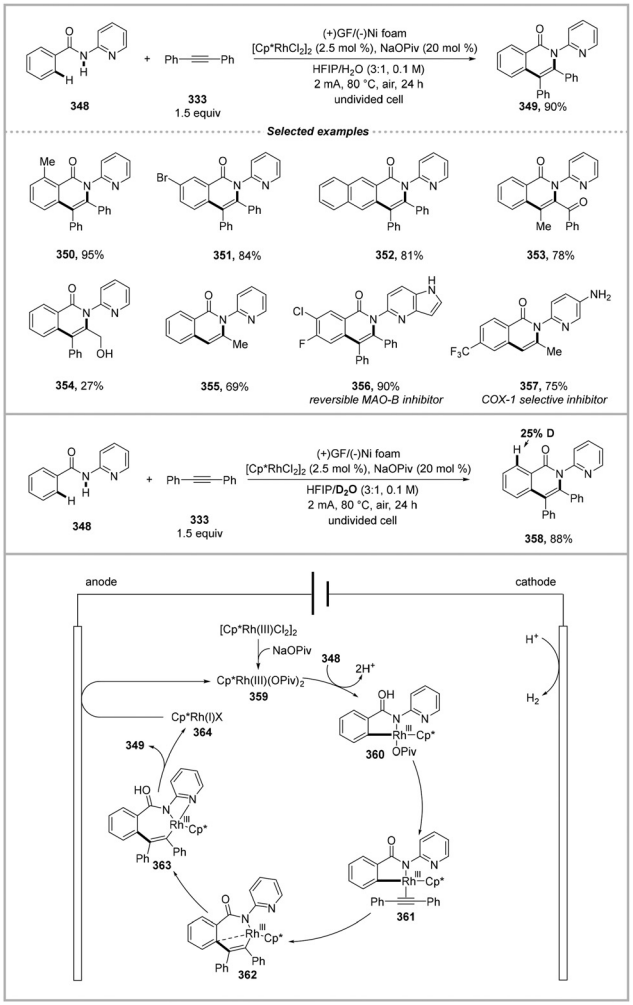

Scheme 28 Rhodium-catalyzed electrochemical late-stage C–H/N–H annulation.

4. Metallic electrooxidative couplings for C–N bond formation

Oxidative couplings have emerged as a powerful mechanism for C–N bond formation.[35,86] Among them, transition metal catalyzed oxidative amination represents the most important strategy,[87] mainly including directed or non-directed oxidative cross-dehydrogenative coupling (CDC), Chan–Lam C–N couplings, and oxidative carbonylative and decarboxylation couplings. With the development of electrocatalysis, the facilitated high-efficiency in the rate-determining steps of elementary

reactions ensured the achievement of mild conditions without strong oxidizing agents and high temperature. This section mainly summarizes the recent advances in metallic electrooxidative C–N bond formation.

4.1 Cu-catalyzed electrooxidative C–N couplings

4.1.1 Chan–Lam C–N couplings. Copper-catalyzed oxidative Chan–Lam coupling represents a modified strategy for C–N coupling at room temperature under weakly basic conditions. However, its limited applicability in the synthetic community is mainly attributed to several deficiencies in the catalytic cycle, such as turnover-limiting transmetalation step of Cu catalyst with electron-deficient boronic acids, slow ligand exchange rate with weak nucleophilic electron-deficient anilines, stoichiometric exogenous oxidant and competitive oxidation of amine substrates. Thus far, great efforts have been made to expand the substrate adaptability, but the necessary chemical oxidants could not be avoided.[88] Catalytic electrooxidative methodologies would be an alternative pathway and the key modification mainly focused on the adjustment of the redox potential, inhibited cathodic reduced catalyst deposition and improved electron transfer kinetics.[89] In this section, Cu-catalyzed electrooxidative Chan–Lam C–N couplings are described to overcome the limitations caused by chemical oxidants and cathodic reduction to achieve greener and more widespread synthesis.

In 2019, Gale-Day and co-workers developed an electrochemically promoted copper-catalyzed Chan–Lam amination coupling in an undivided cell under air (Scheme 29).[90] Both a copper anode and cathode were employed to sustain the homogeneous catalysis and the current was reversed every 10 min, namely electrode switching between two copper thin films, to avoid electrode spoiling by continuously stripping Cu species. During the optimization of the conditions, 2,6-lutidine (1.2 equiv.) and triethylamine (0.2 equiv.) significantly increased the yield of product **365** to 98%, which could be preliminarily explained by the lower oxidation potential of Cu(I) with 2,6-lutidine and triethylamine being favorable for its oxidation to Cu(II). Meanwhile, the significantly reduced yield of 54% with no current revealed that electrocatalysis observably facilitated the classical Chan–Lam reaction. Furthermore, the inhibited reaction activity with no copper precatalyst guaranteed the mediating role of copper rather than an electrode-mediated process. This novel electro-promoted catalytic system effectively resolved the defects of incompatible electron-deficient boronic acids and weak nucleophilic aniline substrates **366–369** and a key factor for success was attributed to the mild potential employed, which was typically demonstrated in the smooth reaction with nitro-substituted boronic acid **369** ($E^{red}_{1/2}$ = −1.19 V *vs.* SCE).

In mechanistic studies, CV studies provided a large amount of reaction information with the results including: (1) excluding the direct anodic oxidation process of Cu(II) to Cu(III) intermediate. (2) The direct reduction of Cu(II) was unlikely to be the redox active species. (3) The Cu(I)/Cu(0) redox couple occurred by stripping of the Cu(0) thin film from the electrode

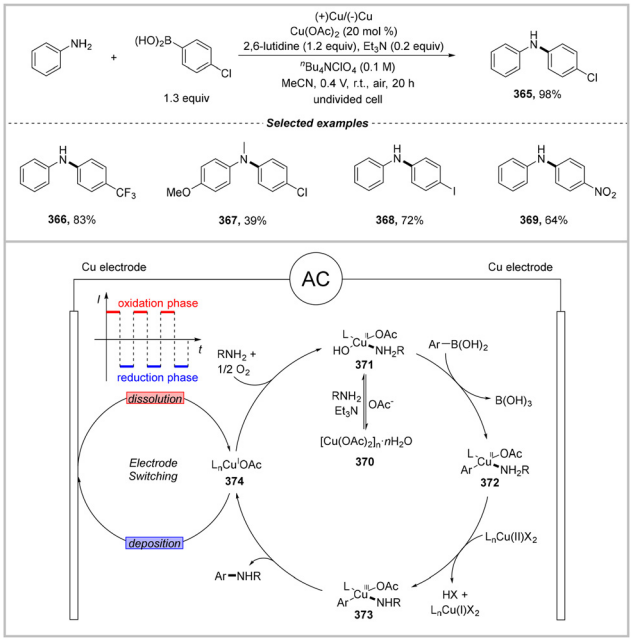

Scheme 29 Copper-catalyzed electrochemical Chan–Lam amination by electrode switching.

surface. (4) 2,6-Lutidine played a key role in reducing the oxidation potential of the Cu(I) species together with the minor role of triethylamine, promoting subsequent aerobic oxidative to Cu(II) species. (5) Removal of the Cu(I) species from the reaction mixture was beneficial for improving the reaction yield and reducing by-products. These CV results were consistent with the conclusions of the experimental optimization.

A probable mechanism was proposed. Firstly, Cu(II)X–amine complex **371** was produced by amine nucleophilic attack to the initial Cu(II)X_2 precatalyst **370**, which underwent transmetalation with the aryl boronic acid coupling partner to give Ar–Cu(II)X–NH_2R intermediate **372**. Next, high-valent Ar–Cu(III)X–NHR **373** was achieved by disproportionation and deprotonation, followed by the generation of Cu(I)X species **374** and the desired product *via* reductive elimination. One step ahead of the thermodynamic Chan–Lam amination with the reoxidation of **374** to **371**, the less stable Cu(I)X species **374** was further plated to the cathode, forming a Cu(0) film, which could diminish by-product formation caused by Cu(I) and increase the yield. Meanwhile, by reversing the current every 10 min, Cu(I) was obtained by the oxidation of the Cu(0) film at the new anode, which next generated Cu(II) through subsequent oxygen oxidation. However, going back to Cu(0) by plating to a new cathode would be a process of balance.

In the aforementioned reaction, as more subsequently generated high-valent Cu(III) species by disproportionation could accelerate the reaction rate with high substrate conversion and product yield, the successful introduction and transformation of low nucleophilic anilines and electron-deficient boronic acids with a catalytic loading of copper salts was mainly attributed to the increased concentrations of Cu(II) species. The

lower oxidation potential of Cu(I) with 2,6-lutidine and triethylamine (probably regarded as ligands) facilitated this process, making it more conducive to be oxidized to Cu(II) species. Meanwhile, the periodic and gradual release of Cu(I) species, namely the interconversion between Cu(0) and Cu(I) by electrode switching, would efficiently inhibit side-product formation and avoid the ineffective consumption of the boronic acid partner. However, the role of electrocatalysis in this reaction was limited to increasing the catalytic turnover and reducing the negative impacts from the Cu(I) species. Though stoichiometric oxidants could directly promote high-valent organometallic intermediates to accelerate the reaction by rapid reductive elimination, excessive oxidation of the substrates was often unavoidable, which prevented the ubiquitous application of Chan–Lam couplings on a large scale. Thus, the advanced development of reaction systems should focus on catalytic conversion under mild conditions without both stoichiometric oxidants and modulated organometallic oxidation potential from the perspective of ligands.

A breakthrough was achieved by Sevov and co-workers in 2021, and the first example of Chan–Lam coupling to form C–N bonds in the absence of stoichiometric oxidants was developed with a new electrooxidative ligandless copper-catalyzed reaction system in an undivided cell (Scheme 30).[91] At the beginning of the reaction, the major challenges were attributed to the kinetically slow anodic oxidation of ligandless Cu(I) and preferential cathodic reduction of Cu(II) ($E_{1/2}$ = −0.8 V *vs.* Fc/Fc^+). Competitive anodic oxidation of amine substrates ($E_{1/2}$ = +0.5 V *vs.* Fc/Fc^+) as well as plated Cu(0) and inhibited H_2 generation on the cathode prevented the reaction from occurring. Encouragingly, a mediator-assisted homogeneous electron transfer strategy was perfectly designed to resolve the above-mentioned problems under a very mild oxidation potential, which has become a great alternative to the electrode switching strategy proposed by Gale-Day.[90] Appropriate and precise screening of the redox potential revealed that ferrocene (Fc) mediator dramatically improved the yield of product **375** to 47% and the preoxidized salt ferrocenium hexafluorophosphate ($Fc^+PF_6^-$) could result in 81% isolated yield with a high conversion of amines.[32,92] The decreased yields and conversions under air without electrochemistry or mediator further highlighted their important role in Cu-catalyzed Chan–Lam reactions. The reaction demonstrated excellent compatibility towards aryl- **376**, heteroaryl- **377–378** or even alkylamines **379–380** under quite mild reaction conditions. It is worth noting that electron-deficient boronic acids **381–382** were coupled in high yields with the opposite trend in reactivity, and no oxygenation or dimerization by-products were detected.

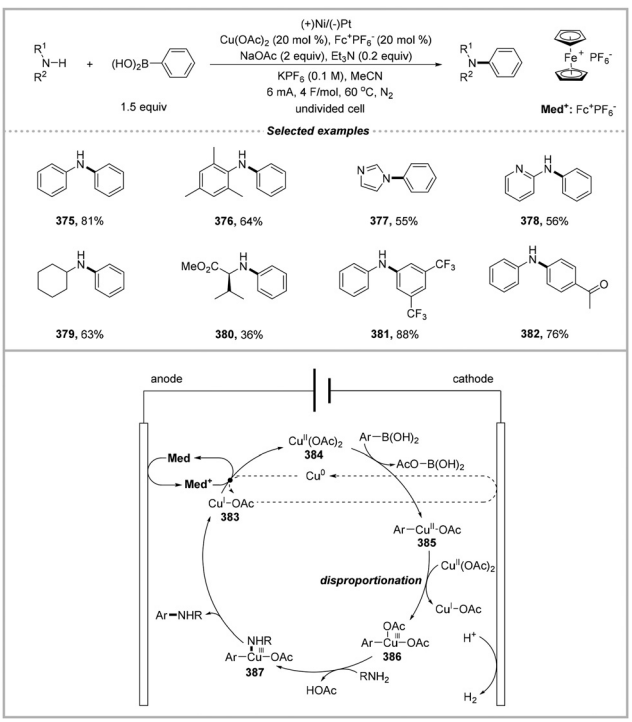

Scheme 30 Copper-catalyzed mediator-assisted electrochemical Chan–Lam amination.

In mechanistic studies, the interaction between Fc^+ and Cu (I) was clearly expressed in the CV studies. In summary, Cu(I) could not be directly oxidized to Cu(II) without Fc^+ under the reaction conditions. Meanwhile, elemental analysis and scanning electron microscopy (SEM) of the cathodic surfaces revealed the exclusive role of the mediator in stripping plated Cu(0) away from cathode to obtain a clean Pt surface for proton reduction and regeneration of Cu(II) species. Furthermore, in contrast to the anodic oxidation potential of +0.8 V (*vs.* Ag/Ag^+) during the unmediated reactions, the lower oxidation potential +0.2 V (*vs.* Ag/Ag^+) for the Fc^+ mediator in this optimized catalytic system completely prevented the oxidation of the amine substrates.

A completely new designed reaction mechanism was proposed. Initially, Cu(II) species **384**, generated from ferrocenium-mediated anodic oxidation of Cu(I)X species **383**, underwent transmetalation with aryl boronic acid and disproportionation with $Cu(OAc)_2$, giving Ar–Cu(III)X_2 intermediate **386**. Subsequently, the obtained Ar–Cu(III)X–NHR **387** from *N*-attack of amine and deprotonation of **386** gave the desired product and Cu(I)X species **383** *via* reductive elimination. The plated Cu(0) film on the cathode as well as less stable **383** were both reoxidized to **384** to finish the catalytic cycle. It should be highlighted that the mediator served multiple key roles during electrolysis, including: (1) an electrochemically generated oxidant to maintain high Cu(II) concentrations. (2) A stripping agent to regenerate the active Cu catalyst and reveal the active Pt surface for proton reduction. (3) An overcharge protector to prevent undesirable anodic reactions.

4.1.2 Non-directed cross-dehydrogenative C–N couplings. Non-directed cross-dehydrogenative C–N couplings, namely direct C(sp^3)–H amination, represent the most concise way for constructing nitrogen-containing skeletons with hydrocarbons and amines. The conventional protocols with stoichiometric oxidants always faced challenges including harsh reaction conditions and limited substrate scope.[93] Current research is mainly

focused on the radical-mediated hydrogen atom transfer (HAT) strategy, capturing the generated carbon-centered radical intermediates with transition-metal-catalyzed platforms.[94] Meanwhile, electrochemistry provides a green redox reagent with electrons, which exhibits superiority to overcome the high oxidation potential of alkanes under mild conditions. In this section, Cu-catalyzed electrooxidative cross-dehydrogenative C–N coupling is described to give a green synthetic protocol.

In 2025, Xia and co-workers developed a novel photoelectrochemical (PEC) copper-catalyzed C(sp^3)–H amination with unactivated hydrocarbons and N-heterocycles (Scheme 31).[95] The conventional graphite rod anode and platinum plate cathode were employed and photoelectro-induced direct hydrogen atom transfer (*d*-HAT) of alkane was proven to be the crucial catalytic cycle to give oxidative coupling product **389**.

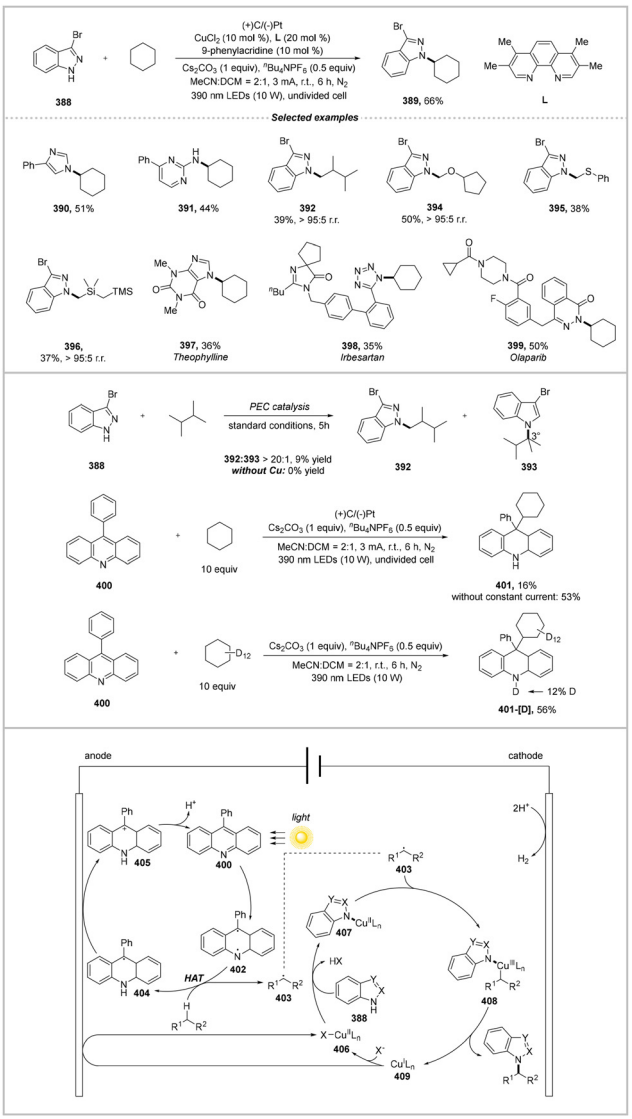

Scheme 31 Copper-catalyzed photoelectrochemical cross-dehydrogenative amination.

During the optimization of the conditions, a light source with a wavelength of 390 nm and photocatalyst 9-phenylacridine **400** were carefully selected to achieve a high isolated yield of 66%, and aerobic conditions were compatible, though with lower yield. The reaction showed broad scope for N-heterocycles **389–390**, (hetero)arylamine **391** and bioactive pharmaceutical agents, such as theophylline **397**, irbesartan **398** and olaparib **399**. It is particularly worth noting that the site-selective characteristics of alkanes **392–393** during amination were unique, which differed from the previously reported tertiary C–H activation. Meanwhile, steric hindrance played a key role in affecting the amination regioselectivity for acyclic alkanes, and α-amination of ethers **394** proceeded smoothly with complete site selectivity. This catalytic system could also be extended to other alkanes containing sulfur **395** and silicon atoms **396**, which exhibited superiority over the scope of peroxide-based C(sp^3)–H amination reactions.

In mechanistic studies, radical scavenger and electron paramagnetic resonance (EPR) experiments both indicated the formation of an alkyl radical. Meanwhile, the photoelectrochemical HAT process between the nitrogen radical of excited 9-phenylacridine was proven by the capture of **401**, and the isotopically labeled product **401-[D]** with deuterated cyclohexane further confirmed this result. Subsequent KIE experiments explained the turnover-limiting step role of the HAT process in the overall reaction. Interestingly, the absence of the desired product **392** of 2,3-dimethylbutane (DMB) with no copper salts indicated that copper-mediated coupling was decisive in the PEC amination. A divided-cell experiment with product around the graphite rod anode also revealed an anodic oxidative C(sp^3)–H amination process.

A plausible reaction mechanism of PEC C–N coupling was proposed. Nitrogen radical species **402** was produced with photoexcited 9-phenylacridin, which next induced a HAT process with unactivated alkane to alkyl radical **403** and triarylmethyl radical **404**. Subsequent anodic oxidation gave triarylmethyl cation **405** and regenerated 9-phenylacridine by elimination and deprotonation. Simultaneously, amine attack and deprotonation of **388** to Cu(II)X_2 species **406** generated Cu(II)X–amino complex **407**, followed by capturing alkyl radical **403** to gain alkyl–Cu(III)X–amino species **408**. Finally, Cu(I)X species **409** was released with the generation of the desired PEC C–N coupling product by reductive elimination. Additional anodic oxidation of **409** to **406** and cathodic reduction of proton to H_2 closed both catalytic cycles.

4.1.3 Photoelectrooxidative decarboxylative C–N couplings. Transition metal-catalyzed decarboxylative amination enables the modular synthesis of alkyl anilines with the corresponding carboxylic acids, in which oxidation of amine substrates is often competitive under stoichiometric chemical oxidants. Late-stage synergistic metallic photoredox catalysis often requires limited activated carboxylic acid,[96] while electrochemistry could avoid these problems through direct anodic oxidation (sometimes combined with other technologies). In this section, Cu-catalyzed photoelectro-oxidative C–N couplings are described to express a direct decarboxylation pathway.

In 2025, Shang and co-workers developed an elegant modular assembly of aniline bioisostere amino-BCP through a photoelectrochemical (PEC) decarboxylative C(sp^3)–N coupling process (Scheme 32).[97] This reaction merged the cooperative ligand-to-metal charge transfer (LMCT) process with copper-catalyzed reductive elimination during amination. Undoubtedly, LMCT photocatalysis for BCP (bicyclo[1.1.1] pentane) radical represented the key issue of the reaction and the significantly reduced anodic oxidation potential compared with direct oxidative decarboxylation not only prevented the oxidation of amine coupling partners but also avoided the probable skeletal rearrangement of small-ring cage BCP carbocations after anodic overoxidation. Meanwhile, the electrochemical potential instead of stoichiometric chemical oxidants in this crucial redox event resulted in very mild reaction conditions, which demonstrated high substrate compatibility and applicability with access to heterocyclic amines **411–412**, previously inaccessible saturated bioisosteres of *para*-, *meta*-, *ortho*-substituted anilines **413–416**, as well as decarboxylative amination of primary and secondary alkyl carboxylic acids **417–419**, respectively.

Mechanistic studies revealed that the anodic oxidation potential of Fe(II) complex was around +0.04 V and the generated Fe(III) species initiated the LMCT process with BCP acid. Moreover, the addition of amine was very beneficial for the oxidation of Cu(I)X–amine to Cu(II)X–amino by reducing the oxidation potential to approximately +0.52 V (*vs.* Ag/Ag^+), and Et_3N promoted this process well. A probable mechanism was proposed. Initially, single-electron anodic oxidation of Fe(II) species **420** and Cu(I)X **423** produced Fe(III) complex **421** and Cu(II)X–amino **424**, respectively. Under irradiation, BCP alkyl radical **422** was released through LMCT homolysis of Fe–OCOR bond in **421**, which next captured **424** to produce high-valent R–Cu(III)X–amino intermediate **425**. Subsequent reductive elimination gave the desired amination product, accompanied by hydrogen evolution through proton reduction at the cathode.

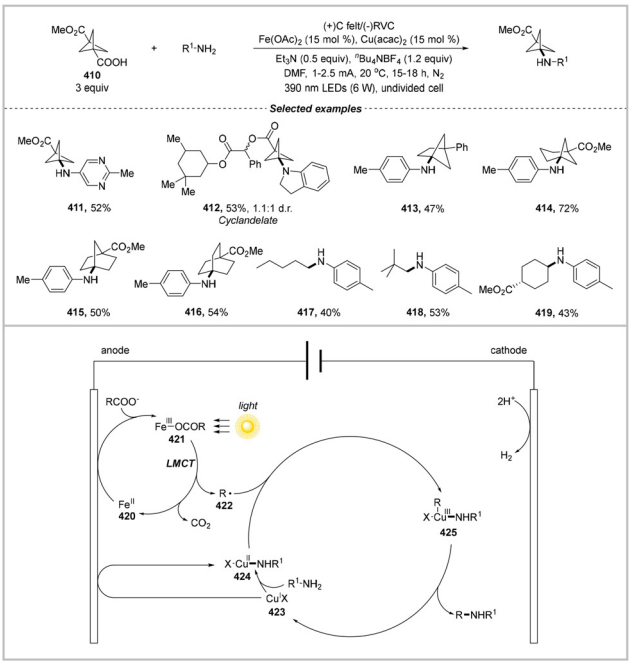

Scheme 32 Copper-catalyzed photoelectrochemical decarboxylative amination.

4.2 Pd-catalyzed electrooxidative carbonylative C–N couplings

Transition metal-catalyzed oxidative carbonylation reactions provide a general method for building amide compounds. The conventional strategies often employed benzaldehydes, carbamoyl chlorides or esters as the carbonyl source, which often suffer the drawbacks of explosive peroxide oxidants and stoichiometric base.[98] Current research is focused on direct oxidative amidation using CO and O_2 as the carbonyl source and oxidant, respectively,[99] while an oxidant-free catalytic system is simultaneously highly required for green synthesis. In this section, metallic electrooxidative carbonylative C–N couplings with no exogenous oxidant are described.

In 2020, Chen, Lei and co-workers reported the electrochemical palladium-catalyzed oxidative aminocarbonylation of alkynes with carbon monoxide under atmospheric pressure in an undivided cell (Scheme 33).[100] This oxygen-free catalytic system demonstrated significant advantages over the developed aerobic palladium-catalyzed oxidation coupling reactions, such as avoiding the ambient explosion risk of the CO/O_2 mixture gas and excellent substrate compatibility with room temperature. During the optimization of the conditions, a controlled potential mode had been separately optimized for the coupling with primary and secondary amines as well as ammonium salts. The reaction demonstrated a broad scope with respect to the substitution patterns and electronic properties of the alkynes, where primary amines **426–427**, cyclic amine **428**, secondary acyclic amine **429** and NH_4NO_3 afforded the rare 3-phenylpropiolamide **430–431** directly with the highest efficiency at 75 °C.

In mechanistic studies with CV experiments, the appropriate applied potential of 0.5 V (*vs.* AgCl/Ag) was decisive for the success of the reaction. All the carbonylation reaction participants, including phenylacetylene, cycloheptylamine, Et_3N, P(*p*-Tol)$_3$, and Pd(MeCN)$_2$Cl$_2$ could not be directly oxidized. Meanwhile, the phosphine ligand and ^{n}BuOH both prevented the direct reduction of the Pd(II) complex and affected the oxidation potential of Pd(0) under a CO atmosphere. The kinetic experiment with *in situ* infrared spectroscopy indicated that anodic oxidation influenced by the anode surface area and concentration of the palladium catalyst was the rate-determining step (RDS) rather than the diffusion of CO. Kinetic isotope effect (KIE) experiments with deuterated phenylacetylene also excluded the RDS role of C–H bond cleavage. The next quick-scanning X-ray absorption fine structure (QXAFS) spectroscopy studies indicated that primary amines rather than phenylacetylene influenced the structure of the palladium complex in the early stage. The X-ray absorption near-edge structure (XANES) and the extended X-ray absorption fine structure

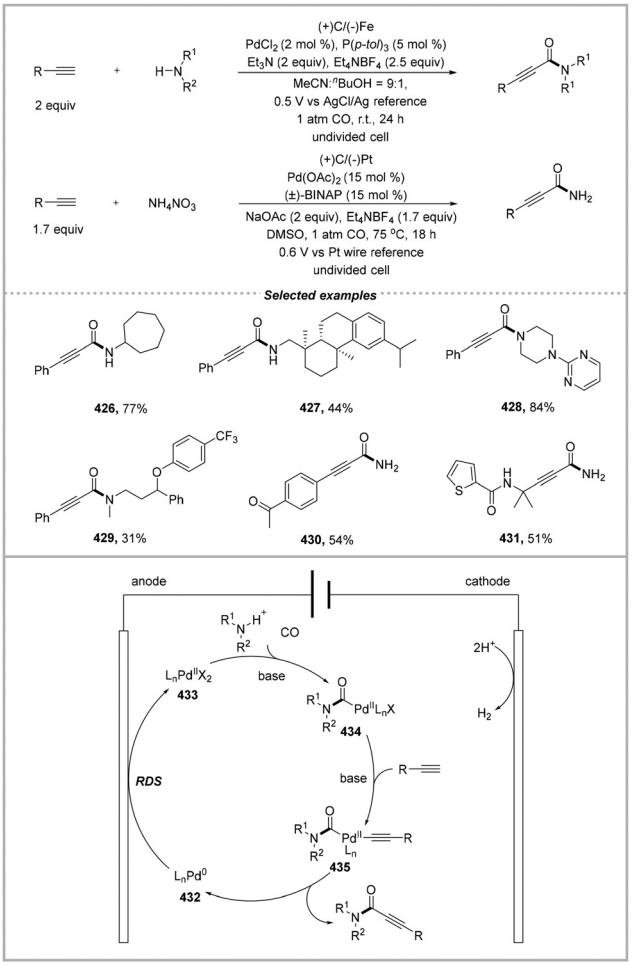

Scheme 33 Palladium-catalyzed electrochemical oxidative aminocarbonylation.

(EXAFS) spectra also provided evidence for the reduction elimination of the Pd(II) complex during the formation of 2-ynamide. Lastly, the intermediate synthesis experiment indicated that the carbamoyl palladium intermediate was facile for subsequent palladium acetylide formation.

A probable mechanism was proposed. In the initial stage of the reaction, carbamoyl intermediate **434** was formed through aminopalladation and CO insertion of Pd(II) species **433** with amines and base, which then reacted with alkyne to generate palladium acetylide **435**. Subsequent reductive elimination afforded the desired product by releasing Pd(0) species **432**. Finally, the rate-determining anodic oxidation of **432** to Pd(II) species **433** and cathodic reduction of proton to H_2 finished the whole electrocatalytic cycle.

4.3 Ni-catalyzed electrooxidative asymmetric cross-dehydrogenative C–N couplings

Transition metal-catalyzed cross-dehydrogenative couplings (CDC) provide a direct approach to C–N bonds with C–H or N–H coupling partners. However, stoichiometric chemical oxidants are often required, limiting the efficient conversion.[101] The mild transformation of CDC amination has been gradually reported under transition metal-assisted or metal-free conditions, especially with electrocatalysis.[102] In this section, asymmetric metallic electrooxidative cross-dehydrogenative aminations are described.

In 2023, Guo and co-workers reported the pioneering electrooxidative nickel-catalyzed enantioselective cross-dehydrogenative amination of acylimidazoles with various nitrogen

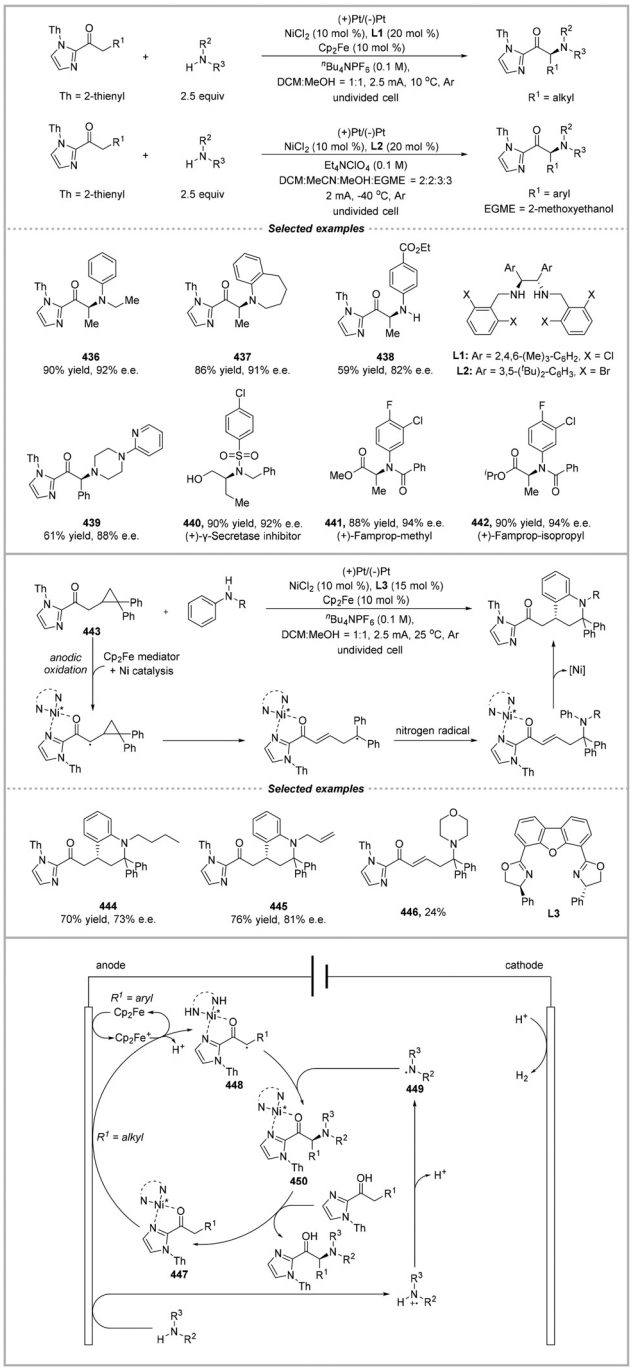

Scheme 34 Enantioselective nickel-catalyzed electrochemical cross-dehydrogenative amination.

nucleophiles as coupling partners to access α-amino carbonyls (Scheme 34).[103] Stereoselective assembly between the anodic oxidative nickel-bound α-keto radical species and aminyl radicals provided a radical–radical coupling pattern to C(sp^3)–N bond formation. During the optimization of the conditions in an undivided cell under a constant current of 2.5 mA at 25 °C, chiral diamine ligand **L1** was successfully employed and lower temperature 10 °C was proven to be the optimal conditions, with 90% yield and 92% enantiomeric excess of product **436**. This stereo-controlled cross-dehydrogenative amination demonstrated excellent compatibility towards primary/secondary (cyclic) amine **436–438** as well as α-alkyl/aryl-substituted acylimidazoles **439** with high enantiomeric excess up to 96%. More importantly, enantio-enriched pharmaceutical and agricultural compounds could be directly late-stage synthesized through the anodic oxidative amination strategy without any loss of enantioselectivity, including (+)-γ-secretase inhibitor **440** and (+)-flamprop-methyl/isopropyl **441–442** from α-amino acylimidazoles.

In mechanistic studies with CV experiments, the significantly decreased onset oxidation potential of α-phenylacylimidazole from +1.27 V to +0.48 V (*vs.* SCE) with the chiral nickel catalyst indicated the formation of a nickel-bound α-keto intermediate. Meanwhile, the interaction between morpholine and the nickel catalyst was not obvious, as the onset oxidation potential of amine was maintained at +0.90 V (*vs.* SCE). The successful amination after controlled potential electrolysis indicated that the α-keto radical and aminyl radical generated from the specific anodic oxidation after the increase in the oxidation potential guaranteed the final C(sp^3)–N coupling. Next, radical clock experiments with ring-expanded product **444–446** from cyclopropyl acylimidazole **443** further verified the formation of the nickel-bound α-keto radical intermediate.

A hypothetical mechanism was proposed. Firstly, nickel-bound enolate complex **447** was generated by the coordination between acylimidazoles and the nickel precatalyst, which underwent direct or ferrocene-mediated SET anodic oxidation to α-keto radical intermediate **448**. Simultaneously, nitrogen-centred aminyl radical **449** was obtained through analogous anodic oxidation after deprotonation. Next, stereoselective assembly of the above-mentioned anodic oxidative **448** and **449** species produced the desired radical–radical coupling intermediate **450** and amination product α-amino acylimidazoles. The release and recoordination of the nickel catalyst and generation of H_2 by cathodic protonic reduction ensured the catalytic cycle.

5. Conclusions and outlook

The continuous evolution of thermodynamic transition metal-catalyzed C–N bond formation had witnessed enhanced reaction efficiency, accompanied with rich ligand libraries, alternative low-cost metal catalysts and reduced temperature. However, the applicable range of reaction conditions and compatibility with specific substrates are still subjected to certain restrictions, which urgently require a wide variety of versatile and common approaches, especially for sustainable and atom-economical conversions. In this regard, metallic electrocatalyzed C–N formations have emerged as elegant protocols to overcome the inherent limitations of conventional methodologies and remarkable progress has been made in this field over the past decade. As summarized in this review, the introduction of metallic catalysts greatly expanded the diversity of intermediates in electrocatalysis and facilitated rate-determining steps in transition metal-catalyzed elementary reactions through maximized atom and energy efficiencies without extra redox reagents or even ligands. Meanwhile, the more advanced photoelectrochemical and continuous flow platforms further provide a multifaceted and reliable toolbox to satisfy new synthetic demands in C–N bond formation.

However, despite these advances, some crucial issues still require a thorough and rigorous discussion. Firstly, the high concentrations of active metallic species generated from the heterogeneous interaction at the surface of electrodes would significantly affect the reaction activity and selectivity, especially in C–N couplings with short-lived intermediates.[100,104] Furthermore, N-centered radicals (NCRs) participating in the metallic electrocatalysis cycle exhibit high potential in facilitating transmetalation or ligand exchange between amines and transition metals with a lower energy barrier.[47] Thus, the development of new protocols, such as mediator-enabled anodic oxidation for NCRs as well as photoelectrocatalytic hydrogen atom transfer, is of great significance.[49–51] Finally, metallic electrocatalyzed asymmetric C–N bond formation is becoming a new research hotspot and this field has higher requirements for in-depth mechanistic insights, such as stereoselectivity control with inner-sphere or outer-sphere process.[7e,103,105] Considering the efficient synergistic integration between electrochemistry and transition metal catalysis, we expect that metallic electrocatalyzed protocols will be a reliable platform for facile and mild access to C–N bonds as well as for the large-scale production of pharmaceutical molecules and industrial synthesis.[106]

Conflicts of interest

There are no conflicts to declare.

Data availability

No primary research results, software or code have been included and no new data were generated or analyzed as part of this review.

The chemdraw files of all schemes in this review were provided and Supplementary Information (SI) is available. See DOI: **https://doi.org/10.1039/d5qo01467k**.

Acknowledgements

We gratefully acknowledge the National Natural Science Foundation of China (No. 22001101), the Natural Science Foundation of Jiangxi Province (No. 20224BAB203014, 20212BAB213027), and the Youth Talent Promotion Project of Nanchang Normal University (24XJQN01) for financial support.

References

1 (*a*) S. A. Lawrence, *Amines: synthesis, properties and applications*, Cambridge University Press, Cambridge, 2004; (*b*) A. Ricci, *Amino group chemistry: from synthesis to the life sciences*, John Wiley & Sons, Weinheim, 2008.

2 (*a*) N. A. McGrath, M. Brichacek and J. T. Njardarson, A Graphical Journey of Innovative Organic Architectures That Have Improved Our Lives, *J. Chem. Educ.*, 2010, **87**, 1348–1349; (*b*) The Njardarson Group, The University of Arizona, Top 200 Pharmaceuticals by Retail Sales, please see: **https://sites.arizona.edu/njardarson-lab/top200-posters**.

3 (*a*) J. Bariwal and E. Eycken, C-N bond forming cross-coupling reactions: an overview, *Chem. Soc. Rev.*, 2013, **42**, 9283–9303; (*b*) J. Feng, L.-L. Xi, C.-J. Lu and R.-R. Liu, Transition-metal-catalyzed enantioselective C-N cross-coupling, *Chem. Soc. Rev.*, 2024, **53**, 9560–9581.

4 (*a*) Y. Park, Y. Kim and S. Chang, Transition Metal-Catalyzed C-H Amination: Scope, Mechanism, and Applications, *Chem. Rev.*, 2017, **117**, 9247–9301; (*b*) A. J. Sterling, N. R. Ciccia, Y. Guo, J. F. Hartwig and M. Head-Gordon, Mechanistic Insights into the Origins of Selectivity in a Cu-Catalyzed C-H Amidation Reaction, *J. Am. Chem. Soc.*, 2024, **146**, 6168–6177.

5 S. Ma and J. F. Hartwig, Progression of Hydroamination Catalyzed by Late Transition-Metal Complexes from Activated to Unactivated Alkenes, *Acc. Chem. Res.*, 2023, **56**, 1565–1577.

6 (*a*) H. Jiang and A. Studer, Chemistry With *N*-Centered Radicals Generated by Single-Electron Transfer-Oxidation Using Photoredox Catalysis, *CCS Chem.*, 2019, **1**, 38–49; (*b*) C. Pratley, S. Fenner and J. A. Murphy, Nitrogen-Centered Radicals in Functionalization of sp^2 Systems: Generation, Reactivity, and Applications in Synthesis, *Chem. Rev.*, 2022, **122**, 8181–8260.

7 (*a*) S. Bhunia, G. G. Pawar, S. V. Kumar, Y. Jiang and D. Ma, Selected Copper-Based Reactions for C-N, C-O, C-S, and C-C Bond Formation, *Angew. Chem., Int. Ed.*, 2017, **56**, 16136–16179; (*b*) C. Le, T. Q. Chen, T. Liang, P. Zhang and D. W. C. MacMillan, A radical approach to the copper oxidative addition problem: Trifluoromethylation of bromoarenes, *Science*, 2018, **360**, 1010–1014; (*c*) Q. Yang, Y. Zhao and D. Ma, Cu-Mediated Ullmann-Type Cross-Coupling and Industrial Applications in Route Design, Process Development, and Scale-up of Pharmaceutical and Agrochemical Processes, *Org. Process Res. Dev.*, 2022, **26**, 1690–1750; (*d*) J. Duker, N. Petersen, N. Richter, P. Feuerer, T. Faber, N. Hölter, N. Kehl, J. Oboril, J. Strippel, A. Gröer, N. Guimond, S. J. Kaldas, M. Lubbesmeyer, G. Volpin, B. König and J. Hillenbrand, Room-Temperature Copper Cross-Coupling Reactions of Anilines with Aryl Bromides, *Org. Lett.*, 2025, **27**, 5566–5571; (*e*) Y. Luo, Y. Li, B. Wu, G. Wang, J. Wu, S.-Y. Zhang, K. N. Houk and Q. Shen, Decoding the redox behaviour of copper in Ullmann-type coupling reactions, *Nature*, 2025, **646**, 1105–1113.

8 (*a*) J. C. Vantourout, H. N. Miras, A. Isidro-Llobet, S. Sproules and A. J. B. Watson, Spectroscopic Studies of the Chan-Lam Amination: A Mechanism-Inspired Solution to Boronic Ester Reactivity, *J. Am. Chem. Soc.*, 2017, **139**, 4769–4779; (*b*) M. J. West, J. W. B. Fyfe, J. C. Vantourout and A. J. B. Watson, Mechanistic Development and Recent Applications of the Chan-Lam Amination, *Chem. Rev.*, 2019, **119**, 12491–12523; (*c*) R. Sang and J. E. Gestwicki, Radical Strategy to the Boron-to-Copper Transmetalation Problem: *N*-Alkylation with Alkylboronic Esters, *J. Am. Chem. Soc.*, 2025, **147**, 23259–23269.

9 C. S. Day and R. Martin, Comproportionation and disproportionation in nickel and copper complexes, *Chem. Soc. Rev.*, 2023, **52**, 6601–6616.

10 (*a*) I. P. Beletskaya and A. V. Cheprakov, The Complementary Competitors: Palladium and Copper in C-N Cross-Coupling Reactions, *Organometallics*, 2012, **31**, 7753–7808; (*b*) P. Ruiz-Castillo and S. L. Buchwald, Applications of Palladium-Catalyzed C-N Cross-Coupling Reactions, *Chem. Rev.*, 2016, **116**, 12564–12649; (*c*) J. Rayadurgam, S. Sana, M. Sasikumar and Q. Gu, Palladium catalyzed C-C and C-N bond forming reactions: an update on the synthesis of pharmaceuticals from 2015–2020, *Org. Chem. Front.*, 2021, **8**, 384–414; (*d*) M. J. Kania, A. Reyes and S. R. Neufeldt, Oxidative Addition of (Hetero)aryl (Pseudo)halides at Palladium(0): Origin and Significance of Divergent Mechanisms, *J. Am. Chem. Soc.*, 2024, **146**, 19249–19260; (*e*) K. Kubota, M. Takahashi, F. Puccetti and H. Ito, Mechanochemical Buchwald-Hartwig Cross-Coupling Reactions of Aromatic Primary Amines and Their Application to Two-Step One-Pot Rapid Synthesis of Unsymmetrical Triarylamines, *Org. Lett.*, 2025, **27**, 5691–5696.

11 (*a*) R. Dorel, C. P. Grugel and A. M. Haydl, The Buchwald-Hartwig Amination After 25 Years, *Angew. Chem., Int. Ed.*, 2019, **58**, 17118–17129; (*b*) P. A. Forero-Cortés and A. M. Haydl, The 25th Anniversary of the Buchwald-Hartwig Amination: Development, Applications, and Outlook, *Org. Process Res. Dev.*, 2019, **23**, 1478–1483; (*c*) X. Liu, X. Han, J. Cai, Q. Wang, L. Liu, X.-H. Duan and M. Hu, Hierarchical phosphorus-enriched organic polymer supports for immobilized palladium catalysts: enabling green and efficient Buchwald-Hartwig amination, *Green Chem.*, 2025, **27**, 9522–9530; (*d*) A. Dusunge,

D. K. Leahy and S. Handa, AshPhos Ligand: Facilitating Challenging Aminations in Five- and Six-Membered Heteroaryl Halides Using Cyclic Secondary and Bulky Amines, *JACS Au*, 2025, **5**, 91–98.

12 J. P. Wolfe and S. L. Buchwald, Nickel-Catalyzed Amination of Aryl Chlorides, *J. Am. Chem. Soc.*, 1997, **119**, 6054–6058.

13 (*a*) M. Marin, R. J. Rama and M. C. Nicasio, Ni-Catalyzed Amination Reactions: An Overview, *Chem. Rec.*, 2016, **16**, 1819–1832; (*b*) C. M. Lavoie and M. Stradiotto, Bisphosphines: A Prominent Ancillary Ligand Class for Application in Nickel-Catalyzed C-N Cross-Coupling, *ACS Catal.*, 2018, **8**, 7228–7250; (*c*) V. M. Chernyshev and V. P. Ananikov, Nickel and Palladium Catalysis: Stronger Demand than Ever, *ACS Catal.*, 2022, **12**, 1180–1200.

14 (*a*) R. A. Green and J. F. Hartwig, Nickel-Catalyzed Amination of Aryl Chlorides with Ammonia or Ammonium Salts, *Angew. Chem., Int. Ed.*, 2015, **54**, 3768–3772; (*b*) C. M. Lavoie, R. McDonald, E. R. Johnson and M. Stradiotto, Bisphosphine-Ligated Nickel Pre-catalysts in C(sp^2)-N Cross-Couplings of Aryl Chlorides: A Comparison of Nickel(I) and Nickel(II), *Adv. Synth. Catal.*, 2017, **359**, 2972–2980; (*c*) T. Harada, Y. Ueda, T. Iwai and M. Sawamura, Nickel-catalyzed amination of aryl fluorides with primary amines, *Chem. Commun.*, 2018, **54**, 1718–1721; (*d*) C. N. Pierson and J. F. Hartwig, Mapping the mechanisms of oxidative addition in cross-coupling reactions catalysed by phosphine-ligated Ni(0), *Nat. Chem.*, 2024, **16**, 930–937.

15 (*a*) Q. Wang, X. Tao, S. Ni, Y. Pan and Y. Wang, Nickel-Catalyzed Amination of Alkyl Electrophiles, *Org. Lett.*, 2023, **25**, 5822–5826; (*b*) J. Zhang, X.-D. Huan, X. Wang, G.-Q. Li, W.-J. Xiao and J.-R. Chen, Recent advances in C(sp^3)-N bond formation via metallaphoto-redox catalysis, *Chem. Commun.*, 2024, **60**, 6340–6361.

16 G. A. Dawson, E. H. Spielvogel and T. Diao, Nickel-Catalyzed Radical Mechanisms: Informing Cross-Coupling for Synthesizing Non-Canonical Biomolecules, *Acc. Chem. Res.*, 2023, **56**, 3640–3653.

17 (*a*) F. Strieth-Kalthoff, A. R. Longstreet, J. M. Weber and T. F. Jamison, Nickel-Catalyzed Radical Mechanisms: Informing Cross-Coupling for Synthesizing Non-Canonical Biomolecules, *ChemCatChem*, 2018, **10**, 2873–2877; (*b*) R. Y. Liu, J. M. Dennis and S. L. Buchwald, The Quest for the Ideal Base: Rational Design of a Nickel Precatalyst Enables Mild, Homogeneous C-N Cross-Coupling, *J. Am. Chem. Soc.*, 2020, **142**, 4500–4507; (*c*) Z.-C. Wang, P.-P. Xie, Y. Xu, X. Hong and S.-L. Shi, Low-Temperature Nickel-Catalyzed C-N Cross-Coupling via Kinetic Resolution Enabled by a Bulky and Flexible Chiral N-Heterocyclic Carbene Ligand, *Angew. Chem., Int. Ed.*, 2021, **60**, 16077–16084; (*d*) V. M. Chernyshev, O. V. Khazipov, M. A. Shevchenko, D. V. Pasyukov, J. V. Burykina, M. E. Minyaev, D. B. Eremin and V. P. Ananikov, Discovery of the N-NHC Coupling Process under the Conditions of Pd/NHC- and Ni/NHC-Catalyzed Buchwald-Hartwig Amination, *Organometallics*, 2022, **41**, 1519–1531.

18 (*a*) C. N. Pierson and J. F. Hartwig, Mapping the mechanisms of oxidative addition in cross-coupling reactions catalysed by phosphine-ligated Ni(0), *Nat. Chem.*, 2024, **16**, 930–937; (*b*) A. Romero-Arenas, M. V. Popescu, M. K. Goetz, R. Bhatnagar, H. Goljani, B. T. Punchihewa, K. M. Sanders, I. A. Guzei, M. Rafiee, D. J. Weix, R. S. Paton and S. S. Stahl, Reductively Induced Aryl Transmetalation: An Alternative Catalytically Relevant Ni-Catalyzed Biaryl Coupling Mechanism, *J. Am. Chem. Soc.*, 2025, **147**, 21697–21707; (*c*) X.-Y. Xu, L.-G. Liu, L.-C. Xu, S.-Q. Zhang and X. Hong, Transfer Learning-Enabled Ligand Prediction for Ni-Catalyzed Atroposelective Suzuki-Miyaura Cross-Coupling Based on Mechanistic Similarity: Leveraging Pd Knowledge for Ni Discovery, *J. Am. Chem. Soc.*, 2025, **147**, 15318–15328.

19 (*a*) R. A. Kelly, N. M. Scott, S. Díez-González, E. D. Stevens and S. P. Nolan, Simple Synthesis of CpNi(NHC)Cl Complexes (Cp = Cyclopentadienyl; NHC = N-Heterocyclic Carbene), *Organometallics*, 2005, **24**, 3442–3447; (*b*) N. H. Park, G. Teverovskiy and S. L. Buchwald, Development of an Air-Stable Nickel Precatalyst for the Amination of Aryl Chlorides, Sulfamates, Mesylates, and Triflates, *Org. Lett.*, 2014, **16**, 220–223; (*c*) J. D. Shields, E. E. Gray and A. G. Doyle, A Modular, Air-Stable Nickel Precatalyst, *Org. Lett.*, 2015, **17**, 2166–2169; (*d*) S. S. Kampmann, B. W. Skelton, D. A. Wild, G. A. Koutsantonis and S. G. Stewart, An Air-Stable Nickel (0) Phosphite Precatalyst for Primary Alkylamine C-N Cross-Coupling Reactions, *Eur. J. Org. Chem.*, 2015, 5995–6004.

20 M. J. Iglesias, A. Prieto and M. C. Nicasio, Well-Defined Allylnickel Chloride/N-Heterocyclic Carbene [(NHC)Ni(allyl)Cl] Complexes as Highly Active Precatalysts for C-N and C-S Cross-Coupling Reactions, *Adv. Synth. Catal.*, 2010, **352**, 1949–1954.

21 Z. Chen, Y. Jiang, L. Zhang, Y. Guo and D. Ma, Oxalic Diamides and *tert*-Butoxide: Two Types of Ligands Enabling Practical Access to Alkyl Aryl Ethers *via* Cu-Catalyzed Coupling Reaction, *J. Am. Chem. Soc.*, 2019, **141**, 3541–3549.

22 S.-T. Kim, M. J. Strauss, A. Cabré and S. L. Buchwald, Room-Temperature Cu-Catalyzed Amination of Aryl Bromides Enabled by DFT-Guided Ligand Design, *J. Am. Chem. Soc.*, 2023, **145**, 6966–6975.

23 J. D. Hicks, A. M. Hyde, A. M. Cuezva and S. L. Buchwald, Pd-Catalyzed *N*-Arylation of Secondary Acyclic Amides: Catalyst Development, Scope, and Computational Study, *J. Am. Chem. Soc.*, 2009, **131**, 16720–16734.

24 (*a*) B. L. Lin, C. R. Clough and G. L. Hillhouse, Interactions of Aziridines with Nickel Complexes: Oxidative-Addition and Reductive-Elimination Reactions that Break and Make C–N Bonds, *J. Am. Chem. Soc.*, 2002, **124**, 2890–2891; (*b*) L. Ilies, T. Matsubara and E. Nakamura, Nickel-Catalyzed Synthesis of Diarylamines

via Oxidatively Induced C-N Bond Formation at Room Temperature, *Org. Lett.*, 2012, **14**, 5570–5573.

25 (*a*) S. Gisbertz, S. Reischauer and B. Pieber, Overcoming limitations in dual photoredox/nickel-catalysed C-N cross-couplings due to catalyst deactivation, *Nat. Catal.*, 2020, **3**, 611–620; (*b*) C.-M. Chan, Y.-C. Chow and W.-Y. Yu, Recent Advances in Photocatalytic C–N Bond Coupling Reactions, *Synthesis*, 2020, 2899–2921; (*c*) G. Song, J. Song, Q. Li, T. Kang, J. Dong, G. Li, J. Fan, C. Wang and D. Xue, Adaptive Photochemical Amination via Co(II) Catalysis, *J. Am. Chem. Soc.*, 2024, **146**, 26936–26946; (*d*) J. Li, P. Wang, B. Bai, Y. Xiao, Y.-F. Wan, Y. Yan, F. Li, G. Song, G. Li, C. Wang, X.-P. Zhang, J. Dong, T. Kang and D. Xue, Synthesis, Characterization, and Catalytic Activity of Ni(0)(DQ)dtbbpy, an Air-Stable, Bifunctional Red-Light-Sensitive Precatalyst, *J. Am. Chem. Soc.*, 2025, **147**, 5851–5859.

26 E. B. Corcoran, M. T. Pirnot, S. Lin, S. D. Dreher, D. A. DiRocco, I. W. Davies, S. L. Buchwald and D. W. C. MacMillan, Aryl amination using ligand-free Ni (II) salts and photoredox catalysis, *Science*, 2016, **353**, 279–283.

27 (*a*) E. R. Welin, C. Le, D. M. Arias-Rotondo, J. K. McCusker and D. W. C. MacMillan, Photosensitized, energy transfer-mediated organometallic catalysis through electronically excited nickel(II), *Science*, 2017, **355**, 380–385; (*b*) C.-H. Lim, M. Kudisch, B. Liu and G. M. Miyake, C-N Cross-Coupling via Photoexcitation of Nickel-Amine Complexes, *J. Am. Chem. Soc.*, 2018, **140**, 7667–7673; (*c*) M. Kudisch, C.-H. Lim, P. Thordarson and G. M. Miyake, Energy Transfer to Ni-Amine Complexes in Dual Catalytic, Light-Driven C-N Cross-Coupling Reactions, *J. Am. Chem. Soc.*, 2019, **141**, 19479–19486.

28 (*a*) K. P. S. Cheung, J. Fang, K. Mukherjee, A. Mihranyan and V. Gevorgyan, Asymmetric intermolecular allylic C-H amination of alkenes with aliphatic amines, *Science*, 2022, **378**, 1207–1213; (*b*) Y.-F. Zhang, B. Wang, Z. Chen, J.-R. Liu, N.-Y. Yang, J.-M. Xiang, J. Liu, Q.-S. Gu, X. Hong and X.-Y. Liu, Asymmetric amination of alkyl radicals with two minimally different alkyl substituents, *Science*, 2025, **388**, 283–291.

29 (*a*) N. E. S. Tay, D. Lehnherr and T. Rovis, Photons or Electrons? A Critical Comparison of Electrochemistry and Photoredox Catalysis for Organic Synthesis, *Chem. Rev.*, 2022, **122**, 2487–2649; (*b*) W. Zeng and Y. Qiu, Electrochemical conversion of organic compounds and inorganic small molecules, *Sci. China:Chem.*, 2024, **67**, 3223–3246; (*c*) Z. Shen, J.-L. Tu and B. Huang, Unleashing the potentiality of metals: synergistic catalysis with light and electricity, *Org. Chem. Front.*, 2024, **11**, 4024–4040.

30 (*a*) Q.-L. Yang, W.-W. Li, Z.-X. Zhang, H.-M. Zhang, X.-J. Li and H.-M. Guo, Electrocatalytic oxidative C-H cycloamination towards tricyclic [1,2,4]triazolo-[3,4-*i*]purine nucleosides mediated by bromide ions, *Org. Chem. Front.*, 2023, **10**, 5369–5374; (*b*) I. Kononov, S. O. Strekalova, V. I. Morozov, K. V. Boyko, V. I. Timashev, M. G. Medvedev, O. B. Babaeva, E. V. Kobeleva, K. A. Ivshin, V. M. Babaev and Y. H. Budnikova, Replacing sulfuric acid with water in electrochemical metal-free mild aromatic C-H amidation: a direct route to *N*-phenylamides, *Org. Chem. Front.*, 2024, **11**, 5820–5830.

31 C. Li, Y. Kawamata, H. Nakamura, J. C. Vantourout, Z. Liu, Q. Hou, D. Bao, J. T. Starr, J. Chen, M. Yan and P. S. Baran, Electrochemically Enabled, Nickel-Catalyzed Amination, *Angew. Chem., Int. Ed.*, 2017, **56**, 13088–13093.

32 W. Zeng, Y. Wang, C. Peng and Y. Qiu, Organo-mediator enabled electrochemical transformations, *Chem. Soc. Rev.*, 2025, **54**, 4468–4501.

33 A. Hazra, M. Organiscak and L. Luo, Deciphering the Synchronization of Alternating Current Frequency with the Nickel Catalytic Cycle in Selective C-N Cross-Coupling, *J. Am. Chem. Soc.*, 2025, **147**, 35139–35148.

34 (*a*) J.-I. Yoshida, K. Kataoka, R. Horcajada and A. Nagaki, Modern Strategies in Electroorganic Synthesis, *Chem. Rev.*, 2008, **108**, 2265–2299; (*b*) M. Yan, Y. Kawamata and P. S. Baran, Synthetic Organic Electrochemical Methods Since 2000: On the Verge of a Renaissance, *Chem. Rev.*, 2017, **117**, 13230–13319; (*c*) S. Möhle, M. Zirbes, E. Rodrigo, T. Gieshoff, A. Wiebe and S. R. Waldvogel, Modern Electrochemical Aspects for the Synthesis of Value-Added Organic Products, *Angew. Chem., Int. Ed.*, 2018, **57**, 6018–6041; (*d*) K. D. Moeller, Using Physical Organic Chemistry To Shape the Course of Electrochemical Reactions, *Chem. Rev.*, 2018, **118**, 4817–4833; (*e*) R. Francke and R. D. Little, Electrons and Holes as Catalysts in Organic Electrosynthesis, *ChemElectroChem*, 2019, **6**, 4373–4382; (*f*) J. C. Siu, N. Fu and S. Lin, Catalyzing Electrosynthesis: A Homogeneous Electrocatalytic Approach to Reaction Discovery, *Acc. Chem. Res.*, 2020, **53**, 547–560.

35 (*a*) M. D. Kärkäs, Electrochemical strategies for C-H functionalization and C-N bond formation, *Chem. Soc. Rev.*, 2018, **47**, 5786–5865; (*b*) H. Zhang and A. Lei, Electrochemical/Photochemical Aminations Based on Oxidative Cross-Coupling between C-H and N-H, *Synthesis*, 2019, 83–96; (*c*) Y. Yuan and A. Lei, Electrochemical Oxidative Cross-Coupling with Hydrogen Evolution Reactions, *Acc. Chem. Res.*, 2019, **52**, 3309–3324; (*d*) N. Dagar, P. P. Sen and S. R. Roy, Electrifying Sustainability on Transition Metal-Free Modes: An Eco-Friendly Approach for the Formation of C-N Bonds, *ChemSusChem*, 2021, **14**, 1229–1257; (*e*) Z. Zhu, P. Li and Y. Qiu, Recent Advance in Electrochemical C(sp^2)-H Amination of Arenes, *Chin. J. Org. Chem.*, 2024, **44**, 871–891; (*f*) C. Liu, J. Liu, W. Li, H. Lu and Y. Zhang, Recent advances in electrochemical C-H bond amination, *Org. Chem. Front.*, 2023, **10**, 5309–5330.

36 (*a*) Y. Zhao and W. Xia, Recent advances in radical-based C-N bond formation via photo-/electrochemistry, *Chem. Soc. Rev.*, 2018, **47**, 2591–2608; (*b*) P. Xiong and H.-C. Xu, Chemistry with Electrochemically Generated N-Centered Radicals, *Acc. Chem. Res.*, 2019, **52**, 3339–3350.

37 (*a*) Z.-W. Hou, Z.-Y. Mao and H.-C. Xu, Recent Progress on the Synthesis of (Aza)indoles through Oxidative Alkyne Annulation Reactions, *Synlett*, 2017, 1867–1872; (*b*) Z. Ye and F. Zhang, Recent Advances in Constructing Nitrogen-Containing Heterocycles via Electrochemical Dehydrogenation, *Chin. J. Chem.*, 2019, **37**, 513–528; (*c*) A. V. Listratova, N. Sbei and L. G. Voskressensky, Catalytic Electrosynthesis of N,O-Heterocycles-Recent Advances, *Eur. J. Org. Chem.*, 2020, 2012–2027; (*d*) Y. Zheng, C. Chen, Y. Lu and S. Huang, Recent advances in electrochemically enabled construction of indoles from non-indole-based substrates, *Chem. Commun.*, 2024, **60**, 8516–8525.

38 (*a*) X. Peng, L. Zeng, D. Wang, Z. Liu, Y. Li, Z. Li, B. Yang, L. Lei, L. Dai and Y. Hou, Electrochemical C-N coupling of CO_2 and nitrogenous small molecules for the electrosynthesis of organonitrogen compounds, *Chem. Soc. Rev.*, 2023, **52**, 2193–2237; (*b*) C. Yang, Z. Li, J. Xu, Y. Jiang and W. Zhu, Electrocatalytic C-N coupling for urea synthesis: a critical review, *Green Chem.*, 2024, **26**, 4908–4933; (*c*) D. Chen, J. Liu, J. Shen, Y. Zhang, H. Shao, C. Chen and S. Wang, Electrocatalytic C-N Couplings at Cathode and Anode, *Adv. Energy Mater.*, 2024, **14**, 2303820; (*d*) Y. Wang, D. Chen, C. Chen and S. Wang, Electrocatalytic Urea Synthesis via C-N Coupling from CO_2 and Nitrogenous Species, *Acc. Chem. Res.*, 2024, **57**, 247–256.

39 (*a*) H. Huang, K. A. Steiniger and T. H. Lambert, Electrophotocatalysis: Combining Light and Electricity to Catalyze Reactions, *J. Am. Chem. Soc.*, 2022, **144**, 12567–12583; (*b*) L. Qian and M. Shi, Contemporary photoelectrochemical strategies and reactions in organic synthesis, *Chem. Commun.*, 2023, **59**, 3487–3506.

40 (*a*) N. Sauermann, T. H. Meyer, Y. Qiu and L. Ackermann, Electrocatalytic C-H Activation, *ACS Catal.*, 2018, **8**, 7086–7103; (*b*) P. P. Sen, N. Dagar, S. Singh, V. J. Roy, V. Pathania and S. R. Roy, Probing the versatility of metallo-electro hybrid catalysis: enabling access towards facile C-N bond formation, *Org. Biomol. Chem.*, 2020, **18**, 8994–9017; (*c*) C. A. Malapit, M. B. Prater, J. R. Cabrera-Pardo, M. Li, T. D. Pham, T. P. McFadden, S. Blank and S. D. Minteer, Advances on the Merger of Electrochemistry and Transition Metal Catalysis for Organic Synthesis, *Chem. Rev.*, 2022, **122**, 3180–3218; (*d*) X.-L. Lai, Y.-K. Lai, P. Xiong and H.-C. Xu, Recent advances in C(sp^3)-H functionalization *via* molecular electrocatalysis, *Org. Chem. Front.*, 2025, **12**, 6631–6661.

41 Y. Kawamata, J. C. Vantourout, D. P. Hickey, P. Bai, L. Chen, Q. Hou, W. Qiao, K. Barman, M. A. Edwards, A. F. Garrido-Castro, J. N. deGruyter, H. Nakamura, K. Knouse, C. Qin, K. J. Clay, D. Bao, C. Li, J. T. Starr, C. Garcia-Irizarry, N. Sach, H. S. White, M. Neurock, S. D. Minteer and P. S. Baran, Electrochemically Driven, Ni-Catalyzed Aryl Amination: Scope, Mechanism, and Applications, *J. Am. Chem. Soc.*, 2019, **141**, 6392–6402.

42 J. Luo, M. T. Davenport, C. Callister, S. D. Minteer, D. H. Ess and T. L. Liu, Understanding Formation and Roles of NiII Aryl Amido and NiIII Aryl Amido Intermediates in Ni-Catalyzed Electrochemical Aryl Amination Reactions, *J. Am. Chem. Soc.*, 2023, **145**, 16130–16141.

43 C. Zhu, A. P. Kale, H. Yue and M. Rueping, Redox-Neutral Cross-Coupling Amination with Weak N-Nucleophiles: Arylation of Anilines, Sulfonamides, Sulfoximines, Carbamates, and Imines via Nickelaelectrocatalysis, *JACS Au*, 2021, **1**, 1057–1065.

44 E. O. Bortnikov and S. N. Semenov, Coupling of Alternating Current to Transition-Metal Catalysis: Examples of Nickel-Catalyzed Cross-Coupling, *J. Org. Chem.*, 2021, **86**, 782–793.

45 F. Daili, S. Sengmany and E. Léonel, Amination of Aryl Halides Mediated by Electrogenerated Nickel from Sacrificial Anode, *Eur. J. Org. Chem.*, 2021, 2462–2469.

46 S. Sengmany, F. Daili, I. Kribii and E. Léonel, Electrogenerated Nickel Catalyst for C-N Cross-Coupling, *J. Org. Chem.*, 2023, **88**, 675–683.

47 (*a*) Y.-N. Zheng, H. Zheng, T. Li and W.-T. Wei, Recent Advances in Copper-Catalyzed C-N Bond Formation Involving N-Centered Radicals, *ChemSusChem*, 2021, **14**, 5340–5358; (*b*) C. Pratley, S. Fenner and J. A. Murphy, Nitrogen-Centered Radicals in Functionalization of sp2 Systems: Generation, Reactivity, and Applications in Synthesis, *Chem. Rev.*, 2022, **122**, 8181–8260.

48 (*a*) S. Z. Zard, Recent progress in the generation and use of nitrogen-centred radicals, *Chem. Soc. Rev.*, 2008, **37**, 1603–1618; (*b*) J. Luo and W.-T. Wei, Recent Advances in Construction of C-N Bonds Through Coupling Reaction between Carbon Radicals and Nitrogen Radicals, *Adv. Synth. Catal.*, 2018, **360**, 2076–2086.

49 (*a*) H. Jiang and A. Studer, Chemistry With N-Centered Radicals Generated by Single-Electron Transfer-Oxidation Using Photoredox Catalysis, *CCS Chem.*, 2019, **1**, 38–49; (*b*) P. Xiong and H.-C. Xu, Chemistry with Electrochemically Generated N-Centered Radicals, *Acc. Chem. Res.*, 2019, **52**, 3339–3350; (*c*) N. Chen and H.-C. Xu, Electrochemical generation of nitrogen-centered radicals for organic synthesis, *Green Synth. Catal.*, 2021, **2**, 165–178.

50 (*a*) Q.-C. Gan, J. Qiao, C. Zhou, R.-N. Ci, J.-D. Guo, B. Chen, C.-H. Tung and L.-Z. Wu, Direct N-H Activation to Generate Nitrogen Radical for Arylamine Synthesis via Quantum Dots Photocatalysis, *Angew. Chem., Int. Ed.*, 2023, **62**, e202218391; (*b*) Z. Zhang, S. Yue, B. Jin, R. Yang, S. Wang, T. Zhang, L. Sun, A. Lei and Hu Cai, *Para*-selective nitrobenzene amination lead by C(sp2)-H/N-H oxidative cross-coupling through aminyl radical, *Nat. Commun.*, 2024, **15**, 4186.

51 J. Wang, S. Li, C. Yang, H. Gao, L. Zuo, Z. Guo, P. Yang, Y. Jiang, J. Li, L.-Z. Wu and Z. Tang, Photoelectrochemical Ni-catalyzed cross-coupling of aryl bromides with amine at ultra-low potential, *Nat. Commun.*, 2024, **15**, 6907.

52 (*a*) E. Rial-Rodríguez, J. D. Williams, D. Cantillo, T. Fuchß, A. Sommer, H.-M. Eggenweiler, C. O. Kappe and G. Laudadio, An Automated Electrochemical Flow Platform to Accelerate Library Synthesis and Reaction Optimization, *Angew. Chem., Int. Ed.*, 2024, **63**, e202412045; (*b*) T.-S. Chen, P. Xiong and H.-C. Xu, Continuous Flow Electrochemistry Unlocks Broadly Applicable Arene C-H Amination, *Angew. Chem., Int. Ed.*, 2025, **64**, e202513864.

53 J. Morvan, K. P. L. Kuijpers, D. Fanfair, B. Tang, K. Bartkowiak, L. Eynde, E. Renders, J. Alcazar, P. J. J. A. Buijnsters, M.-A. Carvalho and A. X. Jones, Electrochemical C-O and C-N Arylation using Alternating Polarity in flow for Compound Libraries, *Angew. Chem., Int. Ed.*, 2025, **64**, e202413383.

54 (*a*) G. Y. Cho, P. Rémy, J. Jansson, C. Moessner and C. Bolm, Copper-mediated cross-coupling reactions of *N*-unsubstituted sulfoximines and aryl halides, *Org. Lett.*, 2004, **6**, 3293–3296; (*b*) C. Moessner and C. Bolm, Cu $(OAc)_2$-Catalyzed *N*-Arylations of Sulfoximines with Aryl Boronic Acids, *Org. Lett.*, 2005, **7**, 2667–2669; (*c*) N. Yongpruksa, N. L. Calkins and M. Harmata, Efficient palladium-catalyzed *N*-arylation of a sulfoximine with aryl chlorides, *Chem. Commun.*, 2011, **47**, 7665–7667; (*d*) H. Zhou, W. Chen and Z. Chen, Pd/Norbornene Collaborative Catalysis on the Divergent Preparation of Heterocyclic Sulfoximine Frameworks, *Org. Lett.*, 2018, **20**, 2590–2594.

55 (*a*) C. Bolm, J. P. Hildebrand and J. Rudolph, Catalytic Coupling of Aryl Sulfonates with sp^2-Hybridized Nitrogen Nucleophiles: Palladium- and Nickel-catalyzed Synthesis of *N*-Aryl Sulfoximines, *Synthesis*, 2000, 911–913; (*b*) A. Wimmer and B. König, *N*-Arylation of *NH*-Sulfoximines via Dual Nickel Photocatalysis, *Org. Lett.*, 2019, **21**, 2740–2744.

56 D. Liu, Z.-R. Liu, C. Ma, K.-J. Jiao, B. Sun, L. Wei, J. Lefranc, S. Herbert and T.-S. Mei, Nickel-Catalyzed *N*-Arylation of *NH*-Sulfoximines with Aryl Halides via Paired Electrolysis, *Angew. Chem., Int. Ed.*, 2021, **60**, 9444–9449.

57 Z.-R. Liu, S. Herbert, H. Schirok, C. Ma and T.-S. Mei, Synthesis of 1,2-Benzothiazine *via* Nickel-Catalyzed Electrochemical Intramolecular Amination, *Org. Lett.*, 2024, **26**, 9034–9039.

58 (*a*) X. Kong, Y. Chen, S. Zhang, K. Feng, X. Chen, L.-H. Dong, M.-H. Li, Y.-Q. Xu and Z.-Y. Cao, Electrochemically promoted defluorinative sulfoximination and fluorosulfonylation of non-activated aryl fluorides at room temperature, *Chem. Sci.*, 2025, **16**, 14161–14169; (*b*) A. Saha, M. Roy, S. Maji, G. Rana, D. Maiti and D. Adhikari, Consecutive Multiphoton-Mediated Defluorinative Amination of Fluoroarenes, *J. Am. Chem. Soc.*, 2025, **147**, 20735–20747.

59 (*a*) J. L. Klinkenberg and J. F. Hartwig, Slow Reductive Elimination from Arylpalladium Parent Amido Complexes, *J. Am. Chem. Soc.*, 2010, **132**, 11830–11833; (*b*) R. A. Green and J. F. Hartwig, Nickel-Catalyzed Amination of Aryl Chlorides with Ammonia or Ammonium Salts, *Angew. Chem., Int. Ed.*, 2015, **54**, 3768–3772; (*c*) K. Choi, J. N. Brunn, K. Borate, R. Kaduskar, C. L. Pueyo, H. Shinde, R. Goetz and J. F. Hartwig, Palladium-Catalyzed Amination of Aryl Halides with Aqueous Ammonia and Hydroxide Base Enabled by Ligand Development, *J. Am. Chem. Soc.*, 2024, **146**, 19414–19424.

60 (*a*) R. Goetz and J. F. Hartwig, An Integrated Carbon Nitride-Nickel Photocatalyst for the Amination of Aryl Halides Using Sodium Azide, *Angew. Chem., Int. Ed.*, 2022, **61**, e202203176; (*b*) L. Karpova, M. Daniel, R. Kancherla, K. Muralirajan, B. Maity and M. Rueping, Excited-State Nickel-Catalyzed Amination of Aryl Bromides: Synthesis of Diphenylamines and Primary Anilines, *Org. Lett.*, 2024, **26**, 1657–1661; (*c*) R. Kancherla, K. Muralirajan, S. Dutta, K. Pal, B. Li, B. Maity, L. Cavallo and M. Rueping, Photoexcitation of Distinct Divalent Palladium Complexes in Cross-Coupling Amination Under Air, *Angew. Chem., Int. Ed.*, 2024, **63**, e202314508; (*d*) G. Song, J. Song, Q. Li, D.-Z. Nong, J. Dong, G. Li, J. Fan, C. Wang, J. Xiao and D. Xue, Werner Salt as Nickel and Ammonia Source for Photochemical Synthesis of Primary Aryl Amines, *Angew. Chem., Int. Ed.*, 2024, **63**, e202314355.

61 G. Song, J. Song, Q. Li, D.-Z. Nong, J. Dong, G. Li, J. Fan, C. Wang, J. Xiao and D. Xue, Werner Salt as Nickel and Ammonia Source for Photochemical Synthesis of Primary Aryl Amines, *Angew. Chem., Int. Ed.*, 2024, **63**, e202314355.

62 J. Huang, X. Li, X. Zhao, Y. Wei and L. Xu, Electrochemically enabled nickel-catalyzed controllable synthesis of monoaryl or diaryl amines from aryl halides and trimethylsilyl azides, *Green Chem.*, 2025, **27**, 5265–5272.

63 Y. Liu, Y. Sun, Y. Deng and Y. Qiu, Electrochemical Amination of Aryl Halides with NH_3, *Angew. Chem., Int. Ed.*, 2025, **64**, e202504459.

64 (*a*) K. Murugesan, T. Senthamarai, V. G. Chandrashekhar, K. Natte, P. C. J. Kamer, M. Beller and R. V. Jagadeesh, Catalytic reductive aminations using molecular hydrogen for synthesis of different kinds of amines, *Chem. Soc. Rev.*, 2020, **49**, 6273–6328; (*b*) T. Irrgang and R. Kempe, Transition-metal-catalyzed reductive amination employing hydrogen, *Chem. Rev.*, 2020, **120**, 9583–9674.

65 T. Wang, F. He, W. Jiang and J. Liu, Electrohydrogenation of Nitriles with Amines by Cobalt Catalysis, *Angew. Chem., Int. Ed.*, 2024, **63**, e202316140.

66 H. Bi, Z. Chen, C. Bi, S. Qu and J. Liu, Electroreductive amination of carboxylic acids by cobalt catalysis, *Nat. Commun.*, 2025, **16**, 7167.

67 J. Xu, Y. Liu, Q. Wang, X. Tao, S. Ni, W. Zhang, L. Yu, Y. Pan and Y. Wang, Electrochemical deoxygenative amination of stabilized alkyl radicals from activated alcohols, *Nat. Commun.*, 2024, **15**, 6116.

68 (*a*) R. Mao, A. Frey, J. Balon and X. Hu, Decarboxylative $C(sp^3)$-N cross-coupling *via* synergetic photoredox and

copper catalysis, *Nat. Catal.*, 2018, **1**, 120–126; (*b*) H. Chen, Y. Liu and X. Liao, Recent Progress in Radical Decarboxylative Functionalizations Enabled by Transition-Metal (Ni, Cu, Fe, Co or Cr) Catalysis, *Synthesis*, 2021, 1–29.

69 Y. Zheng, X. Shao, V. Ramadoss, L. Tian and Y. Wang, Recent Developments in Photochemical and Electrochemical Decarboxylative C(sp^3)-N Bond Formation, *Synthesis*, 2020, 1357–1368.

70 (*a*) Y. Liang, X. Zhang and D. W. C. MacMillan, Decarboxylative sp^3 C-N coupling *via* dual copper and photoredox catalysis, *Nature*, 2018, **559**, 83–88; (*b*) R. Mao, J. Balon and X. Hu, Cross-Coupling of Alkyl Redox-Active Esters with Benzophenone Imines: Tandem Photoredox and Copper Catalysis, *Angew. Chem., Int. Ed.*, 2018, **57**, 9501–9504; (*c*) G. Barzanò, R. Mao, M. Garreau, J. Waser and X. Hu, Tandem Photoredox and Copper-Catalyzed Decarboxylative C(sp^3)-N Coupling of Anilines and Imines Using an Organic Photocatalyst, *Org. Lett.*, 2020, **22**, 5412–5416.

71 Y.-M. Cai, X.-T. Liu, L.-L. Xu and M. Shang, Electrochemical Ni-Catalyzed Decarboxylative C(sp^3)-N Cross-Electrophile Coupling, *Angew. Chem., Int. Ed.*, 2024, **63**, e202315222.

72 (*a*) K.-J. Jiao, C.-Q. Zhao, P. Fang and T.-S. Mei, Palladium catalyzed C-H functionalization with electrochemical oxidation, *Tetrahedron Lett.*, 2017, **58**, 797–802; (*b*) R. L. Carvalho, E. B. T. Diogo, S. L. Homölle, S. Dana, E. N. S. Júnior and L. Ackermann, The crucial role of silver(I)-salts as additives in C-H activation reactions: overall analysis of their versatility and applicability, *Chem. Soc. Rev.*, 2023, **52**, 6359–6378.

73 N. Sauermann, T. H. Meyer, Y. Qiu and L. Ackermann, Electrocatalytic C-H Activation, *ACS Catal.*, 2018, **8**, 7086–7103.

74 (*a*) P. Gandeepan, L. H. Finger, T. H. Meyer and L. Ackermann, 3d metallaelectrocatalysis for resource economical syntheses, *Chem. Soc. Rev.*, 2020, **49**, 4254–4272; (*b*) L. Ackermann, Metalla-electrocatalyzed C-H Activation by Earth-Abundant 3d Metals and Beyond, *Acc. Chem. Res.*, 2020, **53**, 84–104.

75 (*a*) Q.-J. Yao, F.-R. Huang, J.-H. Chen, M.-Y. Zhong and B.-F. Shi, Enantio- and Regioselective Electrooxidative Cobalt-Catalyzed C-H/N-H Annulation with Alkenes, *Angew. Chem., Int. Ed.*, 2023, **62**, e202218533; (*b*) T. Münchow, S. Dana, Y. Xu, B. Yuan and L. Ackermann, Enantioselective electrochemical cobalt-catalyzed aryl C-H activation reactions, *Science*, 2023, **379**, 1036–1042; (*c*) Y. Lin, T. Münchow and L. Ackermann, Cobaltaelectro-Catalyzed C-H Annulation with Allenes for Atropochiral and P-Stereogenic Compounds: Late-Stage Diversification and Continuous Flow Scale-Up, *ACS Catal.*, 2023, **13**, 9713–9723; (*d*) T. Münchow, Y.-R. Liu, R. Parmar, S. E. Peters, S. Trienes and L. Ackermann, Cobaltaelectro-Catalyzed C-H Activation for Central and Axial Double Enantio-Induction, *Angew. Chem., Int. Ed.*, 2024, **63**, e202405423; (*e*) P. Boos, N. K. Pandit, S. Dana, T. Münchow, A. Hashidoko, L. Haberstock, R. Herbst-Irmer, D. Stalke and L. Ackermann, Multiple Atropo Selectivity by κ^2-*N*,*O*-Oxazoline Urea Ligands in Cobaltaelectro-Catalyzed C-H Activations: Decoding Selectivity with Data Science Integration, *ChemistryEurope*, 2025, **3**, e202500071; (*f*) T. Münchow, N. K. Pandit, S. Dana, P. Boos, S. E. Peters, J. Boucat, Y.-R. Li, A. Scheremetjew and L. Ackermann, Enantioselective C-H annulations enabled by either nickel- or cobalt-electrocatalysed C-H activation for catalyst-controlled chemodivergence, *Nat. Catal.*, 2025, **8**, 257–269.

76 P. Kushwaha, A. Saxena, T. von Münchow, S. Dana, B. Saha and L. Ackermann, Metallaelectro-catalyzed alkyne annulations *via* C-H activations for sustainable heterocycle syntheses, *Chem. Commun.*, 2024, **60**, 12333–12364.

77 N. Sauermann, R. Mei and L. Ackermann, Electrochemical C-H Amination by Cobalt Catalysis in a Renewable Solvent, *Angew. Chem., Int. Ed.*, 2018, **57**, 5090–5094.

78 X. Gao, P. Wang, L. Zeng, S. Tang and A. Lei, Cobalt(II)-Catalyzed Electrooxidative C-H Amination of Arenes with Alkylamines, *J. Am. Chem. Soc.*, 2018, **140**, 4195–4199.

79 S.-K. Zhang, R. C. Samanta, N. Sauermann and L. Ackermann, Nickel-Catalyzed Electrooxidative C-H Amination: Support for Nickel(IV), *Chem. – Eur. J.*, 2018, **24**, 19166–19170.

80 Q.-L. Yang, X.-Y. Wang, J.-Y. Lu, L.-P. Zhang, P. Fang and T.-S. Mei, Copper-Catalyzed Electrochemical C-H Amination of Arenes with Secondary Amines, *J. Am. Chem. Soc.*, 2018, **140**, 11487–11494.

81 S. Kathiravan, S. Suriyanarayanan and I. A. Nicholls, Electrooxidative Amination of sp^2 C-H Bonds: Coupling of Amines with Aryl Amides via Copper Catalysis, *Org. Lett.*, 2019, **21**, 1968–1972.

82 Z. Duan, L. Zhang, W. Zhang, L. Lu, L. Zeng, R. Shi and A. Lei, Palladium-Catalyzed Electro-oxidative C-H Amination toward the Synthesis of Pyrido[1,2-*a*]benzimidazoles with Hydrogen Evolution, *ACS Catal.*, 2020, **10**, 3828–3831.

83 Q. Wang, X. Zhang, P. Wang, X. Gao, H. Zhang and A. Lei, Electrochemical Palladium-Catalyzed Intramolecular C-H Amination of 2-Amidobiaryls for Synthesis of Carbazoles, *Chin. J. Chem.*, 2021, **39**, 143–148.

84 Y. Yuan, J. Zhu, Z. Yang, S.-F. Ni, Q. Huang and L. Ackermann, Scalable Rhodaelectro-Catalyzed Expedient Access to Seven-Membered Azepino[3,2,1-*hi*]indoles *via*, [5 + 2] C-H/N-H Annulation, *CCS Chem.*, 2022, **4**, 1858–1870.

85 S. Wu, B. Yuan, Y. Lei, X. Su, T. Münchow, J. C. A. Oliveira, X. Huang, Z. Ding, R. Xu, L. Ackermann and J. Mo, Rhodaelectro-catalyzed C-H activations directed by pharmacophores: enabling modification of bioactive compounds, *Org. Chem. Front.*, 2025, **12**, 5566–5572.

86 Y. Zhao and W. Xia, Recent advances in radical-based C–N bond formation *via* photo-/electrochemistry, *Chem. Soc. Rev.*, 2018, **47**, 2591–2608.

87 (*a*) J. Jiao, K. Murakami and K. Itami, Catalytic Methods for Aromatic C-H Amination: An Ideal Strategy for Nitrogen-Based Functional Molecules, *ACS Catal.*, 2016, **6**, 610–633; (*b*) Y. Park, Y. Kim and S. Chang, Transition Metal-Catalyzed C–H Amination: Scope, Mechanism, and Applications, *Chem. Rev.*, 2017, **117**, 9247–9301; (*c*) Y. N. Timsina, B. F. Gupton and K. C. Ellis, Palladium-Catalyzed C-H Amination of $C(sp^2)$ and $C(sp^3)$-H Bonds: Mechanism and Scope for N-Based Molecule Synthesis, *ACS Catal.*, 2018, **8**, 5732–5776.

88 (*a*) W.-J. Yoo, T. Tsukamoto and S. Kobayashi, Visible-Light-Mediated Chan-Lam Coupling Reactions of Aryl Boronic Acids and Aniline Derivatives, *Angew. Chem., Int. Ed.*, 2015, **54**, 6587–6590; (*b*) J. C. Vantourout, H. N. Miras, A. Isidro-Llobet, S. Sproules and A. J. B. Watson, Spectroscopic studies of the Chan-Lam amination: A mechanism-inspired solution to boronic ester reactivity, *J. Am. Chem. Soc.*, 2017, **139**, 4769–4779; (*c*) Z. Wang, S.-K. Tian and M. Zhang, Generalization of the Chan-Lam reaction via photoinduced copper catalysis, *CCS Chem.*, 2025, DOI: **10.31635/ccschem.025.202506644**; (*d*) H. Xiao, P. Cao, W. Xiong and T. Yang, Overcoming limitations in Chan-Lam amination with alkylboronic esters *via* aminyl radical substitution, *Nat. Commun.*, 2025, **16**, 9121.

89 H.-L. Qi, D.-S. Chen, J.-S. Ye and J.-M. Huang, Electrochemical Technique and Copper-Promoted Transformations: Selective Hydroxylation and Amination of Arylboronic Acids, *J. Org. Chem.*, 2013, **78**, 7482–7487.

90 (*a*) R. P. Wexler, P. Nuhant, T. J. Senter and Z. J. Gale-Day, Electrochemically Enabled Chan-Lam Couplings of Aryl Boronic Acids and Anilines, *Org. Lett.*, 2019, **21**, 4540–4543; (*b*) H.-L. Qi, D.-S. Chen, J.-S. Ye and J.-M. Huang, Electrochemical Technique and Copper-Promoted Transformations: Selective Hydroxylation and Amination of Arylboronic Acids, *J. Org. Chem.*, 2013, **78**, 7482–7487.

91 B. R. Walker, S. Manabe, A. T. Brusoe and C. S. Sevov, Mediator-Enabled Electrocatalysis with Ligandless Copper for Anaerobic Chan-Lam Coupling Reactions, *J. Am. Chem. Soc.*, 2021, **143**, 6257–6265.

92 Z.-J. Huang, J.-H. Qin, M.-L. Huang, Q. Sun, H.-Y. Xie, Y. Li and J.-H. Li, Electrochemical dehydrogenative cyclization/aromatization of aniline-tethered alkylidenecyclo propanes: facile access to benzo[c]carbazoles, *Org. Chem. Front.*, 2023, **10**, 1557–1563.

93 (*a*) Y. Park, Y. Kim and S. Chang, Transition Metal-Catalyzed C-H Amination: Scope, Mechanism, and Applications, *Chem. Rev.*, 2017, **117**, 9247–9301; (*b*) B. L. Tran, B. Li, M. Driess and J. F. Hartwig, Copper-catalyzed intermolecular amidation and imidation of unactivated alkanes, *J. Am. Chem. Soc.*, 2014, **136**, 2555–2563; (*c*) A. G. Bakhoda, Q. Jiang, Y. M. Badiei, J. A. Bertke, T. R. Cundari and T. H. Warren, Copper-catalyzed $C(sp^3)$-H amidation: sterically driven primary and secondary C-H site-selectivity, *Angew. Chem., Int. Ed.*, 2019, **58**, 3421–3425.

94 (*a*) H. Cao, X. Tang, H. Tang, Y. Yuan and J. Wu, Photoinduced intermolecular hydrogen atom transfer reactions in organic synthesis, *Chem. Catal.*, 2021, **1**, 523–598; (*b*) L. Capaldo, D. Ravelli and M. Fagnoni, Direct photocatalyzed hydrogen atom transfer (HAT) for aliphatic C-H bonds elaboration, *Chem. Rev.*, 2022, **122**, 1875–1924.

95 (*a*) J. Yin, C. Shi, A.-M. Hu, M. Luo, C. Yang, L. Guo and W. Xia, Copper-catalyzed $C(sp^3)$-H amination and etherification of unactivated hydrocarbons via photoelectrochemical pathway, *Nat. Commun.*, 2025, **16**, 5123; (*b*) G. Stewart, C. Rapala and C. A. Malapit, Electrochemical Non-Directed Arene C-H Amination, *ChemCatChem*, 2024, **16**, e202400867.

96 (*a*) Y. Liang, X. Zhang and D. W. C. MacMillan, Decarboxylative sp^3 C-N coupling *via* dual copper and photoredox catalysis, *Nature*, 2018, **559**, 83–88; (*b*) Q. Y. Li, S. N. Gockel, G. A. Lutovsky, K. S. DeGlopper, N. J. Baldwin, M. W. Bundesmann, J. W. Tucker, S. W. Bagley and T. P. Yoon, Decarboxylative cross-nucleophile coupling *via* ligand-to-metal charge transfer photoexcitation of Cu(II) carboxylates, *Nat. Chem.*, 2022, **14**, 94–99.

97 K.-N. Yuan, H. Zhuang, J. Wei, Y. Shen, H.-Q. Yao, M.-H. Li, L.-L. Xu and M. Shang, Modular access to saturated bioisosteres of anilines via photoelectrochemical decarboxylative $C(sp^3)$-N coupling, *Nat. Commun.*, 2025, **16**, 920.

98 (*a*) Y. Yasui, S. Tsuchida, H. Miyabe and Y. Takemoto, One-Pot Amidation of Olefins through Pd-Catalyzed Coupling of Alkylboranes and Carbamoyl Chlorides, *J. Org. Chem.*, 2007, **72**, 5898–5900; (*b*) S. C. Ghosh, J. S. Y. Ngiam, A. M. Seayad, D. T. Tuan, C. L. L. Chai and A. Chen, Copper-Catalyzed Oxidative Amidation of Aldehydes with Amine Salts: Synthesis of Primary, Secondary, and Tertiary Amides, *J. Org. Chem.*, 2012, **77**, 8007–8015; (*c*) Y.-L. Zheng and S. G. Newman, Methyl Esters as Cross-Coupling Electrophiles: Direct Synthesis of Amide Bonds, *ACS Catal.*, 2019, **9**, 4426–4433; (*d*) Z. Fu, X. Wang, S. Tao, Q. Bu, D. Wei and N. Liu, Manganese Catalyzed Direct Amidation of Esters with Amines, *J. Org. Chem.*, 2021, **86**, 2339–2358.

99 Y. A. Kolekar and B. M. Bhanage, Pd-Catalyzed Oxidative Aminocarbonylation of Arylboronic Acids with Unreactive Tertiary Amines *via* C-N Bond Activation, *J. Org. Chem.*, 2021, **86**, 14028–14035.

100 L. Zeng, H. Li, J. Hu, D. Zhang, J. Hu, P. Peng, S. Wang, R. Shi, J. Peng, H. Zhang, Y.-H. Chen and A. Lei, Electrochemical oxidative aminocarbonylation of terminal alkynes, *Nat. Catal.*, 2020, **3**, 438–445.

101 (*a*) L. Zhou, S. Tang, X. Qi, C. Lin, K. Liu, C. Liu, Y. Lan and A. Lei, Transition-Metal-Assisted Radical/Radical Cross-Coupling: A New Strategy to the Oxidative $C(sp^3)$-H/N-H Cross-Coupling, *Org. Lett.*, 2014, **16**, 3404–3407; (*b*) Q. Yue, Z. Xiao, Z. Kuang, Z. Su, Q. Zhang and D. Li, Chelation–promoted Efficient C-H/N-H Cross Dehydrogenative Coupling between Picolinamides and Simple Ethers under Copper Catalysis, *Adv. Synth. Catal.*, 2018, **360**, 1193–1198; (*c*) P. Yang, X. Wang, L. Wang,

J. He, Q. Zhang and D. Li, Oxidative cross-dehydrogenative coupling between iodoarenes and acylanilides for C-N bond formation under metal-free conditions, *Org. Chem. Front.*, 2021, **8**, 2556–2562.

102 (*a*) R. W. Evans, J. R. Zbieg, S. Zhu, W. Li and D. W. C. MacMillan, Simple Catalytic Mechanism for the Direct Coupling of α-Carbonyls with Functionalized Amines: A One-Step Synthesis of Plavix, *J. Am. Chem. Soc.*, 2013, **135**, 16074–16077; (*b*) Z.-W. Hou, D.-J. Liu, P. Xiong, X.-L. Lai, J. Song and H.-C. Xu, Site-Selective Electrochemical Benzylic C-H Amination, *Angew. Chem., Int. Ed.*, 2021, **60**, 2943–2947.

103 K. Liang, Q. Zhang and C. Guo, Enantioselective nickel-catalysed electrochemical cross-dehydrogenative amination, *Nat. Synth.*, 2023, **2**, 1184–1193.

104 A. R. Fairhurst, C. Lim, M. Jun, B. J. Ransom, F. Mackowicz, D. Haering and V. R. Stamenkovic, Surface Science: The Foundation of Electrocatalysis, *J. Am. Chem. Soc.*, 2025, **147**, 40035–40044.

105 (*a*) Q. Lin, E. H. Spielvogel and T. Diao, Carbon-centered radical capture at nickel(II) complexes: Spectroscopic evidence, rates, and selectivity, *Chem*, 2023, **9**, 1295–1308; (*b*) C. Gao, X. Liu, M. Wang, S. Liu, T. Zhu, Y. Zhang, E. Hao and Q. Yang, Advances in Asymmetric Electrochemical Synthesis, *Chin. J. Org. Chem.*, 2024, **44**, 673–727; (*c*) E. H. Spielvogel, J. Yuan, N. M. Hoffmann and T. Diao, Nickel-Mediated Radical Capture: Evidence for a Concerted Inner-Sphere Mechanism, *J. Am. Chem. Soc.*, 2025, **147**, 19632–19642; (*d*) C. Ma, J.-F. Guo, S.-S. Xu and T.-S. Mei, Recent Advances in Asymmetric Organometallic Electrochemical Synthesis (AOES), *Acc. Chem. Res.*, 2025, **58**, 399–414; (*e*) W. Liu, C. Zhai, Y. Jiang, L.-P. Wei, H.-C. Li, Z. Cai and C. Zhu, Applying alternating current in paired photo-electrocatalysis for asymmetric cross-coupling of alcohols, *Nat. Synth.*, 2025, **4**, 1534–1545, DOI: 10.1038/s44160-025-00875-8.

106 H. Wang, Y. Cheng, Y. Wang, R. Duan, M. Zhou, S. Liu, W. Zhao, H. Qin, J. Yang, Y. Peng, L. Jing, Y. Xu, Q. Zhu, X. Sun, Q. Qian, J. Zhang, X. Kang and B. Han, Imidazolium radical-mediated electron transfer enhances electrochemical C-N coupling for glycine synthesis, *Nat. Synth.*, 2025, DOI: 10.1038/s44160-025-00892-7.